UNIVERSITÀ DEGLI STUDI ROMA TRE

DOTTORATO IN FISICA – XXX CICLO

Theory of Spin-Charge Interconversion in an Electron Gas

Dottorando: Amin Maleki
Docente Guida: Prof. Roberto Raimondi
Coordinatore: Prof. Giuseppe Degrassi

Ottobre 2017

The sphere upon which mortals come and go,
Has no end nor beginning that we know;
And none there is to tell us in plain truth:
Whence do we come and whither do we go.

Omar Khayyam

Contents

List of Acronyms

2D Two-Dimensional

2DEG Two-Dimensional Electron Gas

3D Three-Dimensional

BIA Bulk-Inversion Asymmetry

CISP Current-Induced Spin Polarization

DP Dyakonov-Perel Spin Relaxation

DSOC Dresselhaus Spin-Orbit Coupling

EE Edelstein Effect

EY Elliott-Yafet Spin Relaxation

EYT Elliott-Yafet torque

GMR Giant magnetoresistance

IEE Inverse Edelstein Effect

ISGE Inverse Spin Galvanic Effect

RSOC Rashba Spin-Orbit Coupling

SGE Spin Galvanic Effect

SHE Spin Hall Effect

SIA Structure Inversion Asymmetry

SO Spin-Orbit

SOC Spin-Orbit Coupling

Chapter 1

Introduction

1.1 Spintronics: Spin-transport electronics vision for the future

Spintronics, or spin-transport electronics, is the science of exploiting the electric spin in addition to the electronic charge for the future electronics applications. The main goal of *spintronics* is to understand the relationship between charge and spin degrees of freedom of carriers and to exploit such understanding to develop new device functionalities. The advantage of using spin-charge based logic devices is that they have substantially more capability and performance, compared to charge-based devices, and can be used to increase data processing speed and memory storage, decrease electric power consumption and make transferring data quicker. In contrast to classic electronics which is based on semiconductors, in *spintronics* applications, both normal and ferromagnetic metals are important as well.

Historically the electric control of the non-equilibrium spin population was based on ferromagnetic interactions. The idea is that the non-equilibrium spin polarization can be generated via paramagnetic materials and then transferred through metallic materials. A typical example of magnetotransport phenomena is the famous giant magnetoresistance (GMR) effect in thin-film structures composed of alternating ferromagnetic and nonmagnetic conductance layers, which exploit the different conductivity properties of the spin populations. The effect is observed by a change in the electric resistance due to the change of the relative magnetization between the two different ferromagnetic layers. More precisely, the resistance is lower when the magnetizations of adjacent ferromagnetic layers are parallel, but is higher for antiparallel alignment. Notice that the magnetization direction of the ferromagnetic layers can be controlled by an external magnetic field. The Nobel prize in 2007 was awarded to Albert Fert and Peter Grünberg for the discovery of GMR [5]. As it is well known, the GMR effect currently has huge applications in electrical devices based on magnetic sensors, which are used in hard disc storage [67], biosensors and micro-electromechanical systems and as well as in magnetoresistive random-access memory as a cell that can store information (For more details, see Ref. [79]).

In addition to paramagnetic materials, the generation of spin-polarized currents can be achieved in different ways such as electrical spin injection, through temperature gradient and many other ways. Traditionally, spin has been oriented by using the optical technique in such away that circular polarized

photons transfer their angular momentum to electrons, and then polarized electron-hole pairs are produced with certain direction [107]. The reverse is also true when the polarized electron (holes) combine with unpolarized holes (electron), polarized light is emitted. This is the principle of spin light emitting diodes (spin LEDs) [61]. In semiconducting structures the spin population is also measured via optical detection of the current-induced spin polarization [14, 42, 65, 93]. Roughly speaking, the optical approach could be specifically designed for detection, manipulation and injection of spin polarization, and exploit the ability to precisely engineer the coupling between electron spin and optical photons. Indeed the merging of electronics, photonics and magnetism will produce new spin-based multifunctional devices such as spin-field effect transistors, quantum bits for quantum computation and communication.

In addition to ferromagnetic interactions, the control of the electric spin could also be obtained with different mechanisms based on spin-orbit coupling (SOC), without the need for magnetic materials. SOC is one of the key microscopic mechanisms to couple charge currents and spin polarizations. Among the many interesting effects which arise from SOC, the two effects, known as inverse spin-galvanic effect (ISGE) and spin Hall effect (SHE), are the focus of intensive experimental and theoretical research both for their intrinsic interest and for their potential exploitation in the realization of new *spintronic* functionalities. Indeed, the SHE and ISGE are deeply connected to each other [11], and we will focus on the effect of ISGE. Through this present chapter, we will give an overview of ISGE, and then introduce the essential tools and concepts that will be extensively used throughout this work. We refer the interested reader to references [3, 32, 34, 95, 103] for details.

1.2 A brief description of inverse spin-galvanic effect

The spin-galvanic effect (SGE) and its inverse manifestation have been intensively investigated over the past decade both for their intrinsic fundamental interest [34] and for their application potential in future generation electronic and *spintronics* technology [3, 95]. The non-equilibrium generation of a spin polarization perpendicular to an externally applied electric field is referred to as the ISGE in the absence of external magnetic field as illustrated in Fig. 1.1, whereas the SGE is its Onsager reciprocal, whereby a spin polarization injected through a nonmagnetic material creates a charge current in the direction perpendicular to the spin polarization. As an all-electrical method of generating and detecting spin polarization in nonmagnetic materials, both of these effects may be used for applications such as spin-based field effect transistors [46, 84, 97] and magnetic random access memory [60, 110].

The ISGE, also known as the Edelstein effect (EE) or current-induced spin polarization (CISP), was originally proposed by Ivchenko and Pikus [40], and observed by Vorob'ev et al. in tellurium [102]. Later, the ISGE was theoretically analyzed by Edelstein in a two-dimensional electron gas (2DEG) with Rashba spin-orbit coupling (RSOC) [21] and also by Lyanda-Geller and Aronov [4, 38]. Notice that the SGE in the spin-charge conversion is sometimes referred to as the inverse Rashba–Edelstein effect. The SGE has been observed experimentally in GaAs quantum wells (QWs) by Ganichev et al. [31, 33], where the spin polarization was detected by measuring the current produced by circularly polarized light. In semiconducting structures, the ISGE can be measured by optical methods such as Faraday rotation, linear-

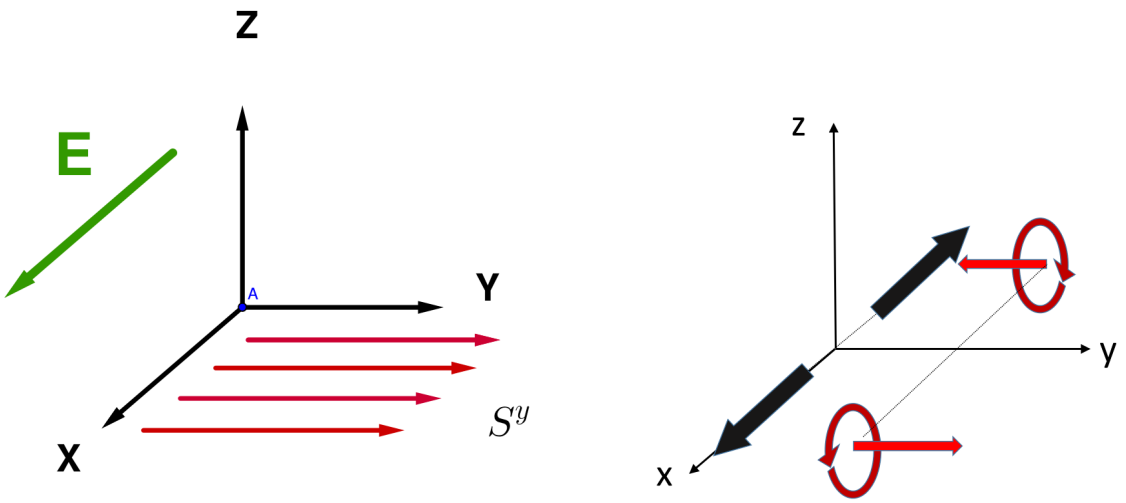

Figure 1.1: Left: Inverse spin galvanic effect. The red lines stand for the direction of spin polarization and the green one is the direction of the external electric field. Right: The parity transformation as a reflection in a mirror. Arrows show the reflection of the components of polar vector J_x (black line) and axial vector S^y (red line) by the mirror reflection through the yz-plane.

circular dichroism in transmission of terahertz radiation and time resolved Kerr rotation [30, 32, 34, 109]. Very recently, a new way of converting spin to charge current has been experimentally developed by Rojas-Sánchez et al., where, by the spin-pumping technique, the non-equilibrium spin polarization injected from a ferromagnet into a Ag/Bi interface yields an electrical current [83]. Successively, the SGE has also been observed in many interfaces with strong spin-orbit splitting, including metals with semiconductor giant SOC or insulators such as $Fe/GaAs$ [15] or Cu/Bi_2O_3 [41]. Phenomenologically, the non-equilibrium spin polarization can be linked to an external electric current by

$$S_i = \sum_j R_{ij} J_j, \tag{1.1}$$

$$J_i = \sum_j Q_{ij} S_j, \tag{1.2}$$

where R_{ij} and Q_{ij} are second rank pseudo tensors. The first equation represents ISGE and the second one is SGE. It is clear that both equations (1.1) and (1.2) linearly couple a polar vector with an axial vector. More precisely, the key mechanism of the effect relies on the symmetry properties of gyrotropic media. [1] In fact, the electrical currents and spin polarizations are polar and axial vector, respectively. In centro-symmetric systems, polar and axial vectors transform differently and no SGE effect is expected. In restricted symmetry conditions, however, polar and axial vectors components may transform similarly. Consider, for instance, the case of electrons confined in the xy plane with the mirror reflection through the yz plane, as shown in Fig. 1.1. Under such a symmetry operation, the electrical currents along the x and y directions transform as $J_x \to -J_x$ and $J_y \to J_y$. The spin polarizations transform as the

[1] See Ref. [34]. A system is called gyrotropic if in its point symmetry group some components of polar vectors and components of axial vectors transform according to the same representation.

components of angular momentum, and we have $S^y \to -S^y$ and $S^x \to S^x$. Hence, one expects a coupling between J_x and S^y or between J_y and S^x. Such a coupling is the SGE. For instance in QWs, under C_{2V} symmetry the only non-vanishing element of the pseudo tensor is Q_{xy} in the restricted symmetry due to the structure inversion asymmetry (SIA). However, in this case, the direction of spin polarization depends not only on SIA, but also on the bulk inversion asymmetry (BIA) resulting in an anisotropy of the current-induced spin polarization.

At a microscopic level, the strength of the coupling is due to the SOC. Usually, the SOC is classified as extrinsic and intrinsic, depending on the origin of the electrical potential. The intrinsic SOC arises due to the crystalline potential of the host material or due to the confinement potential associated with the device structure. On the other hand, the extrinsic SOC is due to the atomic potential of random impurities, which determine the transport properties of a given material. The majority of the studies on SGE/ISGE has focused on the Rashba SOC (RSOC) for electrons moving in the xy plane, which was originally introduced by Rashba [13] to study the properties of the energy spectrum of non-centrosymmetric crystals of the CdS type and later successfully applied to the interpretation of the two-fold spin splitting of electrons and holes in asymmetric semiconducting heterostructures [12]. RSOC is classified as being due to SIA, which is responsible for the confinement of electrons in the xy plane. In addition, one may also consider the SOC arising from BIA, which is usually referred to as DSOC [19]. Both RSOC and DSOC modify the energy spectrum by introducing a momentum-dependent spin splitting. This can also be understood quite generally on the basis of symmetry considerations. In a solid, the spin degeneracy for a couple of states with opposite spin direction, comes from both time reversal invariance and parity (space inversion invariance). By breaking the parity, as for instance, in a confined 2DEG, the spin degeneracy is lifted and the Hamiltonian requires an effective momentum-dependent magnetic field, which is the SOC. As a result, electron states can be classified with their chirality in the sense that their spin state depends on their wave vector. In such a situation, scalar disorder, although not directly acting on the spin state, influences the spin dynamics by affecting the wave vector of the electrons and holes. Spin relaxation arising in this context is usually referred to as the Dyakonov–Perel (DP) mechanism. Extrinsic SOC originates from the potential that is responsible for the scattering from an impurity. Spin relaxation due to extrinsic SOC is usually referred to as the Elliott–Yafet (EY) spin relaxation [108]. In this case, the spin relaxation time scales is as the momentum relaxation time. Therefore, when extrinsic SOC is present, the scattering amplitude of electrons by impurities can be divided in the two different parts, spin-independent and spin-dependent contributions. The spin-independent part yields the standard elastic scattering time, whereas the spin-dependent one is responsible for the EY spin relaxation. As explained by Lifshits and Dyakonov [52], the different combinations of the scattering amplitudes correspond to specific physical processes. Through this present work, we will review it more carefully.

However all the recent publications on spin-charge conversion involve the different SOC mechanisms, including the interaction between an external electric field and charged particles in semiconductor, this conversion between spin and charge can also be demonstrated in cold atomic gases, both the bosonic and fermionic as well as the mixture [1]. In cold atomic gases, the quantum states of atoms can interact with the laser light in different ways depending. More precisely the motion of atoms in position-dependent laser

configuration may give rise a spin-dependent gauge field potentials [54, 66, 81, 101, 111], which can lead to an effective SOC in an atomic gases. Hence with a proper laser configuration, an effective SOC, e.g., Rashba and linear Dresselhaus SOC can be obtained by coupling atomic spin states to spatially varying laser fields. The optically induced SOC in atomic gases is currently the focus of intensive experimental and theoretical research both for a new possibilities of studying spintronics, e.g., spin relaxation [96], *Zitterbewegung* [101] and SHE [53, 111]. The exploration of these systems are however beyond the scope of the present work and we refer the interested reader to the literature cited before.

In this present work, we analyze some aspects of the interplay between the intrinsic and extrinsic mechanisms focusing on the description of the of ISGE/EE and SGE/IEE in a 2DEG – we will however also discuss results valid in three-dimensional (3D) gases. To be explicit, as noted in [34], when both intrinsic and extrinsic SOC are present, the non-equilibrium spin polarization of the ISGE will be dependent on the ratio of the DP and EY spin relaxation rates. This was analyzed in [75] by means of the Keldysh non-equilibrium Green function within an SU(2) gauge theory-description of the SOC. Successively, a parallel analysis by standard Feynman diagrams for the Kubo formula will be carried out in Chapter 4. We theoretically confirm that the ratio of DP to EY spin relaxation is able to tune the value of the ISGE. Such tuning is also affected by the value of the spin Hall angle due to the fact that spin polarization and spin current are coupled in the presence of intrinsic RSOC.

In particular, we will show that the interplay of intrinsic and extrinsic SOC gives rise to an additional spin torque in the Bloch equations for the spin dynamics and affects the value of the ISGE. This additional spin torque, which is proportional to both the EY spin relaxation rate and to the coupling constant of intrinsic SOC, will be derived in Chapter 6 in the context of the diagrammatic approach of the Kubo linear response theory. Although the Kubo linear response theory is a very powerful approach in the understanding of the physical origin of this new torque, it is very useful to also show how the same result can be obtained independently by using the SU(2) gauge theory formulation. One of the aims of this work is to present the same physical phenomenon from different viewpoints. Each technique has its own virtues and merits. The present work, by showing the same phenomenon with different techniques, helps to clarify the connections between them. This may have a pedagogical value. In particular, we obtain an analytical formula of the ISGE in the presence of the Rashba, Dresselhaus and impurity SOC. We will show how the intrinsic and extrinsic SOC act in parallel as far as relaxation to the equilibrium state is concerned. In order to compare with experimental results, we solve the Bloch equation numerically, and then extend our results to the case of beyond the diffusive approximation in the QW systems. We will see that the response function is modified.

1.3 Theoretical tools for the description of spin-charge conversion

One of the most obvious and compelling aspects of any system in the physical world is that it is processed through out-of-equilibrium processes. They are ubiquitous in the physical world with many different examples, some very simple, such as a system connected with different sources of temperatures, electrons in conductor driven by an applied electromagnetic field or pumped by external forces and irreversible processes in general. Indeed, the description of physical properties in an isolated system is more often an out-of-equilibrium system. The general method available for gaining knowledge about the dynamics of a system is the perturbation theory, which provides a set of approximation schemes directly related to mathematical perturbation for describing a complicated quantum system in terms of a simpler one. We do not discuss in general nonequilibrium statistical mechanics and refer the interested reader to the fairly rich lectures [18, 77]. One of the approaches to deal with perturbed systems is the quasiclassical formalism [69, 78]. Under certain physical assumptions, the Keldysh formalism can be used within the quasiclassical approximation [43, 77]. The theory is expressed in a such a way that it generalizes the standard perturbative approach typically from the equilibrium quantum field theory to non-equilibrium problems. This idea historically stems from Martin and Schwinger (1959), and then Schwinger [87] in 1961. Then, in 1964, Keldysh applied the quasiclassical technique to the derivation of transport phenomena in electron-phonon systems that was already discussed by Konstantinov and Perel (1960) in a diagrammatic technique. In fact, the quasiclassical was originally formulated by Kadanoff and Baym [7], where the transport equations beyond perturbation theory for the case of interacting electrons and photons are derived. The model was later extended, highly successfully, to deal with superconductivity [78]. Currently the theory has a wide range of applications which go from particle physics to solid state and soft condensed matter.

In particular, the purpose of the present work, is to give an account of the use of real time Green function in transport theory and discuss the relevance of our results within current research. The theory deals with different transport phenomena by deriving the appropriate kinetic equation, starting from Dyson equations in their general form. The main assumption in this theory is that all energy scales concerning the external fields, interactions and disorder must be small compared to the Fermi energy. Another important assumption is its relying on perfect particle-hole symmetry. In other words, the quasiclassical equations are obtained by neglecting the dependence on the modulus of momentum or energy variable of the density of states and of the velocity, which are fixed at their values at the Fermi surfaces. However, when the spin-orbit coupling is present, there are two Fermi surfaces and one needs to be more careful about the precise relationships involved here. It is such phenomena that allow us to generalize the quasiclassical approach to situations that the electron-hole symmetry is broken. More precisely, we will use the quasiclassical approach to describe the effects of spin-orbit coupling in terms of the SU(2) gauge field theory and derive a generalized Boltzmann equation concerning the charge and spin distribution function. This method has advantages greater than the linear-response theory by allowing non-linear situations to be considered.

Although the SU(2) gauge field theory is a very powerful method, in our case, the linear-response theory can be more convenient than quasiclassical Keldysh formula to attempt to elucidate more the physical origin of the results, which in the SU(2) Keldysh formula derivation is not easy to grasp. The linear response limit is a tremendous simplification compared with conditions, since the linear response is uniquely determined by the equilibrium properties of the system. More generally though, when the system is perturbed ever so slightly, its response function will be linear in the perturbation [77]. Among the numerous applications of linear response theory, one can mention the diagrammatic standard Kubo formula approach [48] to evaluate the response function with respect to the spin-current transport. However the Kubo formula generally is an equation which expresses the linear response of an observable quantity due to a time-dependent perturbation.

1.4 Outline

The layout of the present work is organized as follows:

Chapter 2 is dedicated to the SOC in solid state systems. We will explain how the effective Hamiltonian arises due to the different SOC. Some additional details can be found in Appendix A.

In Chapter 3, we will introduce the central tools used in this present work: the Green functions, the Keldysh technique and quasiclassical theory, and the diagrammatic Kubo formula approach. We will develop the general formalisms dealing with the non-equilibrium situation. After introducing the retarded and advanced Green functions, we develop the perturbation theoretic structure in terms of the quasiclassical and diagrammatic approach. We provide a precise formula definition of our theory in terms of the Kubo formula and Keldysh non-equilibrium Green functions. We recall the weak localization corrections of a disordered system. At the end of the chapter, we will pay some attention to the full scattering amplitude in the presence of SOC.

Chapter 4 is based on the work published in [75]. Here we will formulate the ISGE in a 2DEG. Compared with previous work in [75], we consider both the Rashba and Dresselhaus SOC as well as the SOC from impurity scattering. However in this Chapter, we will not consider the effect of two spin-orbit split bands at the Fermi level in the EY mechanism. In evaluating the Kubo formula for the spin polarization response to an electric field, we will explicitly take into account the side-jump and skew scattering effects.

Chapter 5 is dedicated to the frequency-dependent ISGE when the interplay of SOC is present. In particular, we will find that the size and form of the ISGE is greatly modified by the presence of the various sources of SOC. We use a diagrammatic Kubo formula approach to evaluate the spin polarization charge-current response functions. The main reason for using the linear response theory is to understand the origin of additional spin torque in a situation which is technically simpler to treat with respect to the SU(2) Keldysh technique.

In Chapter 6, the derivation is based on the SU(2) gauge-field formulation of the Rashba-Dresselhaus SOC. Our main result is to the identification of a spin-generation torque arising from EY scattering, which opposes a similar term arising from DP relaxation. Such a torque, which to the best of our knowledge has gone unnoticed so far, is of a basic nature, i.e. it should be effective whenever EY processes are present in a system with intrinsic SOC, irrespective of further specific details. We also discuss the extension results to the three dimensional electron gas, which may be relevant for the interpretation of experiments in thin films.

Chapter 7 starts with a rather general discussion of the ISGE and gives a brief introduction of experimental techniques based on Kerr rotation and spin pumping, and then moves to treat some aspects of our results in connection with the experimental one. More precisely, this present chapter is based on the work published in [64]. We will later numerically show that the non-equilibrium spin polarization does not align along the internal magnetic field due to the spin-orbit coupling.

In Chapter 8, the ISGE will evaluate beyond the diffusive regime. In particular, we derive the Eilenberger equation in the presence of a generic intrinsic spin-orbit field by using the quassiclassical

Green function. Hence the Bloch equations governing spin dynamics of the carriers are evaluated in the linear, cubic and both linear-cubic SOC. The quasiclassical approach allows us to study spin-charge interconversion in the two different regimes, the diffusive and beyond the diffusive approximation. The results also show numerically to make the comparison easier between the two approximations.

1.5 Publications

- A. Maleki Sheikhabadi and R. Raimondi. Inverse Spin Galvanic Effect in the Presence of Impurity Spin-Orbit Scattering: A Diagrammatic Approach. *Condensed Matter*, 2(2):17, 2017
- C. Gorini, A. M. Sheikhabadi, and et al. Theory of current-induced spin polarization in an electron gas. *Phys. Rev. B*, 95:205424, May 2017
- A. M. Sheikhabadi, R. Raimondi, and K. Shen. The Edelstein Effect in the Presence of Impurity Spin-Orbit Scattering. *Acta Physica Polonica A*, 132(1):135–139, 2017

Chapter 2

Spin-orbit coupling in solid-state systems

Charge carriers in materials with structure inversion asymmetries experience a momentum-dependent magnetic field in their frame of motion, even in the absence of an external magnetic field, which is the so-called spin-orbit field. To show how the SOC appears in solid state systems, we start with its atomic derivation in the non-relativistic limit of the Dirac equation [20]. Then we will show how it appears in different semiconductor structures following the so-called $\mathbf{k}\cdot\mathbf{p}$ method [105], within the extended Kane model [80]. Then we will use these techniques in the case of quasi-2D systems [6, 107]. At the end of this chapter, we will derive the generic form of intrinsic Rashba-Dresselhaus [12, 13, 19] SOC and an extrinsic one arising from the random scattering from impurities.

The exploration of SOC physics is currently at the heart of the new research field of *spin-orbitronics*, which is a new branch of spintronics [57], focusing on the manipulation of non-equilibrium spin polarization using SOC. Here is a brief recall of SOC in solid state systems, and for more details we refer the interested reader to the literature cited before.

2.1 The origin of spin-orbit coupling: the Dirac equation

Before we discuss SOC in semiconductors, it is helpful to briefly review the origin of SOC following the approach of the Dirac equation, i.e. the basic equation for describing electronic systems including the electron spin and its relativistic behaviour. In principle, the SOC arises from the non-relativistic limit of the Dirac equation. Assuming a time-dependent problem, the Dirac equation can be written in the following form:

$$\left(\hat{\beta}m_0c^2 + c\hat{\alpha}\cdot\hat{\mathbf{p}} + \hat{V}\right)\psi = i\hbar\partial_t\psi, \tag{2.1}$$

where

$$\hat{\beta} = \begin{pmatrix} 1 & 0 \\ 0 & -1 \end{pmatrix}, \quad \hat{\alpha} = \begin{pmatrix} 0 & \sigma \\ \sigma & 0 \end{pmatrix}, \quad \hat{V} = e\Phi\hat{I}, \quad \hat{\mathbf{p}} = \mathbf{p}\hat{I}, \quad \psi = \begin{pmatrix} \psi_1 \\ \psi_2 \end{pmatrix}. \tag{2.2}$$

The Dirac function is written based on a two-component spinor, ψ_1 and ψ_2, where ψ_1 are the larger components. We will derive the explicit form of ψ, when the V and cp are small compared with the Dirac gap $2m_0c^2$ in the non-relativistic limit. Taking zero energy at m_0c^2, the Dirac equation gives us

$$\sigma \cdot \mathbf{p}\psi_2 = \frac{1}{c}\left(i\hbar\partial_t - e\Phi\right)\psi_1 \tag{2.3}$$

$$\sigma \cdot \mathbf{p}\psi_1 = \frac{1}{c}\left(i\hbar\partial_t + (2m_0c^2 - e\Phi)\right)\psi_2. \tag{2.4}$$

Using the second equation and making an expansion in terms of $1/2m_0c^2$, we can easily show

$$\psi_2 \simeq \frac{1}{2m_0c}\left(1 - \frac{i\hbar\partial_t}{2m_0c^2} + \frac{e\Phi}{2m_0c^2}\right)\sigma \cdot \mathbf{p}\psi_1. \tag{2.5}$$

The probabilistic interpretation of the Dirac theory requires the normalization condition as

$$\int d\mathbf{r}\psi^\dagger\psi = \int d\mathbf{r}\left(\psi_1^\dagger\psi_1 + \psi_2^\dagger\psi_2\right) = 1. \tag{2.6}$$

Therefore, this suggests that we can work with a new two-component wave function $\tilde{\psi}$ defined by

$$\tilde{\psi} = \left(1 + \frac{(\sigma \cdot \mathbf{p})^2}{8m_0^2c^2}\right)\psi_1. \tag{2.7}$$

which satisfies $\langle\tilde{\psi}|\tilde{\psi}\rangle = 1$ up to order $1/c^2$. The equation for $\tilde{\psi}$ from Eq. (2.3) reads

$$i\hbar\partial_t\tilde{\psi} = \left(1 - \frac{(\sigma \cdot \mathbf{p})^2}{8m_0^2c^2}\right)\left[e\Phi + \frac{1}{2m_0}\sigma \cdot \mathbf{p}\left(1 + \frac{e\Phi}{2m_0c^2}\right)\sigma \cdot \mathbf{p}\right]\left(1 + \frac{(\sigma \cdot \mathbf{p})^2}{8m_0^2c^2}\right). \tag{2.8}$$

Then the effective Hamiltonian up to terms of order $1/c^2$ reads

$$H_{eff} = e\Phi + \frac{p^2}{2m_0} - \frac{p^4}{8m_0^3c^2} + \frac{e\hbar\Delta\Phi}{8m_0^2c^2} + \frac{e\hbar}{4m_0^2c^2}\sigma \cdot \nabla\Phi \times \mathbf{p}. \tag{2.9}$$

The above equation can also be derived using Löwdin partitioning and invariants theory [28]. The first two terms are equivalent to the classical non-relativistic Hamiltonian, whereas the third one is the first relativistic correction to the energy and does not have a classical analogy. The fourth term is the so-called Darwin term, and finally the latest one yields the SOC as

$$H_{SOC} = \frac{\lambda_0^2}{4}\sigma \cdot (-i\nabla) \times \nabla(e\Phi), \quad \text{with } \lambda_0 = \frac{\hbar}{m_0c} \tag{2.10}$$

where $\lambda_0 \simeq 10^{-10}cm$ is the Compton wave length, which is very small compared to the characteristic lengths. In solids, when we describe the SOC, one should consider the effective Compton wavelength, which brings a big enhancement of the strength of the SOC. For instance in GaAs, the effective Compton wavelength is ten times bigger than the vacuum one. At the atomic scale, the $e\Phi$ is the central field due to the coulomb potential of the atomic core and to the screening electrons. In a crystalline solid, the derivation is quite different, but we will derive the effective Hamiltonian such as that one presented in Eq. (2.10). In the following sections, we will evaluate these effective terms according to the $k \cdot p$ approach and the Kane model.

2.2 The band structure and $k \cdot p$ approach

The main goal of this section is to describe the motion of charge carriers in terms of the effective Hamiltonian in the semiconductor structures. In theoretical studies, the methods are based on the

envelope function approximation, which allows us to develop a comprehensive description of electron- and hole-like states. We can cope with the periodic crystal potential, as well as perturbations such as external electric and magnetic fields, impurities and, more importantly, the SOC. Details of the underlying crystal potential are included in terms of band structure. All these details are achieved within the framework of the Luttinger-Kohn method, also known as the $k \cdot p$ model and the Kane model.

In the first step, we will treat the problem in the absence of any external fields and impurities, and then we will show how to include them. The derivation of the $k \cdot p$ method is based on the Schrödinger equation for the Bloch functions $\psi_{vk}(\mathbf{r})$ described by the microscopic lattice periodic crystal potential $U(\mathbf{r})$,

$$H_{eff}\psi_{vk}(x) = \left[\frac{(-i\hbar\nabla)^2}{2m_0} + U(\mathbf{r}) + \frac{\lambda_0^2}{4}\nabla U(\mathbf{r}) \times (-i\hbar\nabla) \cdot \sigma\right] \psi_{vk}(\mathbf{r}) = \epsilon_v(\mathbf{k})\psi_{vk}(\mathbf{r}), \tag{2.11}$$

where v denotes the band index, and m_0 is the free-electron mass. From now on we will work with natural units such that $\hbar = c = 1$. The translational symmetry of the lattice requires that the wave function to be of Bloch form, i.e.,

$$\psi_{vk}(\mathbf{r}) = e^{i\mathbf{k}\cdot\mathbf{r}}u_{v\mathbf{k}}(\mathbf{r}) \equiv e^{i\mathbf{k}\cdot\mathbf{r}}\langle\mathbf{r}|v\mathbf{k}\rangle \tag{2.12}$$

with $u_{v\mathbf{k}}(\mathbf{r})$ represents the periodic function of the lattice. In many solid state systems, like GaAs, the minimum of the conduction band and the maximum of valence band are at the Γ point $\mathbf{k} = 0$. [1] Therefore, the eigenfunctions of Eq. (2.12) can be expanded in terms of the band edge Bloch function $u_{v0}(\mathbf{r})$, as

$$u_{v\mathbf{k}}(\mathbf{r}) = \sum_{v'} c_{vv'\mathbf{k}}u_{v'0}(\mathbf{r}) \tag{2.13}$$

Now we multiply Eq. (2.11) from the left by $\langle u_{v0}|$ and using the eigenvalue equation for $|u_{v'0}\rangle$ we can obtain an algebraic eigenvalue problem for the dispersion $\epsilon_v(\mathbf{k})$

$$\begin{aligned}[H_0]_{vv'} &= \langle u_{v0}|H_0|u_{v'0}\rangle \\ &= \left[\left(\epsilon_{v0} + \frac{k^2}{2m}\right)\delta_{vv'} + \frac{1}{m_0}\mathbf{k}\cdot\pi_{vv'}\right],\end{aligned} \tag{2.14}$$

with ϵ_{v0} the energy offset of the band at $\mathbf{k} = 0$

$$\left[\frac{(-i\nabla)^2}{2m} + U + \frac{1}{4m_0}\nabla U \times (-i\nabla) \cdot \sigma\right] |u_{v0}\rangle = \epsilon_{v0}|u_{v0}\rangle, \tag{2.15}$$

and

$$\begin{aligned}\pi_{vv'} &= \langle u_{v0}|(-i\nabla) + \frac{1}{4m_0}\sigma \times \nabla U|u_{v'0}\rangle \\ &\approx \langle u_{v0}|(-i\nabla)|u_{v'0}\rangle.\end{aligned} \tag{2.16}$$

One should notice that the $\mathbf{p} = -i\nabla$ represents the atomic momentum associated with the rapid oscillations of the lattice function u_{v0}, whereas the $\mathbf{k}$ represents the slow crystal momentum at the bottom of band. Therefore, we can neglect the spin-orbit term in Eq. (2.16) and clearly the spin-orbit term only appears in diagonal terms ϵ_{v0}. For a real treatment, the expansion of Eq. (2.13) must be truncated at the bands close to the gap. In this way, we will use the so-called 8×8 Kane model based on the two spin degenerate s-wave conduction and six p-wave valence band (shown schematically in Fig. 2.1).

[1] However, it is straightforward to evaluate $u_{v\mathbf{k}}(\mathbf{r})$ to any other points with $\mathbf{k} \neq 0$. For more details see [106].

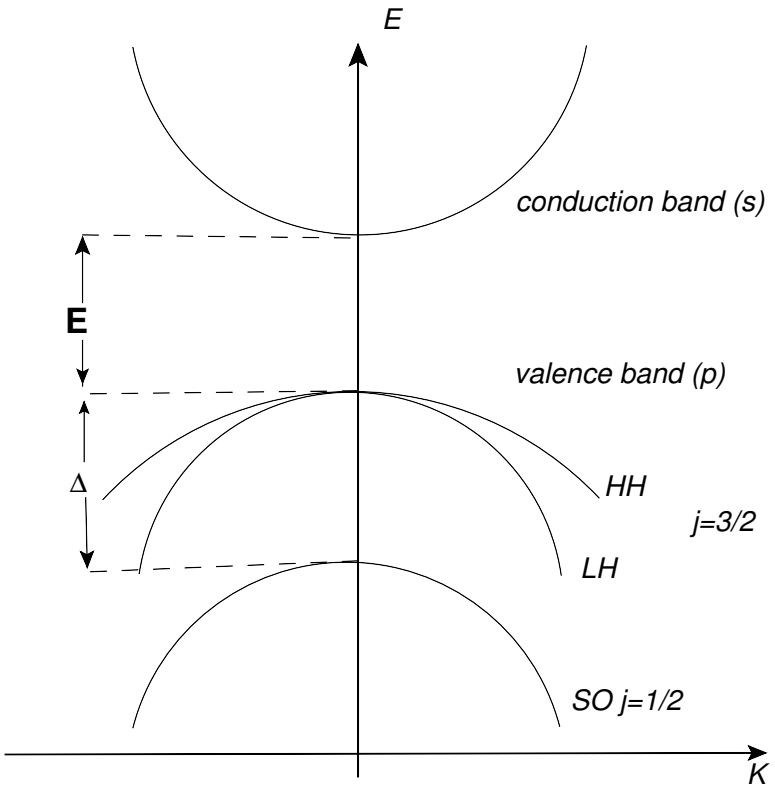

Figure 2.1: Schematic of the band structure of a bulk semiconductor close to the Γ-point for 8×8 Kane model. The s-type conduction-band states separated by a direct band gap E_0 from the p-type valence band states. When SOC is present, the six p-like valence levels split into the light hole band (LH, $J = \pm 1/2$) and heavy hole band (HH,$J = \pm 3/2$) at the Γ point, and both are separated in energy by the so-called spin-orbit gap Δ_0 from the split-off band (SO, $J = 1/2$) [106].

In the presence of the SOC, the six p-like bands partially split into two groups: the fourfold degenerate levels, the light and heavy hole bands (with $J = 3/2$), and another one known as split-off levels (with $J = 1/2$). Obviously the extended model to 14×14 Kane model provides the more accurate description of band structure. Nevertheless, the 8×8 Kane Hamiltonian provides a quite good description of SOC in solid state systems and is more convenient. The envelope function approximation allows one to describe the electron and hole state in the presence of perturbing potentials V–i.e. anything other than the crystal potential U. Let us consider the Hamiltonian as

$$(H_0 + V)\,\psi = \epsilon\psi \tag{2.17}$$

where V varies slowly as compared to U. Similarly to the derivation of the $k \cdot p$ approach, we can expand the wave function in terms of band-edge Bloch functions $|u_{v0}\rangle$ as follows

$$|\psi\rangle = \sum_v \phi_v(\mathbf{r})|u_{v0}\rangle \tag{2.18}$$

where $\phi_v(\mathbf{r})$ contains all information about low energy phenomena introduced by V, but its scale is much bigger than the lattice potential. Then the equation of motion can be written as

$$H_{vv'}\phi_{v'}(\mathbf{r}) = \epsilon\phi_v(\mathbf{r}) \tag{2.19}$$

The envelope function approximation allows one to describe the systems in the more general case of an applied electromagnetic field and to take the total non-crystal potential V, which can be caused by impurities, confinement, strains, and more importantly, the driving electric field. By analogy with Eq. (2.14), the matrix element $H_{vv'}$ is

$$\begin{aligned} H_{vv'} &= \langle u_{v0}|H_0|u_{v'0}\rangle \\ &= \left[\left(\epsilon_{v0} + \frac{(-i\nabla + e\mathbf{A})^2}{2m} + V\right)\delta_{vv'} + \frac{1}{m_0}(-i\nabla + e\mathbf{A})\cdot\mathbf{\Pi_{vv'}}\right] \end{aligned} \tag{2.20}$$

We remark that, the offset energies ϵ_{v0} are not modified because of the factorization Eq. (2.18) in terms of the band edge. The final step is to obtain a lower-dimensional effective Hamiltonian for describing the motion of electrons in the conduction band. The Hamiltonian obtained in Eq. (2.20) can be block-diagonalized by using the Löwdin technique. Thus, the 8×8 Kane Hamiltonian can be written in the matrix notation as [2]

$$H\begin{pmatrix}\phi_c\\ \phi_v\end{pmatrix} = \begin{pmatrix} H_{c,2\times 2} & H_{cv,2\times 6}\\ H^{\dagger}_{cv,6\times 2} & H_{v,6\times 6}\end{pmatrix}\begin{pmatrix}\phi_c\\ \phi_v\end{pmatrix} = \epsilon\begin{pmatrix}\phi_c\\ \phi_v\end{pmatrix} \tag{2.21}$$

where ϕ_c and ϕ_c are a two-dimensional and a six-dimensional spinor for conduction and valence band states, respectively. Under the assumption that the energy gap, E_g, between the two groups of states is the biggest energy scale, and they are weakly coupled to each other– i.e. H_{cv}, $H^{\dagger}_{cv} << H_v \sim E_g$. This assumption allows one to write Eq. (2.21) in terms of a 2×2 equation for the electrons of the conduction band

$$H(\epsilon)\overline{\phi} = \epsilon\overline{\phi} \tag{2.22}$$

where

$$H(\epsilon) = H_c + H_{cv}(\epsilon - H_v)^{-1}H^{\dagger}_{cv} \tag{2.23}$$

with $\overline{\phi}$ a renormalized condition band spinor. According to this way, when the Hamiltonian in Eq. (2.23) is expanded for energies close to the minimum band and then inserted back into the Schrödinger equation (2.22), the effective eigenvalue equation for $\overline{\phi}$ is obtained. This leads us to write the eigenvalue equation in the presence of perturbed potentials V and an external electromagnetic field as

$$\left(\frac{(-i\nabla + e\mathbf{A})^2}{2m^{\star}} + V - \frac{g^{\star}\mu_B}{2}\sigma\cdot\mathbf{B} + \frac{\lambda^2}{4}\nabla V\times[(-i\nabla) + e\mathbf{A}]\cdot\sigma\right)\overline{\phi} = \epsilon\overline{\phi} \tag{2.24}$$

with μ_B the Bohr magnetic field and $\mathbf{B} = \nabla\times\mathbf{A}$ the external magnetic field. One should notice that all effects of coupling with the valence band are included into a renormalization of the effective mass $m^{\star}$, the effective Compton wavelength λ and the g-factor $g^{\star}$. The explicit expression of each quantity is presented in terms of the matrix elements of the Hamiltonian and its derivations are given in Appendix A. The new quantity λ is one of fundamental importance for our purpose. In solid systems, its values can be much bigger than the vacuum constant λ_0, and in some cases like GaAs, it can be as much as six orders of magnitude larger than λ_0. For more clarity, here we show the value of this new parameter

$$\frac{\lambda^2}{4} \simeq \left(\frac{1}{E_g^2} - \frac{1}{(E_g+\Delta)^2}\right) \tag{2.25}$$

[2] For details regarding the structure of each matrix see Appendix A.

where Δ is the spin-orbit splitting between the HH and LH valence bands. This simple Eq. (2.25), together with Eq. (2.24), shows how the SOC can appear in conduction band as soon as this is subject to a non-crystal potentials V. We will classify the SOC as extrinsic and intrinsic mechanisms depending on the origin of the potential V. The extrinsic SOC arises due to the impurity potential, whereas the intrinsic one can be arise due to the confinement potential associated with device structure and/or to the crystalline potential of the host materials. We will talk about both the intrinsic and extrinsic mechanisms.The Hamiltonian derived in Eq. (2.24) can be rewritten as follows

$$H = \frac{k^2}{2m} + V - \mathbf{b}(\mathbf{k}) \cdot \sigma \tag{2.26}$$

where

$$b(\mathbf{k}) \to b_{ext} + b(\mathbf{k}) \tag{2.27}$$

with $k = -i\nabla + e\mathbf{A}$, and $\mathbf{b}(\mathbf{k})$ contains the information about the external magnetic field b_{ext} and k-dependent effective magnetic field $b(\mathbf{k})$. It is important to remark that the 8×8 Kane model describes quite well the conduction band in semiconductors, as GaAs, InSb, GaSb, which have a zinc blend lattice. In some materials like Platinum, where the symmetries of the crystal are different, we must change the Hamiltonian. The material with a crystal structure like the ones presented here (8×8 Kane model) has no inversion symmetry. There is a general argument connecting the spin degeneracy and inversion symmetry in space and time. Both symmetry operations change the wave vector $\mathbf{k}$ to $-\mathbf{k}$, where the time inversion also flips the spin according to Kramers theorem. Hence, the combination of symmetry operations shows a twofold degeneracy of the single-particle energies, $E_{\pm}(\mathbf{k}) = E_{\mp}(\mathbf{k})$, $\pm \leftrightarrow$ spin up/down, i.e.,

$$E_{\pm}(\mathbf{k}) \xrightarrow{\mathcal{T}} E_{\mp}(-\mathbf{k}) \xrightarrow{\mathcal{S}} E_{\mp}(\mathbf{k}) \Rightarrow E_{\pm}(\mathbf{k}) = E_{\mp}(\mathbf{k}) \tag{2.28}$$

where $\mathcal{T}$ and $\mathcal{S}$ are time and space reversal transformations. Thus, when the potential through which the electrons move is inversion asymmetric, the spin degeneracy of the spin state is removed even in the absence of external magnetic fields. In quasi-2D QWs and heterostructures, this spin splitting can be consequences of a SIA of the confinement potential [13] or/and of a BIA of the underlying crystal (e.g. a zinc blende structure [19]). In the case of 2DEG, the potential V given in Eq. (2.26) can be characterized by an asymmetric confinement potential $V(z)$. To lower the order in $\mathbf{k}$, the SIA spin splitting in the conduction band is given by the Rashba SOC term

$$b(\mathbf{k}) \cdot \sigma \to b_R(\mathbf{k}) \cdot \sigma = \alpha(k_x \sigma^y - k_y \sigma^x) \tag{2.29}$$

where $\mathbf{p} = (p_x, p_y) = p(cos\phi, sin\phi)$ is the vector of the components of the momentum operator, and α is the relative strength of the Rashba spin splitting. In principle, α is a function of $V(z)$ and can be tunable via the gates. In the absence of disorder and any external electromagnetic fields, $b_{ext} = 0$, the Rashba Hamiltonian reads

$$H_R = \frac{k^2}{2m^\star} - b_R(\mathbf{k}) \cdot \sigma \tag{2.30}$$

In a 2DEG, the solution of time-independent Schrödinger equation leads to

$$\psi_{\pm\mathbf{k}}(\mathbf{r}) = \frac{e^{i\mathbf{k}\cdot\mathbf{r}}}{\sqrt{2A}} \begin{pmatrix} 1 \\ \pm i e^{i\theta_{\mathbf{k}}} \end{pmatrix} \tag{2.31}$$

with the dispersion energy

$$E_{\pm}(\mathbf{p}) = \frac{p^2}{2m} \pm \alpha p \tag{2.32}$$

where $\theta_{\mathbf{k}}$ is the angle between k and the x-axis, and A is the area of the two-dimensional quantum well. Nevertheless, the schematic of the spin splitting is illustrated in Fig. 2.2, where the spins are oriented perpendicular to the corresponding wavevector $\mathbf{k}$. It is important to remember that an additional mechanism which arises from BIA is also possible. The BIA-induced spin splitting already occurs in 3D materials without an inversion center. For instance, let us consider with more precision, the 12×12 Kane model for the zinc-blend crystal. Here the Dresselhaus term is obtained by an expansion in a power series of $\mathbf{k}$ in the conduction band [20, 58]

$$\mathbf{b}_D^{(3D)} \cdot \sigma \to \mathcal{C}\left[(k_y^2 - k_z^2)\sigma_x k_x + (k_z^2 - k_x^2)\sigma_y k_y + (k_x^2 - k_y^2)\sigma_z k_z\right] \tag{2.33}$$

where $\mathcal{C}$ is a crystal dependent potential and $3D$ stands for three dimensional. For a quasi-2D system, both the k-linear and k-cubic terms in the Hamiltonian are allowed. At low electron energies, the k-cubic may be neglected compared with linear terms, whereas at higher wavevector corresponding to, for instance, large momentum concentration or high temperature, the k-cubic one should be considered as well. In the case of QWs grown in the crystallographic direction (001), the k-linear terms are regarded first. The transition from H_D^{3D} to H_D^{2D} is possible by the replacement of k_z and k_z^2 by their average values $\langle k_z \rangle = 0$ and $\langle k_z^2 \rangle \approx (\pi/d)^2$, d being the width of wall. Hence, the k-linear Dresselhaus SOC reads

$$H_D = \mathbf{b}_D^{lin} \cdot \sigma = \beta_1(-\sigma_x k_x + \sigma_y k_y) \tag{2.34}$$

with $\beta_1 \approx \mathcal{C}(\pi/d)^2$ is used to give its relative strength. Fig. 2.2 shows the distribution of spin orientations for the 2D Fermi energy for different strengths of the k-linear BIA and SIA terms. Now the remaining terms of Eq. (2.33) lead to the $\mathbf{k}$-cubic Dresselhaus terms [39]

$$H_D^{cub} = \mathbf{b}^{cub}(\mathbf{k}) \cdot \sigma = \beta_3(\sigma_x k_x k_y^2 - \sigma_y k_y k_x^2). \tag{2.35}$$

Now we are able to write the complete Dresselhaus contribution to $b_D(\mathbf{k})$ as [107]

$$H_D = b_D(\mathbf{k}) \cdot \sigma = (-\beta_1 cos\phi - \beta_3 cos3\phi)\sigma_x + (\beta_1 sin\phi - \beta_3 sin3\phi)\sigma_y \tag{2.36}$$

with

$$\beta_1 = \mathcal{C}k(\langle k_z^2 \rangle - \frac{1}{4}k^2), \qquad \beta_3 = \mathcal{C}\frac{k^3}{2} \tag{2.37}$$

Here $k^2 = k_x^2 + k_y^2$, and $tan\phi = k_y/k_x$. It is worthwhile to remark that, in the second case of SOC, the BIA is essentially a fixed property of a given sample depending on the material density and geometry of the system. On other hand, in the Rashba model, the SIA can be changed, for example by an external gate [12], applied along the growth direction. Fig. 2.2 shows an overview of different band structures in the case of just a $\mathbf{k}$-linear SOC. The upper panel shows the band structure with (a) only one type of SIA or BIA, and with (b) both types at equal strength values. If the two strength values of BIA and SIA are close to each other, the 2D band structure consists of two paraboloids of revolution, as shown in Fig. 2.2, symmetrically shifted in opposite direction with respect to $\mathbf{k} = 0$ [82]. We assumed the

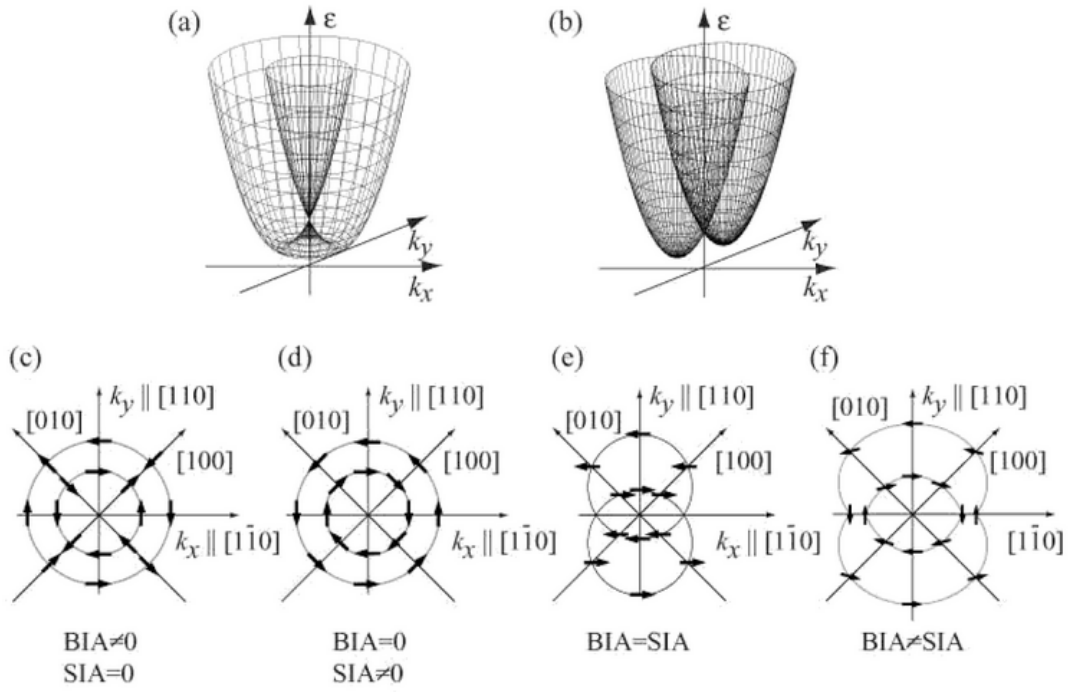

Figure 2.2: Schematic 2D band structure with **k**-linear terms. The energy is plotted as a function of $\mathbf{k} = (k_x, k_y)$ in (a) with only one type of BIA or SIA, and in (b) with equal strength values of the BIA and SIA. The bottom panels represent the distribution of spin orientation in the xy-plane Fermi energy for the different values of the BIA and SIA terms. Taken from [82].

positive coefficients as $\alpha, \beta > 0$. The bottom panel shows the distribution function for the most common communication with BIA and SIA.

As we have seen in Eq. (2.10) for the Dirac equation, the SOC appears as the gradient expansion of the potential. This potential can arise from any type of inversion asymmetry, SIA and BIA, and also of impurity potential, i.e. $\nabla U(\mathbf{r}) \rightarrow \nabla V(\mathbf{r})$. This leads us to write the Hamiltonian in the absence of intrinsic terms

$$H_{imp} = \frac{p^2}{2m} - \frac{\lambda^2}{4}\sigma \times \nabla V(\mathbf{r}) \cdot \mathbf{k} + V(\mathbf{r}) \tag{2.38}$$

where the second term represents the extrinsic SOC with λ the effective spin-orbit wavelength (shown in Eq. (2.25)). This new term affects the spin splitting through different mechanisms, such as EY spin relaxation, side-jump and skew-scattering, which we will explain in more detail in the following Chapters.

Chapter 3

Enter the formalism

Let us consider a generic system whose dynamics are controlled by a given Hamiltonian. We are interested in studying what happens when we modify the Hamiltonian by adding a coupling with an external field. As its title suggests, this chapter will provide the technical details. The main objects of the discussion are the SU(2) gauge-field formalism and the diagrammatic Kubo formula of non-equilibrium problems. We will recall the SU(2) approach for the intrinsic SOC to obtain the SU(2) Boltzmann equation. Here we limit ourselves to recalling the key aspects of the approach to make this presentation self-contained. After that we recall the impurities technique for disordered electron systems. Then we will evaluate both spin and charge currents in a 2DEG with Rashba-Dresselhaus SOC using the SU(2) techniques.

If the system is perturbed ever so slightly, the response function will be linear with respect to the perturbation. Although this system is in a non-equilibrium regime, all the properties of system characterizing its response can be inferred from its equilibrium state. This regime is known as the linear response regime. Hence, the next step is to develop a general scheme of the linear response Kubo formula to an external perturbation. Then we will derive the Kubo formula for a specific case of the transport phenomena. At the end, the most important spin relaxation mechanisms are introduced in the different regimes.

For this purpose, we consider various sections and refer the interested reader to the fairly rich literature [16, 18, 69, 70, 76, 77, 86, 89]. The basic background of interest to all readers is found in Ref. [18, 77]. For a recent pedagogical introduction, see Ref. [71].

3.1 Green functions and the quasiclassical approximation

In the method of quantum field theory, the Green functions or the propagator, is one of the most useful analytical tools, which plays a fundamental role in the treatments of many particle assemblies. It appears also in the theory of differential equations. This function is defined by

$$G_{\sigma\sigma'}(x_1, x_2) = -i\langle T_t \psi_\sigma(x_1)\psi^\dagger_{\sigma'}(x_2)\rangle, \tag{3.1}$$

where T_t is the time-ordering operator defined on a time contour c_K, as depicted in Fig. 3.1. For brevity,

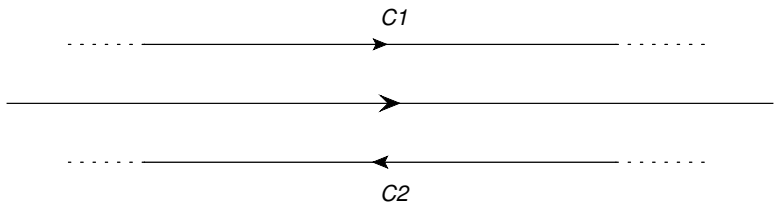

Figure 3.1: The representation of the Keldysh contour c_K in the complex plane of variable t [77].

we used $\psi_\sigma(x_1) = \psi_\sigma(\mathbf{r}_1, t_1)$ and $\psi_\sigma(x_2) = \psi_\sigma(\mathbf{r}_2, t_2)$, where ψ_σ is the Heisenberg field operator with the spin indices σ. The Schwinger's closed time path c_K, also called the Schwinger–Keldysh or real-time contour [77], starts at time $t = -\infty$ and proceeds to time $t = \infty$, and then back again to point $t = \infty$, as illustrated in Fig. 3.1. Now we are able to describe the time-ordered Green functions in the Keldysh space. In the Green function (3.1) the time t_1 and t_2 belong to one of the two parts of a contour c_k (upper and lower). For instance, if the both t_1 and t_2 belongs to the upper part, Eq. (3.1) defines the time-ordered G_{11}. Similarly when both t_1 and t_2 belong to the lower part, Eq. (3.1) defines the anti-time-ordered G_{22}. The G_{12} and G_{21} correspond to the situation when the two times belong to the different parts. Hence, the contour-ordered Green function in Eq. (3.1) is mapped onto a 2×2 matrix structure in the Keldysh space

$$\hat{G} = \begin{pmatrix} \hat{G}_{11} & \hat{G}_{12} \\ \hat{G}_{21} & \hat{G}_{22} \end{pmatrix}. \tag{3.2}$$

We then define the generalized Green functions as

$$\hat{G}_{11} = -i\{\theta(t_1 - t_2)\langle\psi(x_1)\psi^\star(x_2)\rangle - \theta(t_2 - t_1)\langle\psi^\star(x_2)\psi(x_1)\rangle\} \tag{3.3}$$

$$\hat{G}_{12} = i\langle\psi^\star(x_2)\psi(x_1)\rangle \tag{3.4}$$

$$\hat{G}_{21} = -i\langle\psi(x_1)\psi^\dagger(x_2)\rangle \tag{3.5}$$

$$\hat{G}_{22} = -i\{\theta(t_2 - t_1)\langle\psi(x_1)\psi^\star(x_2)\rangle - \theta(t_1 - t_2)\langle\psi^\star(x_2)\psi(x_1)\rangle\}. \tag{3.6}$$

The various Green functions differ in the way the field operators are ordered since the field operators have non-trivial commutation. A convenient way to simplify Eq. (3.2) was introduced by Larkin and Ovchinnikov [50]

$$\check{G} \to \frac{1}{\sqrt{2}}[\hat{\sigma}_0 - i\hat{\sigma}_2]\hat{\sigma}_3\hat{G}\frac{1}{\sqrt{2}}[\hat{\sigma}_0 + i\hat{\sigma}_2]. \tag{3.7}$$

According to this matrix rotation, we get

$$\check{G} = \frac{1}{2}\begin{pmatrix} G_{11} - G_{12} + G_{21} - G_{22} & G_{11} + G_{12} + G_{21} + G_{22} \\ G_{11} - G_{12} - G_{21} + G_{22} & G_{11} + G_{12}G_{21} - \hat{G}_{22} \end{pmatrix}. \tag{3.8}$$

One should notice that the Green functions defined in Eqs. (3.3-3.6) are not all independent and can easily show that there exists the relation

$$G_{11} + G_{22} = G_{12} - G_{21}. \tag{3.9}$$

As a result, there exists three independent Green functions as [78]

$$\check{G} = \begin{pmatrix} G_{11} - G_{12} & G_{12} + G_{21} \\ 0 & G_{11} - G_{21} \end{pmatrix} = \begin{pmatrix} G^R & G^K \\ 0 & G^A \end{pmatrix}, \tag{3.10}$$

where the retarded G^R, Keldysh G^K and advanced G^A components [77] are defined by

$$G^R(1,2) = -i\theta(t_1 - t_2)\langle\{\psi(x_1), \psi^\star(x_2)\}\rangle \tag{3.11}$$

$$G^A(1,2) = i\theta(t_2 - t_1)\langle\{\psi(x_1), \psi^\star(x_2)\}\rangle \tag{3.12}$$

$$G^K(1,2) = i\langle[\psi(x_1), \psi^\star(x_2)]\rangle. \tag{3.13}$$

One sees that the retarded and advanced Green functions are complex conjugates of each other. To grasp the physical meaning of each component of the Green functions, let us consider the simple case of the Fermi gas. In this case, the field operator is

$$\psi_\sigma(x) = \frac{1}{\sqrt{V}} \sum_{\mathbf{k}} e^{i\mathbf{k}\cdot\mathbf{r}} e^{-i\epsilon(\mathbf{k})t} c_{\mathbf{k}\sigma}, \tag{3.14}$$

where $c_{\mathbf{k}\sigma}$ and $c^\star_{\mathbf{k}\sigma}$ represent the creation and annihilation operators with the spin indices σ. Let us start with the anticommutator on the right hand side of G^R and G^A components

$$\begin{aligned} \langle\{\psi(x_1), \psi^\star(x_2)\}\rangle &= \frac{1}{V} \sum_{\mathbf{k}_1\mathbf{k}_2} e^{i\mathbf{k}_1\cdot\mathbf{r}_1 - i\mathbf{k}_2\cdot\mathbf{r}_2} e^{-i\epsilon(\mathbf{k}_1)t_1 - i\epsilon(\mathbf{k}_2)t_2} \langle\{c_{\mathbf{k}_1\sigma_1}, c^\star_{\mathbf{k}_2\sigma_2}\}\rangle \\ &= \frac{1}{V} \sum_{\mathbf{k}\sigma} e^{i\mathbf{k}\cdot(\mathbf{r}_1 - \mathbf{r}_2)} e^{-i\epsilon(\mathbf{k})(t_1 - t_2)}, \end{aligned} \tag{3.15}$$

where the anticommutation relation of $c_{\mathbf{k}\sigma}$ has been used. Since the systems are translationally invariant, we recall the Fourier transform with respect to the space $\mathbf{r}_1 - \mathbf{r}_2$ and time $t_1 - t_2$

$$G(\mathbf{r}_1 - \mathbf{r}_2, t_1 - t_2) = \frac{1}{V} \sum_{\mathbf{k}} e^{i\mathbf{k}.(\mathbf{r}_1 - \mathbf{r}_2)} \int_{-\infty}^{\infty} \frac{d\omega}{2\pi} e^{-i\omega(t_1 - t_2)} G(\mathbf{k}, \omega), \quad \frac{1}{V}\sum_k \equiv \int \frac{d\mathbf{k}}{(2\pi\hbar)^d} \tag{3.16}$$

with d as the dimensionality of the space where the particles move. In the limit of infinite volume, the sum over the momentum reduces to an integral over the momentum. The Green functions of the non-interacting Fermi gas are easily found by inserting Eq. (3.16) inside Eq. (3.11)

$$G^{R/A}(\mathbf{k}, \omega) = \frac{1}{\hbar\omega - \epsilon(\mathbf{k}) \pm i0^+}, \tag{3.17}$$

where $\epsilon(k) = (k^2/2m) - \mu$, with the chemical potential μ and the Fermi momentum p_F. The antitrasform of Eq. (3.16) possesses a problem due to the pole at $\omega = \epsilon(\mathbf{k})/\hbar$. To make the integral over time, one has to regularize the pole in the lower (or upper) of the complex plane for $t > 0$ (or $t < 0$). In principle, if the pole is in the lower (upper) plane, the integral differs from zero only when $t > 0$ (or $t < 0$). Hence, the regularization of the integrals corresponds to choosing a solution defined for ω. The superscript R (or D) stands for "retarded" (or "advanced") when the contour is in the lower (or upper) complex plane for $\omega > 0$ (or $\omega < 0$). By performing a similar analysis for G^K, we have

$$\langle[\psi(x_1), \psi^\dagger(x_2)]\rangle = \delta_{\sigma_1\sigma_2}\delta_{\mathbf{k}_1\mathbf{k}_2}\left(1 - 2f(\epsilon(\mathbf{k}))\right) \tag{3.18}$$

Hence, the Keldysh Green function under the Fourier transform reads

$$G^K(\mathbf{k},\omega) = \left[G^R(\mathbf{k},\omega) - G^A(\mathbf{k},\omega)\right](1-2f(\epsilon(\mathbf{k}))) \tag{3.19}$$

$$= -2\pi i\delta(\omega-\epsilon(\mathbf{k}))\,(1-2f(\epsilon(\mathbf{k})))\,, \tag{3.20}$$

In general, the G^R and G^A carry information about the spectrum of the excitation, while G^K contains the information of the statistical occupation. The equation of motion for G^k can be thought of as the generalization of the Boltzmann equation. In the next section, we will briefly review the SU(2) approach employed to build the kinetic equation in the presence of the RSOC and DSOC.

3.1.1 Quasiclassical approximation and SU(2) gauge-field approach

The ultimate goal of this section is to see how to compute the weak localization corrections of the disordered Fermi gas in the presence of the Rashba-Dresselhaus SOC. In general, the transport coefficient can classically be derived through the U(1) gauge-invariant kinetic Boltzmann equation. In a disordered system, the semiclassical limit enters in the Boltzmann equation in the two main points, the distribution function and the relaxation mechanism. The physical hypothesis is that there is a hierarchy of time and length scales in the system. In the case of an external field, one assumes that the mean free path l is much longer than the Fermi wave length λ_F, the characteristic wave length of quantum particle

$$\lambda_F << l \tag{3.21}$$

The above inequality justifies the description in terms of the Boltzmann equation and also suggests how one can find the correction to that limit. This idea can also be incorporated into the Keldysh formalism in the quasiclassical limit. The first step is to determine the solution of the Dyson equation, i.e. the equation of the motion for the Green functions. We recall the Dyson equation and its complex conjugate in general form

$$\left(\check{G}_0^{-1}(x_1,x_3) - \check{\Sigma}(x_1,x_3)\right)\otimes\check{G}(x_3,x_2) = \delta(x_1-x_2) \tag{3.22}$$

$$\check{G}(x_1,x_3)\otimes\left(\check{G}_0^{-1}(x_3,x_1) - \check{\Sigma}(x_3,x_1)\right) = \delta(x_1-x_2) \tag{3.23}$$

where we have used space-time coordinates $x_1 \equiv (t_1,\mathbf{r}_1)$, etc., and quantities with a "check" $(\check{G}_0^{-1},\check{G},\check{\Sigma})$, which are the matrices in Keldysh space (as shown in Eq. (3.10)). In the above equations, the symbol $\otimes$ implies integration over x_3 and matrix multiplication both in Keldysh and spin spaces,

$$\check{A}(x_1,x_3)\otimes\check{B}(x_3,x_2) \equiv \int dx_3 \begin{pmatrix} A^R & A^K \\ 0 & A^A \end{pmatrix}(x_1,x_3)\begin{pmatrix} B^R & B^K \\ 0 & B^A \end{pmatrix}(x_3,x_2). \tag{3.24}$$

The self-energy Σ denotes the effects of the Hamiltonian interaction, which can arise from the electron-electron, electron-phonon as well as disorders due to defects or impurities. In the next section, we will introduce the self-energy in disordered systems. Now, in this part, we briefly review the SU(2) approach employed to build the kinetic equation in the presence of the Rashaba-Dresselhaus SOC, where the k-cubic terms are neglected compared to the k-linear SOC contributions. With the exception of the last chapter, this work will deal with a general Hamiltonian in the presence of the electromagnetic field

$$H = \frac{p^2}{2m} + \alpha(p_y\sigma_x - p_x\sigma_y) + \beta(p_x\sigma_x - p_y\sigma_y) + V(\mathbf{r}) - \frac{\lambda_0^2}{4}\boldsymbol{\sigma}\times\nabla V(\mathbf{r})\cdot\mathbf{p}, \tag{3.25}$$

A convenient way to deal with the RSOC and DSOC of the Hamiltonian of Eq. (3.25) is the SU(2) approach, where the SOC is described in terms of a spin-dependent gauge field [36]. This formalism, introduced in the context of quark-gluon kinetic theory [23, 104], was also recently extended to superconducting structures with SOC [9, 10]. For a recent pedagogical introduction, see Ref. [71]. Here we limit ourselves to recall the key aspects of the approach to make this presentation self-contained. Neglecting for the time being the extrinsic SOC, the RSOC and DSOC of (3.25) can be written in the compact form of a spin-dependent vector potential and the Hamiltonian reads

$$H = \frac{(\mathbf{p} + e\boldsymbol{\mathcal{A}}^a\sigma^a/2)^2}{2m} - \frac{e\Psi^a\sigma^a}{2} + V(\mathbf{r}), \tag{3.26}$$

where V is the impurity potential, and we will describe it later in the next section. The only non-zero components of $\boldsymbol{\mathcal{A}}^a$ are

$$e\mathcal{A}_x^x = 2m\beta,\ e\mathcal{A}_x^y = -2m\alpha,\ e\mathcal{A}_y^x = 2m\alpha,\ e\mathcal{A}_y^y = -2m\beta. \tag{3.27}$$

Relations 3.27 follow by comparing 3.26 with 3.25. In the Hamiltonian we have also included a Zeeman term

$$H_Z = -\frac{\Delta^a\sigma^a}{2} \equiv -\frac{e\Psi^a\sigma^a}{2}, \tag{3.28}$$

which can be seen as a spin-dependent scalar potential. In the above $\Delta = g_L\mu_B B_{exter}$, g_L is the gyromagnetic factor, μ_B the Bohr magneton and B_{exter} the external magnetic field. In this way the theory can be written in terms of a SU(2) gauge theory of electrons coupled to a d-potential gauge field $(\Psi, \boldsymbol{\mathcal{A}})$, where each component of the d-vector is expanded in Pauli matrices. Notice that in this description the standard scalar and vector potentials can be included as the identiy σ^0 components. For the sake of generality, we formulate the theory in d dimensions. Whereas our first motivation is the description of the spin dynamics in a 2DEG, our conclusions apply also to the three-dimensional electron gas. This is specially relevant in experimental situations where one deals with semiconducting thin films. In the following formula, we make use of the compact (relativistic) space-time notations for the potentials,

$$\mathcal{A}^\mu = (\Psi, \boldsymbol{\mathcal{A}}),\ \mathcal{A}_\mu = (-\Psi, \boldsymbol{\mathcal{A}}), \tag{3.29}$$

the coordinate and momentum,

$$x^\mu = (t, \mathbf{r}),\ x_\mu = (-t, \mathbf{r}),\ p^\mu = (\epsilon, \mathbf{p}),\ p_\mu = (-\epsilon, \mathbf{p}) \tag{3.30}$$

and the corresponding derivatives

$$\partial^\mu \equiv \frac{\partial}{\partial x_\mu},\ \partial_\mu \equiv \frac{\partial}{\partial x^\mu},\ \partial_p^\mu \equiv \frac{\partial}{\partial p_\mu},\ \partial_{p,\mu} \equiv \frac{\partial}{\partial p^\mu}. \tag{3.31}$$

In this way the product $p^\mu x_\mu = -\epsilon t + \mathbf{p}\cdot\mathbf{r}$ has the correct Lorentz metrics. We also introduce mixed Wigner coordinates given by the center-of-mass coordinates $(t, \mathbf{r})$ and energy-momentum variables $(\epsilon, \mathbf{p})$, which are the Fourier-transformed variables of the relative coordinates. According to the analysis of [36], a semiclassical Boltzmann kinetic equation can be derived from a microscopic Keldysh formulation in the presence of non-Abelian gauge fields. The starting point is the subtraction of two Eqs. (3.22) and (3.23)

$$\left[\check{G}_0^{-1}(x_1, x_3)\overset{\otimes}{,}\check{G}(x_3, x_2)\right] = \left[\check{\Sigma}(x_1, x_3)\overset{\otimes}{,}\check{G}(x_3, x_2)\right], \tag{3.32}$$

Furthermore,

$$\check{G}_0^{-1}(x_1, x_3) = (i\partial_{t_1} - H)\,\delta(x_1 - x_3), \tag{3.33}$$

where H is the Hamiltonian operator (3.26). The self-energy $\check{\Sigma}$ appearing in the collision kernel (on the right hand side of (3.32)) will be specified later. The key step, with respect to the standard way of obtaining semiclassical transport theories à la Boltzmann from their microscopic counterparts, is the introduction of a locally covariant Green function $\check{\tilde{G}}(x_1, x_2)$ (to be defined in the following section). To understand how the mechanism works, let us consider the convolution of two quantities

$$(A \otimes B)(x_1, x_2) = \int dx_3 A(x_1, x_3) B(x_3, x_2), \tag{3.34}$$

which can be equivalently expressed in terms of the center-of-mass and relative coordinates

$$\begin{aligned}(A \otimes B)(x_1, x_2) &= \int dx_3 A\left(\frac{x_1 + x_3}{2}, x_1 - x_3\right) B\left(\frac{x_3 + x_2}{2}, x_3 - x_2\right) \\ &= \int dx_3 A\left(\frac{x_1 + x_2 - x_2 + x_3}{2}, x_1 - x_3\right) B\left(\frac{x_1 + x_2 - (x_1 - x_3)}{2}, x_3 - x_2\right),\end{aligned} \tag{3.35}$$

By Taylor expanding A with respect to $x_1 - x_3$ and B with respect to $x_3 - x_2$, and after applying the Fourier transform, we can show

$$A(x,p)B(x,p) + \frac{i}{2}(\partial_\mu A(x,p))(\partial_p^\mu B(x,p)) - \frac{i}{2}(\partial_p^\mu A(x,p))(\partial_\mu B(x,p)). \tag{3.36}$$

Then the left hand side of Dyson equation (3.32) becomes

$$-i[\check{G}_0^{-1}, \check{G}] + \frac{1}{2}\{\partial^\mu \check{G}_0^{-1}, \partial_{p\mu}\check{G}\} + \frac{1}{2}\{\partial_p^\mu \check{G}_0^{-1}, \partial_\mu \check{G}\}. \tag{3.37}$$

From the Wigner transformed covariant Green function $\check{\tilde{G}}(p, x)$ one can define the SU(2) covariant distribution function to obtain the SU(2) Boltzmann equation. The introduction of the covariant Green function in the presence of non-Abelian gauge fields generalizes the well known shift in the momentum dependence of the Green function when one wants to make it gauge invariant under U(1) gauge transformations [2, 49]. In the SU(2) case, as shown in Ref. [36], such a shift, due to the non commutative nature of the symmetry group, can be carried out in terms of Wilson lines of the gauge field. The Hamiltonian defined in Eq. (3.26) is invariant under a gauge transformation $O(x)$ by defining the local rotation of the spinor field

$$\Psi'(x) = O(x)\Psi(x), \quad \Psi'^\dagger(x) = \Psi(x)^\dagger O(x), \quad O(x)O(x)^\dagger = 1. \tag{3.38}$$

The Green function, however, is not locally covariant. The reason is that its transformation depends on two distinct space-time points

$$\check{G}(x_1, x_2) \to O(x_1)\check{G}(x_1, x_2)O(x_2) \tag{3.39}$$

Now it is useful to define the *locally* covariant Green function as

$$\check{\tilde{G}}(x_1, x_2) = U_\Gamma(x, x_1)\check{G}(x_1, x_2)U_\Gamma(x_2, x) \tag{3.40}$$

where

$$U_\Gamma(x, x_1) = \mathcal{P} \exp\left(-i \int_{x_1}^{x} eA^\mu(y) \mathrm{d}y_\mu\right). \tag{3.41}$$

The line integral of the gauge field is referred to as the Wilson line. In Eq. (3.41) $\mathcal{P}$ is a path-ordering operator. Since the Wilson line transforms covariantly under a gauge transformation $O(x)$

$$U_\Gamma(x,x_1) \to O(x)U_\Gamma(x,x_1)O^\dagger(x_1), \tag{3.42}$$

the covariant Green function $\check{\tilde{G}}$ transforms in a locally covariant way

$$\check{\tilde{G}}(x_1,x_2) \to O(x)\check{\tilde{G}}(x_1,x_2)O^\dagger(x). \tag{3.43}$$

To the lowest order in the gauge field, one may expand the exponential of the Wilson line. Then by taking the Fourier transform with respect to the relative coordinate, one obtains

$$\tilde{\Phi}(p,x) = \Phi(p,x) - \frac{1}{2}\left\{e\mathcal{A}^\mu, \partial_{\mu,p}\Phi(p,x)\right\}, \tag{3.44}$$

where $\Phi(p,x)$ is any quantity in the Wigner representation to which the shift can be applied. The inverse transformation reads

$$\Phi(p,x) = \tilde{\Phi}(p,x) + \frac{1}{2}\left\{e\mathcal{A}^\mu, \partial_{\mu,p}\tilde{\Phi}(p,x)\right\}. \tag{3.45}$$

For our purposes, we assumed that the energy scale of the perturbation is small compared to the Fermi energy, then we can perform the shift to lowest order in the gauge field. In the spirit of the gradient expansion, we assumed $\partial^\mu\partial_{\mu,p} \ll 1$ and $eA^\mu\partial_{\mu,p} \ll 1$, and will do so throughout this work. In order to obtain the SU(2) Boltzmann equation from the quantum kinetic equation we will apply the transformation (3.44) to the Eq. (3.32) and to the matrix Keldysh Green function obtained in Eq. (3.10)

$$\check{G} = \begin{pmatrix} G^R & G^K \\ 0 & G^A \end{pmatrix} \to \check{\tilde{G}} = \begin{pmatrix} \tilde{G}^R & \tilde{G}^K \\ 0 & \tilde{G}^A \end{pmatrix}, \tag{3.46}$$

where as a result we get

$$\tilde{G}^R - \tilde{G}^A = -2\pi i\delta(\epsilon - \epsilon_{\mathbf{p}}), \tag{3.47}$$

$$\tilde{G}^K = -2\pi i\delta(\epsilon - \epsilon_{\mathbf{p}})\left[1 - 2f(\mathbf{p},x)\right], \tag{3.48}$$

where $\epsilon_{\mathbf{p}} = p^2/2m - \mu$ measures the energy with respect to the chemical potential μ. Notice that the SU(2)-shifted spectral density ($\sim \tilde{G}^R - \tilde{G}^A$) has no spin structure: the latter is all in the distribution function $f(\mathbf{p},x)$. The fact is that the locally-covariant $\tilde{G}^{R,A}$ does not depend on the gauge fields, which is the great advantage of the approach that will appear later. Finally, the equation for $\check{\tilde{G}}$ reads

$$V^\mu\left[\tilde{\partial}_\mu\check{\tilde{G}} + \frac{1}{2}\left\{e\mathcal{F}_{\mu\nu}, \partial_p^\nu\check{\tilde{G}}\right\}\right] = \check{\tilde{I}}_K, \tag{3.49}$$

where $V^\mu = (1, \mathbf{p}/m)$ is the d-current operator and we have introduced the covariant derivative

$$\tilde{\partial}_\mu\check{\tilde{G}} = \partial_\mu\check{\tilde{G}} + i\left[e\mathcal{A}_\mu, \check{\tilde{G}}\right] \tag{3.50}$$

and the field strength

$$\mathcal{F}_{\mu\nu} = \partial_\mu\mathcal{A}_\nu - \partial_\nu\mathcal{A}_\mu + ie\left[\mathcal{A}_\mu, \mathcal{A}_\nu\right]. \tag{3.51}$$

An intuitive way to understand Eq. (3.49) is by noticing that the combination $V^\mu\partial_\mu$ is the ordinary hydrodynamical derivative entering the Boltzmann equation, $\partial_t + \mathbf{v}\cdot\nabla_{\mathbf{r}}$, written in the compact d-vector

notation. Furthermore, in the case of the Abelian U(1) electromagnetic gauge field, the combination $V^{\mu}F_{\mu\nu}\partial_p^{\nu}$ yields the familiar Lorentz force. Eq. (3.49) representing its extension to the SU(2) scenario. In the next section, the right hand side of Eq. (3.49) will be followed by applying the covariant transformation to the Keldysh collision kernel, $I_K = -i\left[\Sigma, G\right]^K$ and taking advantage of the unitarity of the Wilson line. Let us set it to zero and we will go back to it in the next section. By taking the Keldysh component of (3.49) and separating time and space components we get

$$\left(\tilde{\partial}_t + \frac{\mathbf{p}}{m}\cdot\tilde{\nabla}_{\mathbf{r}}\right) f(\mathbf{p},\mathbf{r},t) - \frac{1}{2}\Big\{\mathbf{F}\cdot\nabla_{\mathbf{p}}, f(\mathbf{p},\mathbf{r},t)\Big\} = 0 \tag{3.52}$$

where $\mathbf{F}$ is the spin-dependent force due to the SU(2) gauge fields

$$F_i = e\mathcal{F}_{0i} + e\frac{p_k}{m}\mathcal{F}_{ki} = e\mathcal{E}_i + e\epsilon_{ikj}\frac{p_k}{m}\mathcal{B}_j. \tag{3.53}$$

Here $\mathcal{E}_i = \mathcal{F}_{0i}$ and $\mathcal{B}_i = \frac{1}{2}\epsilon_{ijk}\mathcal{F}_{jk}$ are the SU(2) electric and magnetic fields, respectively. Hence, we have obtained a generalization Boltzmann equation in terms of the space-time covariant derivatives. The density and current might be introduced by integrating over the momentum

$$\rho(\mathbf{p},t) = \sum_{\mathbf{p}} f(\mathbf{p},\mathbf{r},t), \qquad \mathbf{J}(\mathbf{r},t) = \sum_{\mathbf{p}} \frac{\mathbf{p}}{m} f(\mathbf{p},\mathbf{r},t). \tag{3.54}$$

Hence the integration over momentum in Eq. (3.52) leads to the continuity equation with the covariant derivatives as

$$\tilde{\partial}_t \rho(\mathbf{r},t) + \tilde{\nabla}_{\mathbf{r}}\cdot\mathbf{J}(\mathbf{r},t) = 0. \tag{3.55}$$

We will use the above equation later, where the Bloch equations governing the spin dynamics are evaluated in terms of SU(2) approach. Now, in the next section, we will recall the impurities technique for disordered electron gas. For this purpose, we will derive first the dressed Green function by impurities, and then the Boltzmann collision integral in the Born approximation. At the end, we will derive the explicit expressions for the particle and spin currents.

3.2 The standard model of disordered systems

In this section we describe the weak localization corrections of disordered electron systems in quasiclassical treatment of Eq. (3.21). We start with the Dyson equation, which is a summary of the Feynman-Dyson theory in a particularly compact form. In that way, the exact Green function consists of two terms, the unperturbed Green function G_0 and all connected terms with the potential described by the so-called self energy Σ. The corresponding analytical expression of the Dyson equation is given by

$$G_{\alpha\beta}(x_1,x_2) = G^0_{\alpha\beta}(x_1,x_2) + \int dx dx' G^o_{\alpha\Gamma}(x_1,x)\Sigma_{\Gamma\mu}(x,x')G_{\mu\beta}(x',x_2), \tag{3.56}$$

where the Green function G is determined by the self energy Σ, and also Σ determined by G. According to the standard model of disorder potential as illustrated in Fig. 3.2, the impurity potential V is taken as the Gaussian random variable with zero mean and the variance given by

$$\langle V(\mathbf{r})\rangle = 0, \quad \langle V(\mathbf{r})V(\mathbf{r}')\rangle = n_i v_0^2 \delta(\mathbf{r}-\mathbf{r}') \tag{3.57}$$

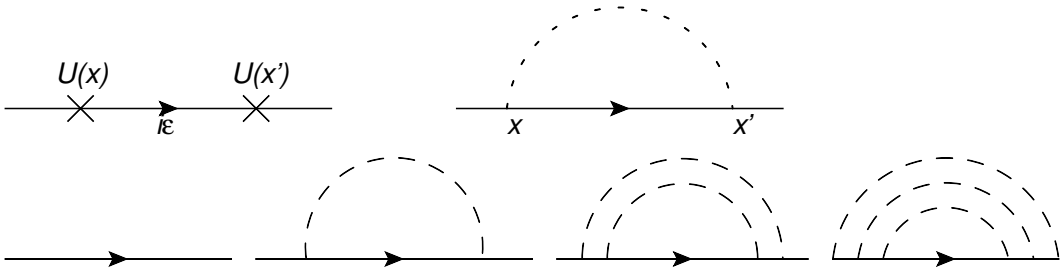

Figure 3.2: Lowest order self-energy in the Born approximation for before (top left) and after (top right) averaging over the impurity distributions. The dashed line denotes the impurity average. The bottom panel is illustrating the sequence of the rainbow diagrams selected by the self-consistent solution for the Green function [18].

where n_i and v_i are the impurity density and scattering amplitude. Since the interaction is invariant under transformation and the system is spatially uniform, we can find an algebraic expression of the Green function in the momentum-energy space

$$G(\mathbf{p},\epsilon) = \frac{1}{\omega - \epsilon(\mathbf{p}) - \mathbf{\Sigma}(\mathbf{p},\omega)}, \tag{3.58}$$

The Green functions, G_o and G, are all diagonal in the matrix indices in the absence of the SOC. The simple model potential given in Eq. (3.57) shows that only an even number of cross insertions are different from zero. Hence, the lowest order impurity-average, the so-called Born approximation represented by Fig. 3.2, plays an important role in the effective self-energy in the impurity technique. Let us consider the retarded self-energy shown in Fig. 3.2

$$\Sigma_1^R(\mathbf{p},\omega) = n_i v_0^2 \sum_{\mathbf{p}'} G_0(\mathbf{p}',\omega), \tag{3.59}$$

To evaluate the above equation we have to pass from momentum to energy variable

$$\sum_{\mathbf{p}'}(\cdots) \to N_0 \int_{-\mu}^{\infty} d\epsilon(\mathbf{p}')(\cdots) \to N_0 \int_{-\infty}^{\infty} d\epsilon(\mathbf{p}')(\cdots) \tag{3.60}$$

where N_0 represents the density of states in the absence of perturbation. In the above equation, we assumed that the biggest energy scale is the Fermi energy. In the large values of $\mathbf{p}'$, the real part of the integral divergence over $\mathbf{p}'$, its values do not depend on ω and $\mathbf{p}$. In fact, this is the consequences of the simple model taken from the scattering potential. A more realistic model cures this problem by introducing a cutoff frequency for the scattering process with a large momentum. In the following, we will consider the imaginary part of the self-energy, since the real part has been absorbed in just a shift of the chemical potential. By performing the integral, the imaginary part of the self-energy in the limit of the Born approximation reads

$$\Sigma_1^R(\mathbf{p},\omega) \equiv -\frac{i}{2\tau_0}, \tag{3.61}$$

where $\tau_0 = 2\pi N_0 n_i v_0^2$ represents the elastic quasiparticle relaxation time. To proceed in the perturbative expansion, one should consider the above result into the Green function and compute it again for the

next iteration for Σ_2. This leads to the replacement of the imaginary part of the integral G_0. But as the integral does not depend on its modulus, this yields a self-consistent solution of Dyson equation for the Green function, as illustrated in Fig. 3.2. Hence, we can consider the Σ_1 as a total self-energy Σ. To evaluate the integral over the momentum, we assumed that the variation of the integrand, set up by the position of the pole, is much smaller than the lower limit of the integral $-\mu$. Here we confirm this expression of the small expansion parameter

$$\frac{1}{\tau} << \mu \approx \epsilon_F \to p_F l >> 1, \tag{3.62}$$

where $l = v_F\tau$ is the mean free path. As shown in Eq. (3.58) for the Dyson equation, the disorder-dressed Green functions becomes

$$G^{R/A}(\mathbf{p},\omega) = \frac{1}{\omega - \epsilon(p) \pm i/2\tau_0}. \tag{3.63}$$

However, these results are obtained in the lowest order Born approximation, but we can go beyond that order. At the end of the chapter, we will take care of the side-jump and skew scattering corrections, when the extrinsic SOC is also present. What we have learned up to now is that the disorder effects can be taken into account via the inclusion of the self-energies. Now we will obtain an explicit expression for the collision integral describing the scattering from impurities. We recall the Boltzmann collision integral in Eq. (3.52),

$$I \equiv \int \frac{\mathrm{d}\epsilon}{2\pi i} I_K = -\int \frac{\mathrm{d}\epsilon}{2\pi} \left[\check{\Sigma}, \check{G}_{\mathbf{p}}\right]^K, \tag{3.64}$$

Now we have to transform it to the locally covariant formalism according to the transformation of Eq. (3.44). This procedure is the same with the transformation of the kinetic equation obtained in the previous section. In particular, the covariant transformation of the Keldysh collision integral gives us

$$U_\Gamma(x,x_1)\left[\check{\Sigma}(x_1,x_3)\overset{\otimes}{,}\check{G}(x_3,x_2)\right]U_\Gamma(x_2,x) = \left[\check{\tilde{\Sigma}}(x_1,x_3)\overset{\otimes}{,}\check{\tilde{G}}(x_3,x_2)\right] \tag{3.65}$$

after using the unitarity of the Wilson line by inserting

$$U_\Gamma(x_3,x)U_\Gamma(x,x_3) = 1$$

between the self-energy and the Green function. The locally covariant self-energy according to the shift of Eq. (3.44) and Eq. (3.45) yields

$$\check{\tilde{\Sigma}} = n_i v_0^2 \sum_{\mathbf{p}'} \left(\check{\tilde{G}}_{\mathbf{p}'} + \frac{1}{2}\{\mathbf{A}^\mu(\partial_{\mathbf{p}',\mu} - \partial_{\mathbf{p},\mu}), \check{\tilde{G}}_{\mathbf{p}'}\}\right) = n_i v_0^2 \sum_{\mathbf{p}'} \check{\tilde{G}}_{\mathbf{p}'}, \tag{3.66}$$

where the derivative with respect to ϵ, cancels in the two terms. The derivative with respect to $\mathbf{p}$, vanishes and another one with respect to $\mathbf{p}'$ can be neglected because it is constant after integrating. Hence, the locally covariant self-energy has the same functional form as the original self-energy. The Keldysh component of the collision integral has the form

$$\begin{aligned} \tilde{I}^K &= -i\left[\check{\tilde{\Sigma}}, \check{\tilde{G}}\right]^K \\ &= -in_i v_0^2 \sum_{\mathbf{p}'} \left((\tilde{G}^R_{\mathbf{p}'} - \tilde{G}^A_{\mathbf{p}'})\tilde{G}^K_{\mathbf{p}} - (\tilde{G}^R_{\mathbf{p}} - \tilde{G}^A_{\mathbf{p}})\tilde{G}^K_{\mathbf{p}'}\right) \end{aligned} \tag{3.67}$$

By using Eqs. (3.47-3.48) for the locally covariant Green functions, the Boltzmann collision integral for the impurity scattering process yields

$$I[f] = -2\pi n_i v_0^2 \sum_{\mathbf{p}'} \delta(\epsilon_{\mathbf{p}} - \epsilon_{\mathbf{p}'})(f(\mathbf{p},\mathbf{r},t) - f(\mathbf{p}',\mathbf{r},t)). \tag{3.68}$$

Now we are able to obtain the solution of the Boltzmann Eq. (3.52) in the diffusive approximation. Notice that, by taking integration over the momentum $\mathbf{p}$, the collision integral vanishes and reproduces the continuity equation derived in Eq. (3.55) with the density and current defined in Eq. (3.54). In diffusive approximation, the distribution function can be expanded in the spherical harmonic as

$$f(\mathbf{p},\mathbf{r},t) \equiv \langle f \rangle + 2\hat{\mathbf{p}} \cdot \mathbf{f}, \tag{3.69}$$

where the terms kept up to the order of p-wave symmetry and $\langle \cdots \rangle$ denote the integration over the momentum direction. Hence, the collision integral becomes

$$I(f) = -\frac{1}{\tau} 2\hat{\mathbf{p}} \cdot \mathbf{f}. \tag{3.70}$$

We multiply both side of Eq. (3.52) by $\hat{p} = (cos(\phi), sin(\phi))$, and then take the integration over angle ϕ. We get

$$-\frac{1}{\tau}\mathbf{f} = \frac{p}{2m}\tilde{\nabla}_{\mathbf{r}}\langle f \rangle - \frac{e}{2}\langle\{\hat{p}\mathbf{E}\cdot\nabla_{\mathbf{p}}, \langle f\rangle\}\rangle - \frac{e}{2m}\langle\{\hat{\mathbf{p}}(\mathbf{p}\times\mathbf{B}\cdot\nabla_{\mathbf{p}}), 2\hat{\mathbf{p}}\cdot\mathbf{f}\}\rangle, \tag{3.71}$$

where the $U(1) \times SU(2)$ fields are given by

$$\mathbf{E} = -\partial_t \mathbf{A} - \nabla_{\mathbf{r}}\phi + ie[\phi, \mathbf{A}], \tag{3.72}$$

$$B_i = \frac{1}{2}\epsilon_{ijk}F^{jk}. \tag{3.73}$$

The first term, according to Eq. (3.54) for the current term, is the *diffusive* contribution including the covariant derivative with respect to the SU(2) gauge fields. Under uniform circumstance, this term differs from zero due to the covariant nature of derivatives. The second term is the usual *drift* contribution due to the external electric field, whereas the third one yields a *Hall* contribution. Then we get

$$\mathbf{f} = -\frac{\tau p}{2m}\tilde{\nabla}_{\mathbf{r}}\langle f\rangle + \frac{e\tau}{4}\{\mathbf{E}, \partial_p\langle f\rangle\}\rangle + \frac{e\tau}{2m}\{\mathbf{B}\times, \mathbf{f}\}\rangle \tag{3.74}$$

where the gradient with respect to the momentum is replaced by $\nabla_{\mathbf{p}} = \hat{\mathbf{p}}\partial_p - \hat{\phi}\partial_\phi/p$ with $\hat{\phi} = (-sin\phi, cos\phi)$. As shown in the definitions of density and current in Eq. (3.54), we can write the expression for the number and spin components

$$n = \mathrm{Tr}[\rho], \quad \mathbf{J}^0 = \mathrm{Tr}[\sigma^a\rho] \tag{3.75}$$

$$S^a = \frac{1}{2}\mathrm{Tr}[\sigma^a\rho], \quad \mathbf{J}^a = \frac{1}{2}\mathrm{Tr}[\sigma^a\mathbf{J}]. \tag{3.76}$$

Let us start with the drift term as

$$\mathbf{J}_{drift} = \sum_{\mathbf{p}} \frac{p}{m}\frac{e\tau}{4}\{\mathbf{E}, \partial_p\langle f\rangle\} = eN_0 \int d\epsilon_{\mathbf{p}} D(\epsilon_{\mathbf{p}}) \frac{1}{2}\{\partial_{\epsilon_{\mathbf{p}}}\langle f\rangle, \mathbf{E}\} = -\frac{e}{2}\{\sigma(\mu), \mathbf{E}\}, \tag{3.77}$$

where the diffusion coefficient is given by

$$D(\epsilon_{\mathbf{p}}) = \frac{\tau}{m}\epsilon_{\mathbf{p}}, \quad \text{with} \quad \epsilon_{\mathbf{p}} = \frac{p^2}{2m} \tag{3.78}$$

and $\mu = \rho/N_0$ is the spin-dependent chemical potential, and $\sigma(\mu) = N_0 D(\mu)$. In equilibrium, the density current is defined by $\rho_{eq} = N_0\epsilon_F + N_0\Psi$. By expanding $D(\mu)$ around ϵ_F, we have $D^0 \approx D(\epsilon_F)$ and $D^a \approx \tau S^a/(N_0 m)$, and therefor

$$\sigma(\mu) = N_0 D(\epsilon_F)\sigma^0 + \frac{\tau}{m} S^a \sigma^a. \tag{3.79}$$

Hence, the particle and spin currents of drift term reads

$$\mathbf{J}^0_{drift} = -eN_0 D^0 \mathbf{E}^0 - \frac{e}{2} N_0 D^a \mathbf{E}^a, \quad \mathbf{J}^a_{drift} = -\frac{e}{4} N_0 D^0 \mathbf{E}^a - \frac{e}{2} N_0 D^a \mathbf{E}^0. \tag{3.80}$$

By taking the integration over momentum, the diffusion term becomes

$$\mathbf{J}_{diff} = -N_0 \int d\epsilon_{\mathbf{p}} \tilde{\nabla}_{\mathbf{r}} \langle f \rangle = -\frac{1}{2}\{D(\mu), \tilde{\nabla}_{\mathbf{r}}\rho\}. \tag{3.81}$$

Then we get

$$\mathbf{J}^0_{diff} = -D^0 \nabla_{\mathbf{r}} n - 2D^a [\tilde{\nabla}_{\mathbf{r}} S]^a, \quad \mathbf{J}^a_{diff} = -\frac{1}{2} D^a \nabla_{\mathbf{r}} n - D^0 [\tilde{\nabla}_{\mathbf{r}} S]^a. \tag{3.82}$$

By using the same procedure, we obtain the Hall terms as

$$\mathbf{J}^0_{Hall} = \frac{e\tau}{m} \mathbf{B}^0 \times \mathbf{J}^0 + \frac{e\tau}{m} \mathbf{B}^a \times \mathbf{J}^a, \quad \mathbf{J}^a_{Hall} = \frac{e\tau}{m} \mathbf{B}^0 \times \mathbf{J}^a + \frac{e\tau}{4m} \mathbf{B}^a \times \mathbf{J}^0. \tag{3.83}$$

Hence, the particle and spin currents in general, may be written as

$$\mathbf{J} = -eN_0 D^0 \mathbf{E}^0 - \frac{e}{2} N_0 D^a \mathbf{E}^a - D^0 \nabla_{\mathbf{r}} n - 2D^a [\tilde{\nabla}_{\mathbf{r}} S]^a + \frac{e\tau}{m} \mathbf{B}^0 \times \mathbf{J}^0 + \frac{e\tau}{m} \mathbf{B}^a \times \mathbf{J}^a \tag{3.84}$$

and

$$\mathbf{J}^a = -\frac{e}{4} N_0 D^0 \mathbf{E}^a - \frac{e}{2} N_0 D^a \mathbf{E}^0 - \frac{1}{2} D^a \nabla_{\mathbf{r}} n - D^0 [\tilde{\nabla}_{\mathbf{r}} S]^a + \frac{e\tau}{m} \mathbf{B}^0 \times \mathbf{J}^a + \frac{e\tau}{4m} \mathbf{B}^a \times \mathbf{J}^0. \tag{3.85}$$

In Chapter 6, we will use the above equations, together with the continuity-like equation derived in Eq. (3.55) to analyze some aspects of the current-induced spin polarizations in a disordered Rashba-Dresselhaus model, where we will consider the effect of extrinsic SOC as well. Although the SU(2) gauge field is a powerful method, it is useful to show how the same results can be obtained in a different way. In the next section we will introduce the diagrammatic Kubo formula for various spin transport coefficients.

3.3 Linear response theory

In this part we develop a general scheme of linear response theory. The idea is that the external perturbation is small enough, which means that the system response would be a linear function of the perturbation strength. We assume that the Hamiltonian consists of two different parts. The first part is the time-independent Hamiltonian, H_0, which describes the dynamics in an unperturbed system. The second one is an additional time-dependent Hamiltonian, $H_{ext}(t)$, which is the perturbation due to the external field. More precisely, the perturbation involves the coupling of an external field, $U_B(x', t)$, with an observable $\hat{O}_B$ system. Then we are able to describe H_{ext} as

$$H_{ext} = \int dx' U_B(x', t) \hat{O}_B(x). \tag{3.86}$$

In general, we want to calculate the statistical average of any operator $\langle \hat{O}_A \rangle$, which we wish to measure in the presence of the perturbation $U_B(x', t)$. In the Eq. (3.86), the external field, $U_B(x', t)$, is a function of time, and so is the associated Hamiltonian. The exact state vector in the Schrödinger picture $|\psi_\sigma(t)\rangle$ satisfies the Schrödinger equation as

$$i\hbar\partial_t|\psi_\sigma(t)\rangle = (H_0 + H_{ext}(t))|\psi_\sigma(t)\rangle. \tag{3.87}$$

Suppose that the perturbation started at t_0 by turning on an additional time-dependent Hamiltonian. We will use the interaction adiabatically, i.e. if $t \to -\infty$, and $H_{ext} \to 0$, which means

$$|\psi(t_0 \to -\infty)\rangle = |\psi_0\rangle. \tag{3.88}$$

This leads us to write the state vector as

$$|\psi_\sigma(t)\rangle = |\psi_\sigma(0)\rangle - i\int_{-\infty}^{t} dt' H_{ext}(t')|\psi_\sigma(0)\rangle. \tag{3.89}$$

All the physical information of interest is contained in the average of the Schrödinger picture operator $\langle O_A \rangle$, i.e.,

$$\langle O_A \rangle = \langle \psi_\sigma(t)|O_A|\psi_\sigma(t)\rangle = \langle\psi_0|O_A|\psi_0\rangle + i\langle\psi_0|\int_{-\infty}^{t} dt'[H_{ext}(t'), O_A]|\psi_0\rangle \tag{3.90}$$

where only the linear terms of $H_{ext}(t)$ have been left. The first term is the average over the unperturbed system, which is not of interest here, whereas the second one is the linear response of the ground-state expectation value of the operator

$$\begin{aligned}
\delta\langle O_A(x,t)\rangle &= \langle O_A\rangle - \langle O_A\rangle_0 \\
&= -i\langle\psi_0|\int_{-\infty}^{t} dt'[O_A, H_{ext}(t')]|\psi_0\rangle \\
&= \int_{-\infty}^{\infty} dt' \int dx' R^{AB}(x, x', t-t')U_B(x', t'),
\end{aligned} \tag{3.91}$$

which gives the information of the perturbation on the average of the operator. Then the response function is defined as

$$R^{AB}(x, x', t-t') = -i\theta(t-t')\langle\psi_0|[O_A(x,t), O_B(x', t')]|\psi_0\rangle \tag{3.92}$$

where θ is the step function. One should note that since H_0 is time-independent, the response function only depends on the time difference of the two Heisenberg operators. The above equation is the famous Kubo formula, which expresses the properties of the perturbed system in the zero-temperature limit. In the Fourier space, with respect to both space and time, the response function is rewritten as

$$R^{AB}(x, x', t-t') = \frac{1}{v}\int_{-\infty}^{\infty}\frac{d\omega}{2\pi}\sum_p e^{-i\omega(t-t')}e^{iq.x+iq'.x'}R^{AB}_{qq'}(\omega). \tag{3.93}$$

We assumed that the unperturbed system is translationally invariant, which implies that the response function only depends on the difference of the space argument. It is sufficient to write

$$R^{AB}(x, x', t-t') = R^{AB}(x-x', t-t') \tag{3.94}$$

$$R^{AB}_{\mathbf{qq'}}(\omega) = R^{AB}_q(\omega)\delta_{\mathbf{q}+\mathbf{q'}}. \tag{3.95}$$

Hence, according to Eq. (3.93), the response function in momentum space can be defined as

$$R_q^{AB}(\omega) = -i\int_{-\infty}^{\infty} dt e^{-i\omega t}\theta(t)\langle[O_A(\mathbf{q},t), O_B(-\mathbf{q},0)]\rangle. \tag{3.96}$$

Then Eq. (3.91) in the Fourier space has the form

$$\delta\langle O_A(q,\omega)\rangle = R_q^{AB}(\omega)\hat{U}_B(q,\omega), \tag{3.97}$$

where $\hat{U}_B(q,\omega)$ represents the Fourier transform of the external potential. For uniform and static limit of perturbing field, the response function is given by

$$\chi_{AB} = \frac{\delta O_A}{\delta U_B} = \lim_{q\to 0}\lim_{\omega\to 0}\hat{R}_{\mathbf{q}}^{AB}(\omega). \tag{3.98}$$

Now we are going to show a few remarkable properties of the response function. By using the identity $\sum_n |n\rangle\langle n| = 1$ between the two operators, we can easily show that

$$\begin{aligned} R_{\mathbf{q}}^{AB}(t) &= -i\theta(t) \quad \sum_{lm} \quad \left[\langle m|\hat{O}_A(\mathbf{q},t)|l\rangle\langle l|\hat{O}_B(-\mathbf{q},0)|m\rangle - \langle m|\hat{O}_B(\mathbf{q},0)|l\rangle\langle l|\hat{O}_A(-\mathbf{q},0)|m\rangle\right] \\ &= -i\theta(t) \quad \sum_{lm} \quad \left(e^{-i\omega_{lm}t}A_{ml}(\mathbf{q})B^{\star}_{ml}(-\mathbf{q}) - e^{i\omega_{lm}t}A^{\star}_{ml}(\mathbf{q})B_{ml}(-\mathbf{q})\right), \end{aligned} \tag{3.99}$$

where $\omega_{lm} = (E_l - E_m)$, and E_l represents eigenvalues of H_0 in the set of eigenstates $|l\rangle$ and

$$A_{ml}(\mathbf{q}) = \langle m|\hat{O}_A(\mathbf{q})|l\rangle \tag{3.100}$$

$$B^{\star}_{ml}(-\mathbf{q}) = \langle l|\hat{O}_B(\mathbf{q})|m\rangle. \tag{3.101}$$

Since the operators are hermitian and we have assumed the space inversion symmetry, we have

$$A^{\star}_{ml}(\mathbf{q})B_{ml}(-\mathbf{q}) = A_{ml}(\mathbf{q})B^{\star}_{ml}(-\mathbf{q}) \tag{3.102}$$

where by exploiting the formula

$$-i\int_0^{\infty} e^{i(\omega-\omega_{lm}+io^+)} = \frac{1}{\omega-\omega_{lm}+io^+} \tag{3.103}$$

we can obtain the Fourier transform with respect to the time of the response function

$$R_{\mathbf{q}}^{AB}(\omega) = \sum_{lm} A_{ml}(\mathbf{q})B^{\star}_{ml}(-\mathbf{q})[\frac{1}{\hbar\omega-\hbar\omega_{lm}+i0^+}], \tag{3.104}$$

which is not analytic in terms of the complex variable ω. This is clear from the fact that the term on the right hand side is an analytical in the upper complex plane of ω. Eq. (3.104) obeys the Kramers-Kronig relation

$$R_{\mathbf{q}}^{AB}(\omega) = \frac{1}{\pi}\int_{-\infty}^{\infty} d\omega' \frac{ImR_{\mathbf{q}}^{AB}(\omega')}{\omega'-\omega-io^+}, \tag{3.105}$$

By means of the property

$$\frac{1}{x-i0^+} = \mathcal{P}(\frac{1}{x}) + i\pi\delta(x) \tag{3.106}$$

the imaginary part reads

$$ImR_{\mathbf{q}}^{AB}(\omega) = -\frac{\pi}{\hbar}\sum_{lm} A_{ml}(\mathbf{q})B^{\star}_{ml}(-\mathbf{q})\delta(\omega-\omega_{lm}). \tag{3.107}$$

From the expression in Eq. (3.107), together with Eq. (3.102), we see that

$$ImR^{AB}_{-\mathbf{q}}(-\omega) = -ImR^{AB}_{\mathbf{q}}(\omega). \tag{3.108}$$

Now we are able to transform θ function to the time-ordering operator T_t product as

$$P^{AB}(x-x',t-t') = -i\langle T_t[O_A(x,t), O_B(x',t')]\rangle. \tag{3.109}$$

More precisely, in the Fourier space, the imaginary and real parts of the $R^{AB}_q(\omega)$ according to Eq. (3.104) are

$$ReR^{AB}_q(\omega) = ReP^{AB}_q(\omega) \tag{3.110}$$

$$ImR^{AB}_q(\omega) = sgn(\omega)ImP^{AB}_q(\omega). \tag{3.111}$$

Hence, the P^{AB}_q and R^{AB}_q contain the same information. The linear response theory of any operator O_A to an external perturbation couples to an operator O_B that has been derived in terms of the response function R^{AB}. Now we will consider a specific case of linear response theory to an electromagnetic field and gauge invariance.

3.3.1 The Kubo formula for transport phenomena

The explicit expression of linear response theory to an external perturbation has been obtained in Eq. (3.109). Now we consider the linear response to an external electromagnetic field. As a specific case in the Kubo formula, we consider a system with the positive charge $e > 0$ and the density operator $\hat{\rho} = -e\hat{n}(\mathbf{r})$ in the presence of external scalar ϕ and vector potential $\mathbf{A}$. The corresponding Hamiltonian is described by

$$H_{ext} = \frac{1}{c}\int dx A^{\mu}(x) J_{\mu}(x), \tag{3.112}$$

where the Greek indices μ are dedicated to time ($\mu = 0$) and space indices ($\mu = 1, \cdots, d$) and we used the compact notation of space-time $x = (t, \mathbf{r})$. Here we adopt the relativistic notations for the lower and upper indices, e.g. $J_{\mu} = (c\hat{\rho}, -\mathbf{J})$ and $A^{\mu} = (c\phi, \mathbf{A})$. By using Eq. (3.92), the linear response to an external electromagnetic field is given by

$$\langle J^{\mu}(x)\rangle = \frac{1}{c}\int dx' R^{\mu\nu}(x,x') A_{\mu}(x') \tag{3.113}$$

where the response Kernel is

$$R^{\mu\nu}(x,x') = -i\langle \mathrm{T}_t[J_{\mu}(x), J_{\nu}(x')]\rangle, \tag{3.114}$$

which contains both the current-current and density-density response function. Since the unperturbed system is time-independent and translationally invariant, we can use the Fourier transform as

$$R^{\mu\nu}(x-x',t-t') = \int_{-\infty}^{\infty}\frac{d\omega}{2\pi}\sum_{\mathbf{k}} e^{i\mathbf{k}\cdot(x-x')}e^{-i\omega(t-t')}R^{\mu\nu}(\mathbf{k},\omega). \tag{3.115}$$

In the limit of an infinite system, the sum is replaced by an integral over all spaces. By applying the Fourier transform, Eq. (3.115) becomes local

$$J^{\mu}(q) = \frac{1}{c}R^{\mu\nu}(q)A_{\nu}(q). \tag{3.116}$$

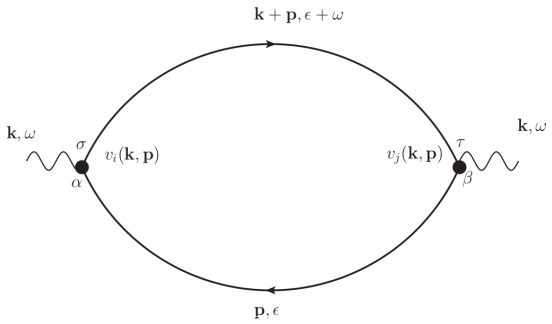

Figure 3.3: Feynman bubble diagram for the current-current response function.

where $q = (\omega, \mathbf{q})$. Since the electric field is derived by taking the time derivation of a time dependent vector gauge $\mathbf{E} = -\partial_t \mathbf{A}/c$, the electrical conductivity reads

$$\sigma_{\mu\nu}(\omega) = -\lim_{q\to 0} \frac{R^{\mu\nu}(\mathbf{k}, \omega)}{i\omega} \tag{3.117}$$

Now we are able to evaluate the conductivity according to the linear Kubo formula. In the following equation, the charge current operator is expressed as bilinear forms of the field operators

$$\mathbf{J} \quad = \quad -i\frac{e}{2m}\sum_{\sigma}\left(\psi^{\dagger}_{\sigma}(x,t)\nabla\psi_{\sigma}(x,t) - (\nabla\psi^{\dagger}_{\sigma}(x,t))\psi_{\sigma}(x,t)\right) - \frac{e^2}{m}\mathbf{A}\psi^{\dagger}_{\sigma}(x,t)\psi_{\sigma}(x,t). \tag{3.118}$$

By inserting the current operator Eq. (3.118) in the response function of Eq. (3.114) and transforming in the Fourier space, we obtain

$$R^{\mu\nu}(\mathbf{k}, t-t') \quad = \quad -i\langle T_t[J_{\mu}(\mathbf{k}, t), J_{\nu}(-\mathbf{k}, t')]\rangle, \tag{3.119}$$

where we considered the current $\mathbf{J}_{\mu}$ caused by an external electric field oriented along the μ-axis and coupled with the current $\mathbf{J}_{\nu}$. In the mixed space $(\mathbf{k}, t)$, the expression (3.119) yields

$$R^{\mu\nu}(\mathbf{k}, t-t') = i(-e)^2\sum_{\mathbf{pk}}\frac{p_{\mu}}{m}\frac{q_{\nu}}{m}\langle T_t(\hat{a}^{\star}_{p-k/2,\sigma}(t)\hat{a}_{p+k/2,\sigma}(t)\hat{a}^{\star}_{q+k/2,\tau}(t')\hat{a}_{q-k/2,\tau}(t'))\rangle, \tag{3.120}$$

where $a_{\mathbf{k}\sigma}$ and $a^{\star}_{\mathbf{k}\sigma}$ represent the creation and annihilation operators. In order to evaluate the average over four operators we recall the Wick's theorem in zero-temperature limit

$$\langle T_t(\hat{a}^{\star}_{p-k/2,\sigma}(t)\hat{a}_{p+k/2,\sigma}(t)\hat{a}^{\star}_{q+k/2,\tau}(t')\hat{a}_{q-k/2,\tau}(t'))\rangle = -\langle T_t(\hat{a}_{p+k/2,\sigma}(t')\hat{a}^{\star}_{p+k/2,\tau}(t))\rangle\langle T_t\hat{a}_{p-k/2,\tau}(t')\hat{a}^{\star}_{p-k/2,\sigma}(t)\rangle \tag{3.121}$$

which permits us to express the average in terms of the product of two single-particle Green functions. At the end, after taking Fourier transform with respect to the $t-t'$, we obtain

$$R^{\mu\nu}(\mathbf{k}, \omega) = ie^2\sum_{p}\int_{-\infty}^{\infty}\frac{d\epsilon}{2\pi}\mathrm{Tr}[v_{\mu}(p)G(p+k/2, \omega+\epsilon)v_{\nu}(p)G(p-k/2, \epsilon)] \tag{3.122}$$

where $v_{\mu,\nu} = p_{\mu,\nu}/m$, and Tr is the sum over the spin states. As illustrated in Fig. 3.3, the Kubo response function can be expressed through a bubble diagram, which can be the starting point for the perturbative expansion.

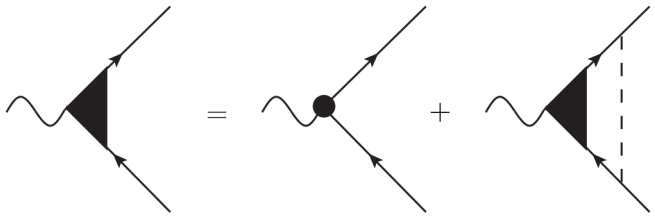

Figure 3.4: Feynman diagrams for the vertex corrections.

The ISGE is the appearance of a spin polarization produced by the action of a perpendicular external electric field. Hence, the quantity we are interested in is to examine the spin polarization $O_A \to \mathbf{S}$, and the external perturbation is the charge current operator $\mathbf{J} = -e\hat{\mathbf{v}}$. After applying the integral over ϵ, the Kubo formula for the ISGE has the form

$$\sigma^{\mu\nu} = \frac{(-e)}{2\pi} \sum_{\mathbf{p}} \mathrm{Tr}[G^R(\mathbf{p},\omega) S^\mu G^A(\mathbf{p}) J_\nu], \tag{3.123}$$

In the above equation, the Green functions are defined by the standard technique for disordered electron systems (3.58). Therefore, we must also correct the bubble diagram with impurity insertions and make the average over disorders. There are two ways to connect the different pairs of impurity, i.e. by dressing the same Green function line and by attaching the upper Green function to the lower one with the vertical and parallel impurity lines. At the leading order $1/(\epsilon_F \tau_0)$ we can neglect the crossed impurity lines. This leads to the so-called vertex correction, illustrated in Fig. 3.4. The vertex correction is applied here to the spin vertex, of which the Dyson equation reads

$$\Gamma^\rho = \frac{\sigma^\rho}{2} + \sum_{\mathbf{p}\mathbf{p}'} S_{\mathbf{p}'\mathbf{p}} G(\mathbf{p}, \epsilon+\omega) \Gamma^\rho G(\mathbf{p},\omega) S_{\mathbf{p}\mathbf{p}'} \tag{3.124}$$

where ρ is the spin direction and $S_{\mathbf{p}\mathbf{p}'}$ represents the scattering amplitude in the presence of extrinsic SOC. The above equation can be solved in the perturbative way. In the following section, we will first derive the full scattering amplitude $S_{\mathbf{p}\mathbf{p}'}$ and then the evolution of the density matrix will study under the scattering process.

3.4 Scattering amplitude in the presence of spin-orbit coupling

Extrinsic SOC originates from the potentials due to random scattering from the impurities. In this case, before and after the scattering events, there is no direct connection between the wave vector and the spin of the electrons. The scattering amplitude can be divided in two parts based on the expression of the spin-independent and spin-dependent contributions [52]

$$f_{\mathbf{k},\mathbf{k}'} = \mathcal{A}(v) + \mathcal{B}(v)\ \hat{\mathbf{k}} \times \hat{\mathbf{k}}' \cdot \hat{\sigma}, \tag{3.125}$$

with $\hat{\mathbf{k}}$ and $\hat{\mathbf{k}}'$ representing the unit vector along the direction of momentum before and after the scattering, and v is the scattering angle. As mentioned in Ref. [52], the different combinations of the amplitudes

$\mathcal{A}$ and $\mathcal{B}$ correspond to specific physical processes. Let us consider them in more details. We start with the density matrix under the scattering process

$$\rho_{\mathbf{k}} \to \rho_{\mathbf{k}'} = S_{\mathbf{k}\mathbf{k}'}\rho_{\mathbf{k}}S^{\star}_{\mathbf{k}\mathbf{k}'}. \tag{3.126}$$

In the following, we will proceed with a formal derivation of scattering amplitude $S_{\mathbf{k}',\mathbf{k}}$ relating to the initial state ($\mathbf{k}$) and the final state ($\mathbf{k}'$)

$$S_{\mathbf{k}',\mathbf{k}} =< \mathbf{k}'|U + UGU + \cdots|\mathbf{k} > \tag{3.127}$$

where $G_{\mathbf{k}}$ represents the Green function. The potential U, due to the impurity scattering in the presence of SOC, is defined by

$$U(\mathbf{r}) = V(\mathbf{r}) + \frac{\lambda^2}{4}\sigma \cdot \nabla V(\mathbf{r}) \times (-i\nabla),\ V(\mathbf{r}) = v_0\delta(\mathbf{r}). \tag{3.128}$$

Thus the scattering amplitude in the Born approximation has the form

$$f_{\mathbf{k}'\mathbf{k}} = \langle \mathbf{k}'|U|\mathbf{k}\rangle = v_0\left[1 - i\frac{\lambda^2}{4}\mathbf{k} \times \mathbf{k}' \cdot \sigma\right]. \tag{3.129}$$

By inserting the solution of the identity in Eq. (3.127), one gets

$$S_{\mathbf{k}',\mathbf{k}} = f_{\mathbf{k},\mathbf{k}'} + \int \frac{d\mathbf{k}''}{(2\pi)^2} f_{\mathbf{k}',\mathbf{k}''}G(\mathbf{k}'')f_{\mathbf{k}'',\mathbf{k}} + \cdots \tag{3.130}$$

In order to obtain Eq. (3.130), it is convenient to write $f_{\mathbf{k}',\mathbf{k}}$ in a 4-vector components

$$f_{\mathbf{k}',\mathbf{k}} = f^0_{\mathbf{k}',\mathbf{k}}\sigma^0 + f^i_{\mathbf{k}',\mathbf{k}}\sigma^i \tag{3.131}$$

and turn it into the matrix form. In a 2DEG, it is sufficient to write

$$f^0_{\mathbf{k}',\mathbf{k}} = v_0 \tag{3.132}$$

$$f^z_{\mathbf{k}',\mathbf{k}} = -i\frac{\lambda^2}{4}v_0(\mathbf{k}' \times \mathbf{k})_z, \tag{3.133}$$

where in-plane of wave vector $\mathbf{k} = (k_x, k_y)$, only z-component of f^i remained. The sum of the series leads to the self-consistent solution for the scattering amplitude

$$S_{\mathbf{k}',\mathbf{k}} = f_{\mathbf{k},\mathbf{k}'} + \int \frac{d\mathbf{k}''}{(2\pi)^2} f_{\mathbf{k}',\mathbf{k}''}G(\mathbf{k}'')S_{\mathbf{k}'',\mathbf{k}}. \tag{3.134}$$

Hence, by inserting Eq. (3.132) and Eq. (3.133), we can find a solution in the form of

$$S_{\mathbf{k}',\mathbf{k}} = S^0_{\mathbf{k}',\mathbf{k}}\sigma^0 + S^z_{\mathbf{k}',\mathbf{k}}\sigma^z, \tag{3.135}$$

if the two components, spin-independent S^0 and spin-dependent scattering amplitude S^z, have the forms

$$S^0_{\mathbf{k}',\mathbf{k}} = v_0 + v_0\int \frac{d\mathbf{k}''}{(2\pi)^2}G(\mathbf{k}'')S^0_{\mathbf{k}',\mathbf{k}} - i\lambda^2 v_0\int \frac{d\mathbf{k}''}{(2\pi)^2}G(\mathbf{k}'')(\mathbf{k}' \times \mathbf{k}'')_z S^z_{\mathbf{k}',\mathbf{k}} \tag{3.136}$$

$$S^z_{\mathbf{k}',\mathbf{k}} = -i\lambda^2(\mathbf{k}' \times \mathbf{k})_z + v_0\int \frac{d\mathbf{k}''}{(2\pi)^2}G(\mathbf{k}'')S^z_{\mathbf{k}',\mathbf{k}} - i\lambda^2 v_0\int \frac{d\mathbf{k}''}{(2\pi)^2}G(\mathbf{k}'')(\mathbf{k}' \times \mathbf{k})_z S^0_{\mathbf{k}',\mathbf{k}}.$$

To solve them we must make a guess about the momentum dependent terms. The Green function has a pole at $|\mathbf{k}''| = k_F$, therefore we have to worry only about the angle dependence. If we insert the first approximation for S^z into the last integral of S^0, we get the following angle integral

$$\int \frac{d\Omega''}{2\pi}(\hat{k} \times \hat{k}'')_z(\hat{k}'' \times \hat{k}')_z = -\frac{1}{2}\hat{k}' \cdot \hat{k}, \tag{3.137}$$

which means that $S^0_{\mathbf{k'k}}$ contains the s-wave and p-wave harmonics terms. We can set

$$S^0_{\mathbf{k'k}} = \tilde{v}_0 + \tilde{v}_1 \hat{k}' \cdot \hat{k}, \tag{3.138}$$

where $\tilde{v}_0$ and $\tilde{v}_1$ are independent of $\mathbf{k}$ and $\mathbf{k}'$. By taking the momentum integration over $\mathbf{k}''$ in the second part of Eq. (3.136), the first integral in $S^z_{\mathbf{k'k}}$ vanishes. The second angle integration in $S^z_{\mathbf{k'k}}$ may lead to the correction to the p-wave part of $S^0_{\mathbf{k'k}}$

$$\int \frac{d\Omega''}{2\pi} (\hat{k}' \times \hat{k}'')_z \hat{k}'' \cdot \hat{k} = \frac{1}{2} \hat{k}' \times \hat{k}. \tag{3.139}$$

Hence, we seek $S^z_{\mathbf{k'k}}$ with the form

$$S^z_{\mathbf{k'k}} = \tilde{v}_2 (\hat{k}' \times \hat{k})_z. \tag{3.140}$$

By using the two coupled equations $S^0_{\mathbf{k'k}}$ and $S^z_{\mathbf{k'k}}$ into Eq. (3.136) we get the system of equations in the following forms

$$\begin{aligned}
\tilde{v}_0 &= v_0 - i\pi N_0 v_0 \tilde{v}_0, && (3.141)\\
\tilde{v}_1 &= \frac{1}{2}(\frac{\lambda^2}{4}) p_F^2 v_0 \tilde{v}_2, && (3.142)\\
\tilde{v}_2 &= -i(\frac{\lambda^2}{4}) p_F^2 v_0 + \frac{1}{2}(\frac{\lambda^2}{4}) p_F^2 v_0 \tilde{v}_1. && (3.143)
\end{aligned}$$

The self-consistent solution of each equation leads to

$$\begin{aligned}
\left(1 + (\pi N_0 v_0)^2\right) \tilde{v}_0 &= v_0 - i\pi N_0 v_0^2, && (3.144)\\
\left(1 - (\frac{\lambda^2 p_F^2 v_0}{8})^2\right) \tilde{v}_1 &= -\frac{i}{2} \left((\frac{\lambda^2}{4}) p_F^2 v_0 \right)^2, && (3.145)\\
\left(1 - \frac{1}{2}(\frac{\lambda^2 p_F^2 v_0}{4})^2\right) \tilde{v}_2 &= -i(\frac{\lambda^2}{4}) p_F^2 v_0. && (3.146)
\end{aligned}$$

Up to the first order in λ^2, we have

$$\begin{aligned}
\tilde{v}_0 &= \frac{v_0 - i\pi N_0 v_0^2}{1 + (\pi N_0 v_0)^2}, && (3.147)\\
\tilde{v}_1 &\approx 0, && (3.148)\\
\tilde{v}_2 &\approx -i(\frac{\lambda^2}{4}) p_F^2 v_0. && (3.149)
\end{aligned}$$

Hence, in the Born approximation and to the first order in λ^2 and in v_0^2, the scattering amplitudes, $\mathcal{A}$ and $\mathcal{B}$, have the forms

$$\mathcal{A} = v_0 - i v_0^2 \pi N_0, \quad \mathcal{B} = -i(\frac{\lambda^2}{4}) p_F^2 v_0. \tag{3.150}$$

Now we can proceed with the formal derivation of the density matrix (3.126). After setting the scattering amplitude $f_{\mathbf{k'k}}$ (3.125) inside the density matrix $\rho_{p'}$ (3.126), we can obtain a system of coupled equations for $\rho_{k'}$ as

$$\rho_{\mathbf{k}'} = \rho^0_{\mathbf{k}} \sigma^0 + \sum_{a=1}^{3} \rho^a_{\mathbf{k}} \sigma^a, \tag{3.151}$$

where, to evaluate the particle $\rho^0_{\mathbf{k}}$ and spin polarization distributions $\rho^a_{\mathbf{k}}$, we can use the following equations

$$\rho^0_{\mathbf{k}'} = \frac{1}{2} \mathrm{T}r(S_{\mathbf{kk}'} \rho_{\mathbf{k}} S^\star_{\mathbf{kk}'}), \quad \rho^a_{\mathbf{k}'} = \frac{1}{2} \mathrm{T}r(\sigma^a S_{\mathbf{kk}'} \rho_{\mathbf{k}} S^\star_{\mathbf{kk}'}). \tag{3.152}$$

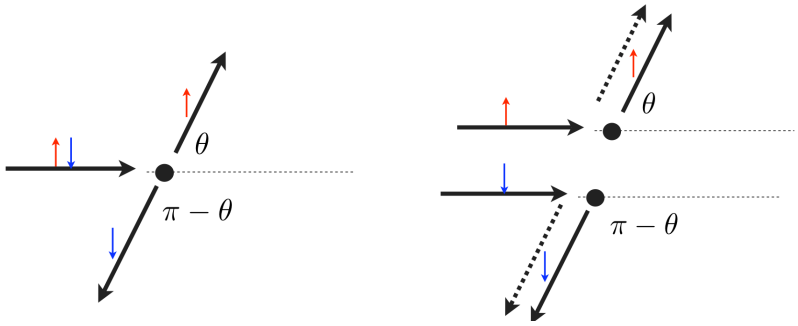

Figure 3.5: Mott Skew Scattering and side-jump at attractive impurities. Shown are the classical trajectories (solid lines), impurities (black holes) and the spin quantization axis perpendicular to the momentum plane. The dashed line represents the horizontal displacement arising from the side-jump effect.

Hence, we get from Eq. (3.151) and Eq. (3.152)

$$\rho^0_{k'} = \left(|\mathcal{A}|^2 + |\mathcal{B}|^2\right)\rho^0_k + \left(\mathcal{A}\mathcal{B}^\star + \mathcal{A}^\star\mathcal{B}\right)\hat{n}\cdot\rho_k, \tag{3.153}$$

$$\rho^a_{k'} = \left(\mathcal{A}\mathcal{B}^\star + \mathcal{A}^\star\mathcal{B}\right)\rho^0_k\hat{n} + i\left(\mathcal{A}\mathcal{B}^\star - \mathcal{A}^\star\mathcal{B}\right)\rho_k\times\hat{n} + |\mathcal{B}|^2\left(2\hat{n}(\hat{n}\cdot\rho_k) - \rho_k\right), \tag{3.154}$$

where $\hat{n} = \hat{\mathbf{k}}'\times\hat{\mathbf{k}}$. In the above equations, the combinations of the amplitudes, $\mathcal{A}$ and $\mathcal{B}$, correspond to the specific physical processes. The $|\mathcal{A}|^2 + |\mathcal{B}|^2$ describes the total standard scattering rate, where $|\mathcal{A}|^2$ and $|\mathcal{B}|^2$ correspond to the spin-independent and EY spin relaxation rates, respectively. Interference terms between the two amplitudes yield coupling among the currents. More in detail, $\mathcal{A}\mathcal{B}^* - \mathcal{A}^\star\mathcal{B}$ gives rise to the side-jump [8] and swapping of spin currents [52, 90], whereas the combination $\mathcal{A}\mathcal{B}^* + \mathcal{A}^\star\mathcal{B}$ describes the skew scattering [94], which is responsible for the coupling between the charge and spin currents, as illustrated in Fig. 3.5. More precisely, when an electron scatters at an impurity potential, the scattering cross section depends on the spin states. The effect also known as Mott skew scattering was originally considered for high energy electrons. The effect does not appear in the order of Born approximation, and needs to go beyond Born approximation at least in the order of v_0^3. In Fig. 3.5 (left), the SS is shown at impurity site with strong SOC. This impurity acts as a potential landscape which makes the trajectories of spin-up and spin-down electrons to different directions. At the order of the Born approximation, the extrinsic SOC will also be effective in another mechanism (arised from $|\mathcal{A}|^2 + |\mathcal{B}|^2$), which is the so-called side-jump (SJ). This mechanism affects the spin splitting by making the lateral displacement of the wave function during the scattering events [8], see Fig. 3.5 (right). This displacement is the same for both the spin-up and spin-down electrons but with opposite sign. Hence the total momentum is still conserved, and then the SJ is an elastic event. The effect appears in the anomalous part of both the spin and charge current. To understand the origin of this effect, from Hamiltonian (2.38) the equation of motion at a semiclassical level has the form

$$\dot{\mathbf{r}} = \frac{i}{\hbar}[H_{imp}, r] = \frac{\mathbf{k}}{m} - \frac{\lambda_0^2}{4}\nabla V(\mathbf{r})\times\sigma, \tag{3.155}$$

$$\dot{\mathbf{k}} = -\nabla V(\mathbf{r}) + \frac{\lambda_0^2}{4}(\sigma\times\mathbf{k}\cdot\nabla)\nabla V(\mathbf{r}). \tag{3.156}$$

To first order of λ_0^2, the equation for $\mathbf{r}$ becomes

$$\dot{\mathbf{r}} = \frac{\mathbf{k}}{m} + \frac{\lambda_0^2}{4}\sigma\times\dot{\mathbf{k}}. \tag{3.157}$$

By integrating over time from $-\infty$ to ∞, which is from before to after the scattering, the trajectory acquires an extra contribution proportional to the transferred momentum upon scattering

$$\Delta\mathbf{r} = \frac{\lambda_0^2}{4}\sigma \times \Delta\mathbf{p} \tag{3.158}$$

This displacement is the so-called SJ effect. In the next Chapter 4, we will use the Kubo formula and diagrammatic approaches to evaluate the SJ and SS contributions to the Edelstein conductivity.

3.5 Spin relaxation mechanisms and the relevant energy scales

Here we present the two main mechanisms contributing to the spin relaxation of the conduction electron, the EY and DP spin relaxation [27]. In the case of the EY mechanism, the spin loses its orientation due to the spin flip scattering, which is the consequence of the k-dependent admixture of the valence band states with conduction band wave function. This admixture of the two states results in the SOC induced by impurities. In principle, the spin relaxation due to the extrinsic SOC, which arises from impurity potential, is usually refereed to as the EY spin relaxation.

Another possibility mechanism, which arises from the intrinsic SOC, is the DP spin relaxation, where the spin precesses about the effective magnetic field between two collisions. Consider an electron with momentum $\mathbf{k}$. Its spin precesses with a rotation frequency ω along the axis given by $\mathbf{b}(\mathbf{k})$ ($\mathbf{k}$-dependent magnetic field arising from the intrinsic SOC). In this system we have $\omega = (e/2\pi)\mathbf{b}(\mathbf{k})$. The electron scatters into the different momentum $\mathbf{k}'$, and so begins to process along the new direction $\mathbf{b}(\mathbf{k}')$, and so on. The elastic scattering randomizes the travel direction, and then the precession direction and frequency change their direction after each collision. This leads to loss of the memory of the initial spin direction. Thus, the system acquires another characteristic time proportional to $\omega\tau$, where ω is the typical precession frequency proportional to $b(\mathbf{k})$. In the relationship between ω and τ, there exists two different limits that can be useful to give the different physical meaning to the result that we will find. The first one is the so-called *dirty* limit that describes the regime of high impurity concentration and we consider $\omega_L\tau << 1$, where ω_l is the effective Larmor frequency at the Fermi energy at zero temperature. In this limit, the precession frequency is high compared to τ, and its spin rotates very slowly compared to τ. Many of these small rotations lead to the loss of memory of the initial spin direction. On the other hand, when the electron scatters rarely and so the relaxation time τ is very long, we can consider the case $\omega_l\tau >> 1$. This limit is the so-called *clean* limit described in the regime of the low impurity concentration. The table 3.1 below summarizes the relationships between the parameters of our model

Table 3.1: The range of parameters

metallic regime	$\epsilon_F >> \hbar/\tau$
small spin-orbit effect	$\epsilon_F >> \omega_L$
clean limit	$\omega_L\tau >> 1$
dirty limit	$\omega_L\tau << 1$

According to these limits, we will define the two regimes, diffusive and beyond diffusive regimes, in which we will study the transport properties of a disordered electron system.

Chapter 4

The inverse spin-galvanic effect in the presence of impurity spin-orbit scattering

In this present Chapter, we will study the ISGE in the presence of the RSOC and DSOC as well as SOC from impurity scattering. To understand the origin of this effect, we will first recall the Edelstein result in the Rashba model. Then we will start with a general review of the problems in the second section, where we immediately "get into the thick of it" by formulating the problem, providing its solution, and highlighting certain experimentally relevant consequences. We base our discussion on physical arguments only, and postpone the technical details substantiating our conclusions to the next Chapters 5-6.

For this purpose, in the end of this Chapter we will introduce the Kubo formula and evaluate the ISGE in a 2DEG without considering the effect of the interplay between the SOC mechanisms. Compared to previous treatments [86] in the Rashba model, we consider here both the Rashba and Dresselhaus SOC. In evaluating the Kubo formula for the spin polarization response to an applied electric field, we explicitly take into account the side-jump and skew-scattering effects. We show that the inclusion of side-jump and skew-scattering modifies the expression of the ISGE. These results have been published in [88].

4.1 The inverse spin-galvanic effect

As maintained in Chapter 1, the ISGE is the appearance of a non-equilibrium spin polarization produced by the action of an external electric field. Belonging to the same category of the physical phenomena is the so-called SGE, in which an electric current is produced by a non-equilibrium spin polarization in the direction perpendicular to the spin direction.

We can interpret these effects in the following manner. The external electric field induces a Zeeman effective field through the SOC. This effective magnetic field is proportional to $\gamma\Delta p$, where γ represents the strength values of the intrinsic SOC and Δp is the shift of the Fermi sphere due to the external electric

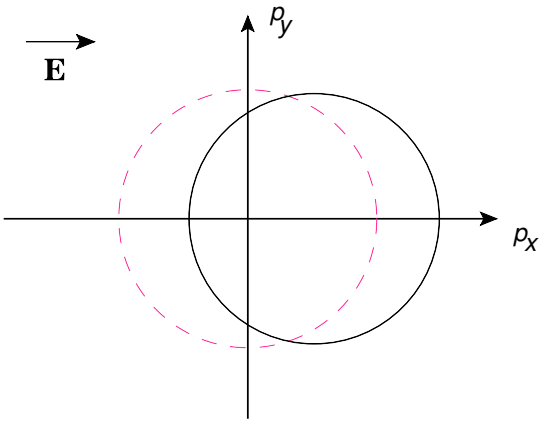

Figure 4.1: Fermi contour of the Rashba model is shifted by the application of an external electric field along the x-direction, whose the spin polarization is along the y-direction.

fields. More precisely, this shift of the Fermi surface in the direction of the electron motion induces an overpopulation of spins in the perpendicular direction of the electric field. In the concrete case of the Rashba model in a 2DEG as shown in Fig. 4.1, the ISGE leads to the Edelstein result as [21]

$$S^y = -eN_0\tau_0\alpha E_x, \tag{4.1}$$

where the external electric field E_x produces a spin polarization S^y in a 2DEG. Phenomenologically, the microscopic origin of the effect lies in the SOC. Usually the SOCs are classified as intrinsic when due to the SIA (Rashba [12]) and/or BIA (Dresselhaus [19]), whereas extrinsic ones are due to random scattering from impurities. The interplay between the two types of the SOCs depends on the ratio of the two main spin relaxation mechanisms caused by each one. Spin relaxation due to SOC from impurities is usually referred to as the EY mechanism and in this case the spin relaxation time scales as the momentum relaxation time. Intrinsic SOC yields in addition the DP spin relaxation due to the precessional mechanism, where the spin relaxation time scales as the inverse of the momentum relaxation time. In the next section, we start with a general review of the problem, where we formulate the problem providing its solution and highlighting certain experimentally relevant consequences. We show how the size and form of the ISGE can modify by the presence of the various sources of SOC.

4.2 The problem and its solution

Consider an ensemble of carriers in a generic solid state environment, where the spin is not a conserved quantity. In a homogeneous sample, in the presence of an exchange/Zeeman field $\mathbf{\Delta}$, the ensemble spin polarization $\mathbf{S}$ will then obey the continuity (Bloch) equation

$$\partial_t S^a = -[\mathbf{\Delta} \times \mathbf{S}]^a + \mathcal{T}^a \tag{4.2}$$

where here and throughout Latin superscritps stand for spin components $a = x, y, z$. The first term on the r.h.s. describes precession around the field $\mathbf{\Delta}$, while $\mathcal{T}^a$ is the a-th component of the torque acting

on the spin polarization, responsible for relaxation to equilibrium. In a simple isotropic medium, it reads

$$\mathcal{T}^a = -\frac{1}{\tau_s}\left(S^a - S^a_{\rm eq}\right), \tag{4.3}$$

where τ_s is the spin relaxation time – of whatever origin – and the equilibrium spin density $\mathbf{S}_{\rm eq} = \chi\boldsymbol{\Delta}$ is given in terms of the Pauli spin susceptibility $\chi = \frac{1}{4}\partial n/\partial\mu$ which at zero temperature reduces to $\chi = N_0/2$, with N_0 the density of states per spin at the Fermi energy.

In the presence of intrinsic SOC a finite drift velocity $\mathbf{v}$ of the ensemble is associated with a non-equilibrium spin polarization. Let us take a drift v_x in the x-direction and RSOC for definiteness' sake. The non-equilibrium spin polarization then reads

$$S^y = \chi B^y, \tag{4.4}$$

with

$$B^y = 2m\alpha v_x \tag{4.5}$$

an effective "drift field" felt by the moving ensemble. When the drift is caused by an electric field, $v_x = -e\tau E_x/m$, Eqs. (4.4) and (4.5) describe the usual ISGE/EE [4, 21]. RSOC also leads to (anisotropic) Dyakonov-Perel spin relaxation

$$1/\tau_s \to \hat{\Gamma}_{DP} = \frac{1}{\tau_{DP}}\begin{pmatrix} 1 & 0 & 0 \\ 0 & 1 & 0 \\ 0 & 0 & 2 \end{pmatrix}, \tag{4.6}$$

with $1/\tau_{DP} = (2m\alpha)^2 D$ and $D = v_F^2\tau/2$ the diffusion constant. This suggests that we modify the Bloch equations (4.2) to

$$\partial_t S^a = -[\boldsymbol{\Omega}\times\mathbf{S}]^a + \mathcal{T}^a_{int}, \tag{4.7}$$

where $\boldsymbol{\Omega} = \boldsymbol{\Delta} + \mathbf{B}$ is the full effective exchange/Zeeman field felt by the drifting carriers and (repeated indices are summed over, unless otherwise specified)

$$\mathcal{T}^a_{int} = -\hat{\Gamma}^{ab}_{DP}\left(S^b - \chi\Omega^b\right) \tag{4.8}$$

is the intrinsic torque, "intrinsic" meaning that spin-orbit effects from impurities are not yet included. This torque has a spin-relaxation component, $-\hat{\Gamma}_{DP}\mathbf{S}$, and a spin-generation one, $\hat{\Gamma}_{DP}\chi\boldsymbol{\Omega}$. The intuitive form of Eqs. (4.7) and (4.8) will be rigorously justified in the section 4.3, and holds for any kind of intrinsic SOC – e.g. RSOC + DSOC – with the appropriate form of $\hat{\Gamma}_{DP}$. It shows that the spin polarization relaxes to a non-equilibrium steady-state value given by

$$\mathbf{S}_{\rm neq} \equiv \chi\boldsymbol{\Omega} = \mathbf{S}_{\rm eq} + \chi\mathbf{B}\,. \tag{4.9}$$

What happens to this intuitive picture once extrinsic SOC is taken into account? This is the central *problem* addressed in our work. While modifications to both the relaxation and the spin generation torques are clearly expected, their precise form is a priori far from obvious. This is because extrinsic SOC gives rise to several phenomena, such as side-jump, skew scattering, and Elliott-Yafet relaxation,

which are not necessarily additive with respect to intrinsic SOC effects [75]. Let us start with the spin relaxation torque, which acquires a contribution due to Elliott-Yafet scattering

$$\hat{\Gamma}_{DP}\,\mathbf{S} \to [\hat{\Gamma}_{DP} + \hat{\Gamma}_{EY}]\,\mathbf{S} \equiv \hat{\Gamma}\,\mathbf{S}, \tag{4.10}$$

with $\hat{\Gamma}_{EY} \sim \lambda_0^4$. Unsurprisingly, spin-flip events at impurities, which are second order in the extrinsic SOC constant λ_0^2, provide a parallel channel for relaxation. However they also crucially affect the non-equilibrium steady-state value $\mathbf{S}_{\rm neq}$ the spins want to relax to. This is subtler, and highlights the difference between a true equilibrium state and a non-equilibrium steady-state. Such state is determined by the spin generation torque, which extrinsic SOC modifies in two ways: First, via side-jump and skew scattering, which together add an extrinsic contribution $\theta_{ext}^{sH} \sim \lambda_0^2$ to the intrinsic spin Hall angle, $\theta_{int}^{sH} \sim (\alpha^2, \beta^2)$ (this can have the same or the opposite sign as the intrinsic angle). Second, via Elliott-Yafet relaxation, which yields a correction *opposite* to the non equilibrium part of the intrinsic spin generation term, i.e., the $\hat{\Gamma}\chi B$ part of $\hat{\Gamma}\chi\Omega$ in Eq. (4.8):

$$\begin{aligned} \hat{\Gamma}_{DP}\chi\boldsymbol{\Omega} \;&\to\; \left[\hat{\Gamma}_{DP} + \hat{\Gamma}_{EY}\right]\chi\boldsymbol{\Delta} + \left[\hat{\Gamma}_{DP} + \hat{\Gamma}_{DP}\frac{\theta_{ext}^{sH}}{\theta_{int}^{sH}} - \hat{\Gamma}_{EY}\right]\chi\mathbf{B} \\ &\equiv\; \hat{\Gamma}\,\mathbf{S}_{\rm eq} + \delta\hat{\Gamma}\,\chi\mathbf{B}\,, \end{aligned} \tag{4.11}$$

where

$$\hat{\Gamma} = \hat{\Gamma}_{DP} + \hat{\Gamma}_{EY}\,, \tag{4.12}$$

and

$$\delta\hat{\Gamma} = \hat{\Gamma}_{DP} + \hat{\Gamma}_{DP}\frac{\theta_{ext}^{sH}}{\theta_{int}^{sH}} - \hat{\Gamma}_{EY}\,. \tag{4.13}$$

The full Bloch equations thus become

$$\partial_t S^a = -[\boldsymbol{\Omega}\times\mathbf{S}]^a - \hat{\Gamma}^{ab}(S^b - \chi\Delta^b) + \delta\hat{\Gamma}^{ab}\chi B^b. \tag{4.14}$$

This is the main result that we are looking for. It shows that, while intrinsic and extrinsic SOC act in parallel as far as relaxation to the equilibrium state is concerned–second term on the r.h.s. of Eq. (4.14)– they compete for the more interesting non-equilibrium contribution–the spin-generation torque, described by the third term on the r.h.s. of Eq. (4.14). In particular, the last term on the right hand side of Eq. (4.13) describes an "Elliot-Yafet spin-generation torque", which *opposes* the more familiar Dyakonov-Perel and spin Hall terms.

Eq. (4.14) shows that the naive Bloch equation (4.8) is modified by extrinsic processes. While this fact had already been recognized in Chapter 5 (and Refs. [75, 91]) some terms (third order in SOC: first order in RSOC and second order in λ_0^2) of the diagrammatic expansion had been neglected leading to an incomplete form of $\delta\hat{\Gamma}$, in which the last term on the right hand side of Eq. (4.13) was missing. [1]

As a result, the numerical calculation of current-induced spin polarization must be reconsidered, hence we will solve Eq. (4.14) numerically in the last Chapter 7. Indeed, Eq. (4.14) implies that the competition between intrinsic and extrinsic torques can generate out-of-plane spin polarizations from in-plane spin-orbit fields. Note that such a mechanism is very basic in nature, in the sense that it does not require

[1] Note that the terms here taken into account are beyond those considered in Ref. [47], where e. g. $\mathcal{O}(\lambda_0^4)$ corrections are neglected, and Ref. [98], where purely orbital mechanisms, not involving the spin of the carriers, are discussed.

finer details such as band non-parabolicities or angle-dependent scattering [25] in order to be effective. As such, it may have important consequences both in the analysis of existing experimental data [42, 93], and in the design of novel setups.

The non-trivial modification of the ISGE/EE arising from Eq. (4.14) implies a corresponding modification of the SGE/IEE, so as to fullfill Onsager relations. To be explicit, in the scenario reciprocal to the one considered in Eqs. (4.4), (4.5), the charge current J_x generated by a non-equilibrium spin polarization $S^y - \chi\Delta^y$ acquires the correction

$$\delta J_x = \frac{2e\alpha\tau}{\tau_{EY}} \left(S^y - \chi\Delta^y\right). \tag{4.15}$$

This ensures reciprocity between the spin response to an electric field E_x and the charge response to a time-dependent magnetic field $-\Delta^y(t)$ [91]. A microscopic derivation of (4.15) in a more general context is discussed in Ref. [99] and will not be pursued here.

In the following sections, we will extend the results of Ref. [75] to the case when both RSOC and DSOC, as well as SOC from impurities, are present. Here the effect of the interplay between SOC mechanisms is not considered. In contrast to what was done in Ref. [75], where the quasiclassical Keldysh Green function technique was used, we adopt here the diagrammatic language and the Kubo formula, which allows to identify the different physical contributions to the ISGE. We will derive the ISGE in a 2DEG and show in particular that the contributions due to RSOC and DSOC can cancel each other for equal RSOC and DSOC strengths. This is in agreement with Refs. [29, 35] when they concluded that the ISGE in semiconductors can be strongly anisotropic due to the interplay of RSOC and DSOC in the presence of impurity scattering [100].

4.3 Linear response theory at $\omega = 0$

The model Hamiltonian for a 2DEG in the presence of the SOC reads

$$H = \frac{p^2}{2m} + \alpha(p_y\sigma_x - p_x\sigma_y) + \beta(p_x\sigma_x - p_y\sigma_y) - \frac{\lambda_0^2}{4}\boldsymbol{\sigma} \times \nabla V(\mathbf{r}) \cdot \mathbf{p} + V(\mathbf{r}), \tag{4.16}$$

with $\mathbf{p} = -i\hbar\nabla_{\mathbf{r}}$ the momentum operator and $V(\mathbf{r})$ representing a short-range impurity potential. In Eq. (4.16) m is the effective mass in the sample, $\boldsymbol{\sigma} = (\sigma_x, \sigma_y, \sigma_z)$ the vector of Pauli matrices, α and β the Rashba and Dressehaus SOC constants. In the linear response theory, the spin polarization along the y direction due to an electric field applied along the x direction is given by

$$S^y = \sigma_{EC}^{yx} E_x \tag{4.17}$$

where σ_{EC}^{yx} is the frequency-independent Edelstein conductivity [21] given by Eq. (3.122) for the Kubo formula [91]

$$\sigma_{EC}^{yx} = \frac{(-e)}{2\pi} \sum_{\mathbf{p}} \mathrm{Tr}[G^A \frac{\Gamma_y}{2} G^R J_x], \tag{4.18}$$

where Γ_y is the spin vertex renormalized by impurity scattering derived in Eq. (3.124), and J_x is the number current vertex. In the presence of RSOC and DSOC, the retarded Green function has a structure in spin space, which can be expanded in Pauli matrix basis in the form

$$G_{\mathbf{p}}^R = G_0^R\sigma_0 + G_x^R\sigma_x + G_y^R\sigma_y \tag{4.19}$$

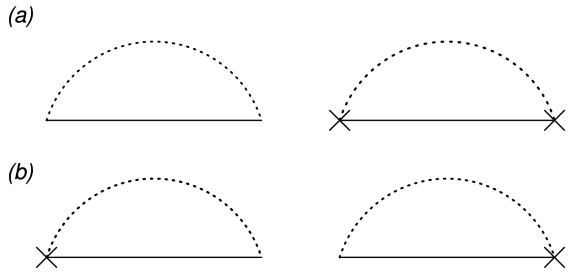

Figure 4.2: Lowest order diagrams for the disorder-averaged self-energy. (a) The self-consistent Born approximation for the spin-independent (Σ_0) and spin-dependent (Σ_{EY}) selfenergies. (b) The extra correction to the self-energy due to the interplay of RSOC and extrinsic SOC. The dashed line denotes the impurity average and the cross denotes the SOC from the impurity potential.

where

$$\begin{aligned} G_0^R &= \frac{G_+^R + G_-^R}{2} \\ G_x^R &= (\alpha\hat{p}_y + \beta\hat{p}_x)\frac{G_+^R - G_-^R}{2\gamma} \\ G_y^R &= -(\alpha\hat{p}_x + \beta\hat{p}_y)\frac{G_+^R - G_-^R}{2\gamma}. \end{aligned} \tag{4.20}$$

with $G_\pm^R = (\epsilon - \frac{p^2}{2m} \mp \gamma p + \frac{i}{2\tau})^{-1}$, and it is clear that the advanced Green function is obtained via the relation $G_\pm^A = (G_\pm^R)^*$. Here, $\gamma^2 = \alpha^2 + \beta^2 + 2\alpha\beta(\hat{p}_x\hat{p}_y + \hat{p}_y\hat{p}_x)$ is the total spin-orbit strength and depends on the direction of the momentum $\hat{p}_x = \cos(\phi)$ and $\hat{p}_y = \sin(\phi)$. Within the self-consistent Born approximation, the self-energy is given by the diagrams of Fig. 4.2(a) and has two contributions due to spin-independent and spin-dependent scatterings [21, 89]

$$\begin{aligned} \Sigma^R &= \Sigma_0^R + \Sigma_{EY}^R \\ &= n_i v_0^2 \sum_{\mathbf{p}'} G_{\mathbf{p}'}^R + n_i v_0^2 (\frac{\lambda_0^2}{4})^2 \sum_{\mathbf{p}'} \sigma^z G_{\mathbf{p}'}^R \sigma^z (\mathbf{p}\times\mathbf{p}')_z^2 \\ &= -\mathrm{i}\frac{1}{2\tau_0} - \mathrm{i}\frac{1}{4\tau_{EY}} = -\mathrm{i}\frac{1}{2\tau}, \end{aligned} \tag{4.21}$$

where $1/2\tau$ is the total quasiparticle relaxation rate. Whereas the first term, to zero order in λ_0^2, yields the standard elastic scattering time, the second one, to second order in λ_0^2, is responsible for the EY spin relaxation. The standard expression for the spin-independent scattering and EY spin relaxation rates is given by

$$\frac{1}{\tau_0} = 2\pi n_i N_0 v^2, \ \frac{1}{\tau_{EY}} = \frac{1}{\tau_0}\left(\frac{\lambda_0 p_F}{2}\right)^4, \tag{4.22}$$

where $N_0 = m/(2\pi)$ and p_F are the density of states and the Fermi momentum, respectively, of the 2DEG in the absence of SOC. In order to evaluate Eq. (4.18) we have introduced the matrix element of the number current vertex J_x from state $\mathbf{p}'$ to state $\mathbf{p}$

$$J_{x,\mathbf{p}\mathbf{p}'} = \delta_{\mathbf{p}\mathbf{p}'}\left(\frac{p_x}{m} - \alpha\sigma_y + \beta\sigma_x\right) + \delta J_{x,\mathbf{p}\mathbf{p}'}. \tag{4.23}$$

The latter term $\delta J_{x,\mathbf{p}\mathbf{p}'}$ is responsible for the side-jump contribution to the Edelstein conductivity and will be discussed further in Section 4.4. The renormalized spin vertex may be expanded in Pauli matrices

as $\Gamma_y = \Sigma_\eta \Gamma_y^\eta \sigma^\eta$ and is obtained by summing ladder diagrams, as illustrated in Fig. 3.4. As a result the vertex obeys an integral equation, which within the standard approximation, becomes an algebraic one [85]

$$\Gamma_y^\eta = \delta_{y\eta} + \frac{1}{2}\sum_{\mu\upsilon i} I_{\mu\upsilon}\mathrm{Tr}[\sigma_\eta\sigma_\mu\sigma_i\sigma_\upsilon]\Gamma_y^i + \frac{1}{2}\sum_{\mu\upsilon i} J_{\mu\upsilon}\mathrm{Tr}[\sigma_\eta\sigma_z\sigma_\mu\sigma_i\sigma_\upsilon\sigma_z]\Gamma_y^i, \tag{4.24}$$

where we have defined

$$I_{\mu\upsilon} = \frac{1}{2\pi N_0\tau_0}\sum_{\mathbf{p}'} G_\mu^R G_\upsilon^A,\ J_{\mu\upsilon} = \frac{1}{4\pi N_0\tau_{EY}}\sum_{\mathbf{p}'} G_\mu^R G_\upsilon^A. \tag{4.25}$$

Symmetry arguments in Eq. (4.24) indicate that, when both Rashba and Dresselhaus are present, the renormalized spin vertex Γ_y is not simply proportional to σ_y, but acquires components on both σ_x and σ_y. Upon the integration over the momentum in Eq. (4.24), some of the integrals $I_{\mu\upsilon}$ are zero and so the equations simplify. As a result we finally obtain

$$\begin{pmatrix}\Gamma_y^y\\ \Gamma_y^x\end{pmatrix} = \begin{pmatrix}1 - I_{00} + J_{00} & -2(I_{yx} - J_{yx})\\ -2(I_{xy} - J_{xy}) & 1 - I_{00} + J_{00}\end{pmatrix}^{-1}\begin{pmatrix}1\\0\end{pmatrix} \tag{4.26}$$

with

$$1 - I_{00} + J_{00} \simeq \tau(\frac{1}{\tau_\alpha} + \frac{1}{\tau_\beta} + \frac{1}{\tau_{EY}}) \simeq \frac{\tau}{\tau_t}, \tag{4.27}$$

$$-2(I_{xy} - J_{xy}) \simeq \frac{2\tau}{\tau_{\alpha\beta}}. \tag{4.28}$$

where the solution of each integral I_{ij} can be found in Appendix B. In the diffusive approximation, for instance, the DP spin relaxation due to RSOC can be defined as

$$\frac{1}{\tau_\alpha} = \frac{1}{2\tau_0}\frac{(2\tau_0\alpha p_F)^2}{1 + (2\tau_0\alpha p_F)^2} \backsimeq (2m\alpha)^2 D, \tag{4.29}$$

where in the diffusive regime we assumed $(2\tau_0\alpha p_F)^2 \ll 1$, which means that the many scattering events are needed to erase the memory of the initial conditions. In the same regime, $\frac{1}{\tau_\beta} \backsimeq (2m\beta)^2 D$ and $\frac{1}{\tau_{\alpha\beta}} \backsimeq (2m)^2\alpha\beta D$ are the DP relaxation times due to DSOC and the interplay of RSOC and DSOC, respectively. Once the renormalized spin vertex is known, the Edelstein conductivity from Eq. (4.18) can be put in the form

$$\sigma_{EC}^{yx} = \sum_{\eta=x,y}\Gamma_y^\eta\Pi_\eta, \tag{4.30}$$

where the bare Edelstein conductivity without the contributions of the side-jump term and skew-scattering mechanisms is given by

$$\Pi_\eta = \frac{(-e)}{2\pi}\sum_{\mathbf{p}}\mathrm{Tr}[G^A\frac{\sigma^\eta}{2}G^R J_x]. \tag{4.31}$$

To derive the CISP, we rewrite Eq. (4.17) by using Eq. (4.30)

$$S^y = \begin{pmatrix}\Gamma_y^y & \Gamma_y^x\end{pmatrix}\begin{pmatrix}\Pi_y\\ \Pi_x\end{pmatrix}E_x. \tag{4.32}$$

By using the standard technique to evaluate the integration over the absolute value of the momentum, the bare conductivities in Eq. (4.31) read

$$\Pi_y = \tau S_\alpha\langle\frac{1}{\tau_\gamma} - \frac{2}{\tau_\gamma}\frac{\beta^2}{\gamma^2}\rangle,\ \Pi_x = -\tau S_\beta\langle\frac{1}{\tau_\gamma} - \frac{2}{\tau_\gamma}\frac{\alpha^2}{\gamma^2}\rangle \tag{4.33}$$

where

$$S_\beta \;=\; -eN_0\tau\beta E_x,\;\; S_\alpha = -eN_0\tau\alpha E_x \tag{4.34}$$

and $\langle ... \rangle$ denotes the average over the momentum directions. Then the ISGE, which is equivalent to the stationary solution of the Bloch equation for spin dynamics, is derived by inserting Eq. (4.26) and Eq. (4.33) into Eq. (4.32)

$$S^y = \left(\frac{1}{\left(\frac{1}{\tau_\alpha}+\frac{1}{\tau_\beta}+\frac{1}{\tau_{EY}}\right)^2 - \left(\frac{2}{\tau_{\beta\alpha}}\right)^2} \right) \langle S_\beta \frac{2}{\tau_{\alpha\beta}} \left(\frac{1}{\tau_\gamma} - \frac{2}{\tau_\gamma}\frac{\alpha^2}{\gamma^2} \right) + S_\alpha \frac{1}{\tau_t} \left(\frac{1}{\tau_\gamma} - \frac{2}{\tau_\gamma}\frac{\beta^2}{\gamma^2} \right) \rangle. \tag{4.35}$$

In Eq. (4.35), $1/\tau_\gamma = (2\gamma p_F \tau)^2/2\tau$ is the total DP spin relaxation for Rashba and Dresselhaus SOCs with "$\gamma^2 = \alpha^2 + \beta^2 + 2\alpha\beta sin(2\phi)$". After taking the angular average of Eq. (4.35) we may write the expression of the ISGE component along the y direction

$$S^y_{int} = \left(\frac{1}{\left(\frac{1}{\tau_\alpha}+\frac{1}{\tau_\beta}+\frac{1}{\tau_{EY}}\right)^2 - \left(\frac{2}{\tau_{\beta\alpha}}\right)^2} \right) \left(S_\alpha (\frac{1}{\tau_\alpha} - \frac{1}{\tau_\beta})(\frac{1}{\tau_\alpha} - \frac{1}{\tau_\beta} + \frac{1}{\tau_{EY}}) \right). \tag{4.36}$$

We have added a suffix *int* to remind that we are only considering the intrinsic mechanism, which can be defined as the term that survives when the extrinsic SOC (λ_0) vanishes. One must however borne in mind that this intrinsic term is modified by the presence of the extrinsic SOC via the appearance of the EY spin relaxation time. The consideration of the extrinsic mechanisms, i.e. those terms which only arise when the extrinsic SOC is present, will be done in the next section.

Eq. (4.36) generalizes to the presence of the DSOC the expression for the *intrinsic* contribution to the Edelstein polarization presented in Eq. (36) of Ref. [75] and, indeed, reduces to it when $\beta = 0$. Furthermore, when also $\lambda_0 = 0$ it reproduces the Edelstein result for the Rashba model [21], as presented in Eq. (4.1). We also note that, in the absence of the extrinsic SOC, the contributions due to the RSOC and DSOC cancel each other when $\alpha = \beta$. In this case indeed Eq. (4.36) predicts that the Edelstein effect vanishes. The fact that the spin vertex Γ_y has both σ_x and σ_y components implies that there will be spin polarization also along the x direction. By performing a similar calculation for the ISGE along the x direction, we have

$$S^x_{int} = \left(\frac{1}{\left(\frac{1}{\tau_\alpha}+\frac{1}{\tau_\beta}+\frac{1}{\tau_{EY}}\right)^2 - \left(\frac{2}{\tau_{\beta\alpha}}\right)^2} \right) \left(S_\beta (\frac{1}{\tau_\alpha} - \frac{1}{\tau_\beta})(\frac{1}{\tau_\alpha} - \frac{1}{\tau_\beta} + \frac{1}{\tau_{EY}}) \right). \tag{4.37}$$

One should remember that the extrinsic SOC affects the ISGE not only through the EY mechanism, but also through the two other mechanisms, side-jump and skew scattering. In the following sections, we will show how the inclusion of the side-jump and skew scattering modifies the ISGE.

4.4 Side-jump and skew-scattering contributions

In this section we evaluate the side-jump and skew-scattering contributions to the Edelstein conductivity. The self-energies, to order λ_0^2, in Fig. 4.2(b) are usually zero in the absence of intrinsic SOC due

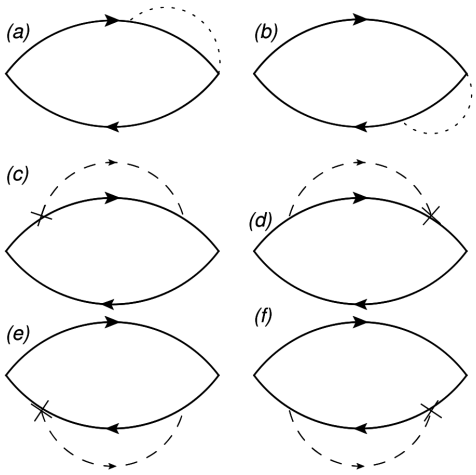

Figure 4.3: Diagrams for the side-jump contribution to the Edelstein effect. The solid lines are Green function and dashed lines represent the average over the impurity potential. The cross denotes the SOC from the impurity potential (a),(b) Side-jump type of diagrams originating from components proportional to λ_0^2 in the current vertices. (c)-(f) The extra corrections to the side-jump contribution due to the extrinsic effect, where the right vertex is for the x component of the charge current.

to symmetry reasons. However, when RSOC and DSOC are present, they no longer vanish and, actually, their contribution is crucial to get the full side-jump contribution to the Edelstein conductivity. Hence, the diagrams we need to consider for the side-jump mechanism are those depicted in Fig. 4.3. Diagrams shown in Figs. 4.3(a) and 4.3(b) correspond to the ordinary side-jump diagrams as those used to evaluate the spin Hall conductivity and originate from the anomalous correction to the current vertex to order λ_0^2 (see Eq. (4.23)). The other diagrams shown in Figs. 4.3(c-f) take into account the self-energy corrections mentioned above. To keep the discussion as simple as possible, we confine first to the case when only RSOC is present. The extension to the DSOC is straightforward.

The anomalous current vertex of Eq. (4.23) from state $\mathbf{p}$ to state $\mathbf{p}'$ can be put in the form

$$\delta J^x_{\mathbf{p},\mathbf{p}'} = \mathrm{i}\frac{v_0\lambda_0^2}{4}(p_y - p'_y)\sigma_z. \tag{4.38}$$

By replacing the spin current $J_{x\mathbf{p}\mathbf{p}'}$ in Eq. (4.31) by $\delta J_{x\mathbf{p}\mathbf{p}'}$, the diagrams in Figs. 4.3(a) and 4.3(b) read

$$\Pi_y^{sj(a+b)} = -\mathrm{i}\frac{ev_0^2 n_i}{2\pi}\frac{\lambda_0^2}{4}\sum_{\mathbf{p}\mathbf{p}'}(p'_y - p_y)\frac{1}{2}\mathrm{Tr}\left[G^A_{\mathbf{p}}\sigma_y G^R_{\mathbf{p}}(G^R_{\mathbf{p}'}\sigma_z - \sigma_z G^A_{\mathbf{p}'})\right]. \tag{4.39}$$

The diagrams in Figs. 4.3(c) and 4.3(f) corresponding to the contributions from the self-energy renormalization of the Green functions are given by

$$\Pi_y^{sj(c+d)} = \mathrm{i}\frac{en_i}{2\pi}v_0^2\frac{\lambda_0^2}{4}\sum_{\mathbf{p}\mathbf{p}'}\mathrm{Tr}\left[\frac{\sigma_y}{2}G^R_{\mathbf{p}}[G^R_{\mathbf{p}'}(\mathbf{p}'\times\mathbf{p})_z\sigma_z + (\mathbf{p}\times\mathbf{p}')_z\sigma_z G^R_{\mathbf{p}'}]G^R_{\mathbf{p}}\frac{p_x}{m}G^A_{\mathbf{p}}\right], \tag{4.40}$$

$$\Pi_y^{sj(e+f)} = \mathrm{i}\frac{en_i}{2\pi}v_0^2\frac{\lambda_0^2}{4}\sum_{\mathbf{p}\mathbf{p}'}\mathrm{Tr}\left[\frac{\sigma_y}{2}G^R_{\mathbf{p}}\frac{p_x}{m}G^A_{\mathbf{p}}\ [(\mathbf{p}\times\mathbf{p}')_z\sigma_z G^A_{\mathbf{p}'} + G^A_{\mathbf{p}'}(\mathbf{p}'\times\mathbf{p})_z\sigma_z]G^A_{\mathbf{p}}\right]. \tag{4.41}$$

After performing the integration over the momentum $\mathbf{p}'$ and using the expansion of the Green function

in Pauli matrices, we obtain

$$\begin{aligned}\Pi_y^{sj(a+b)} &= \mathrm{i}\frac{e}{4\tau_0}\frac{\lambda_0^2}{4}\frac{1}{2\pi}\sum_{\mathbf{p}} p\left(G_+^A G_-^R - G_-^A G_+^R\right) \\ &= \frac{\lambda_0^2 p_F^2}{4} S_0 \end{aligned} \tag{4.42}$$

with $S_0 = -eN_0\alpha\tau$ and

$$\begin{aligned}\Pi_y^{sj(c+d+e+f)} &= (4)(-i)\frac{e}{4\tau_0}\frac{\lambda_0^2}{4}\frac{\alpha}{2\pi}\sum_{\mathbf{p}} p_x^2 \mathrm{Tr}[\sigma_y G_{\mathbf{p}}^R \sigma_y G_{\mathbf{p}}^R G_{\mathbf{p}}^A] \\ &= \frac{\lambda_0^2 p_F^2}{4} S_0. \end{aligned} \tag{4.43}$$

By collecting the result of all the diagrams, one gets

$$\Pi_y^{sj} = \Pi_y^{sj(a+b)} + \Pi_y^{sj(c+d+e+f)} = 2\frac{\lambda_0^2 p_F^2}{4} S_0. \tag{4.44}$$

Then, recalling that the side-jump spin Hall conductivity reads

$$\sigma_{sj}^{SHE} = -\frac{e}{2\pi}\frac{\lambda_0^2 p_F^2}{4}, \tag{4.45}$$

we finally obtain

$$\sigma_{EC,yx}^{sj} = -2\tau_s m\alpha\sigma_{sj}^{SHE}. \tag{4.46}$$

The above term will then give the following contribution to the ISGE

$$S^y = -2m\alpha\tau_s\sigma_{sj}^{SHE}E_x, \tag{4.47}$$

with the total relaxation rate being $\frac{1}{\tau_s} = \frac{1}{\tau_{EY}} + \frac{1}{\tau_\alpha}$. Note that by identifying the side-jump contribution to the spin Hall current as $J_y^z = \sigma_{sj}^{SHE}E_x$, one obtains the same expression as in Ref. [75] as expected in S^y when extrinsic contributions are explicitly taken into account.

In the following, for the treatment of the skew-scattering effect, we need the third moment of the disorder distribution $\langle V(\mathbf{r}_1)V(\mathbf{r}_2)V(\mathbf{r}_3)\rangle = n_i v_0^3\delta(\mathbf{r}_1-\mathbf{r}_2)\delta(\mathbf{r}_2-\mathbf{r}_3)$. Now we proceed to evaluate the diagrams responsible for the skew-scattering contribution to the bare conductivity. The diagrams in Fig. 4.4 give

$$\Pi_y^{ss(a+b)} = -i\frac{e}{2\pi}v_0^3\frac{\lambda_0^2}{4}\sum_{\mathbf{p}\mathbf{p}'\mathbf{p}''} Tr\left[\frac{\sigma_y}{2}G_{\mathbf{p}}^R[G_{\mathbf{p}'}^R\ G_{\mathbf{p}''}^R\frac{p_x''}{m}G_{\mathbf{p}''}^A(\mathbf{p}''\times\mathbf{p})_z\sigma_z + (\mathbf{p}\times\mathbf{p}')_z\sigma_z G_{\mathbf{p}'}^R\frac{p_x'}{m}G_{\mathbf{p}'}^A G_{\mathbf{p}''}^A]G_{\mathbf{p}}^A\right]. \tag{4.48}$$

Similarly to Eqs. (4.40) and (4.41), after taking the integration over $\mathbf{p}'$ and $\mathbf{p}''$ and using the expansion of the Green function, we can obtain

$$\Pi_{yx}^{ss(a+b)} = i\frac{ev_0 p_F^2}{4m}N_0\frac{\lambda_0^2}{4}\sum_{\mathbf{p}} p\frac{1}{2}(G_-^R G_+^A - G_+^A G_-^R). \tag{4.49}$$

Finally the total skew-scattering contribution for a screened impurity potential gives

$$S^y = -2m\alpha\tau_s\sigma_{ss}^{SHE}E_x, \tag{4.50}$$

$$\sigma_{ss}^{SHE} = e\frac{\lambda_0^2}{4}n\frac{mv_0}{2}p_F l, \tag{4.51}$$

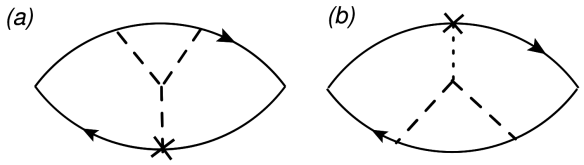

Figure 4.4: Diagrams for the skew-scattering contribution to the Edelstein effect. The cross denotes the correction to the Green function due to spin-orbit scattering.

where σ_{ss}^{SHE} is the spin Hall conductivity associated to the skew-scattering mechanism.

Similar to the side jump, the skew-scattering contribution can be included in the Edelstein conductivity, which amounts to say that $\sigma_{EC,sj}^{yx}$ can be replaced by the sum of both contributions

$$\sigma_{EC,sj}^{yx} \to \sigma_{EC,sj}^{yx} + \sigma_{EC,ss}^{yx}. \tag{4.52}$$

The inclusion of the DSOC is straightforward, although the calculation is lengthy. However, the final result can be guessed by carefully considering the results (4.36) and (4.37). In Eq. (4.36), for instance, one sees that the SOC determines the form of the spin polarization in three respects. First, there is a factor S_α reminiscent of the Edelstein effect in only the RSOC model. Secondly, the DSOC appears only in the specific element of the inverse matrix of the scattering rates. Finally, the factor $1/\tau_\alpha - 1/\tau_\beta$ can be interpreted as due to the intrinsic spin Hall conductivity $\sigma_{int}^{SHE} = (e/8\pi)(2\tau/\tau_\alpha - 2\tau/\tau_\beta)$. For S^x in Eq. (4.37) there is a similar situation with the roles of RSOC and DSOC interchanged. Then, in order to have the side-jump and skew-scattering contributions to the Edelstein conductivity, it is sufficient to replace the intrinsic spin Hall conductivity with $\sigma_{ext}^{SHE} = \sigma_{sj}^{SHE} + \sigma_{ss}^{SHE}$ to read

$$S_{ext}^{y} = \left(\frac{1}{\left(\frac{1}{\tau_\alpha} + \frac{1}{\tau_\beta} + \frac{1}{\tau_{EY}}\right)^2 - \left(\frac{2}{\tau_{\beta\alpha}}\right)^2} \right) \left(S_\alpha \left(\frac{1}{\tau_\alpha} - \frac{1}{\tau_\beta} + \frac{1}{\tau_{EY}}\right) \frac{4\pi}{e\tau} \sigma_{ext}^{SHE} \right) \tag{4.53}$$

and

$$S_{ext}^{x} = \left(\frac{1}{\left(\frac{1}{\tau_\alpha} + \frac{1}{\tau_\beta} + \frac{1}{\tau_{EY}}\right)^2 - \left(\frac{2}{\tau_{\beta\alpha}}\right)^2} \right) \left(S_\beta \left(\frac{1}{\tau_\alpha} - \frac{1}{\tau_\beta} + \frac{1}{\tau_{EY}}\right) \frac{4\pi}{e\tau} \sigma_{ext}^{SHE} \right) \tag{4.54}$$

The sum of Eqs. (4.36) and (4.53) gives the total expression for the Edelstein polarization along the y direction. Similarly Eqs. (4.37) and (4.54) provide the corresponding expression for the polarization along the x direction. The four equations represent then the main result of this chapter. One interesting consequence of these equations is that, by invoking the Onsager reciprocity, along, say the y, direction, should in principle yield a charge current both along the x and y directions, an effect which can be tested experimentally.

Chapter 5

The frequency-dependent inverse spin-galvanic effect

As its title suggests, in this Chapter we will describe the frequency-dependent ISGE in the diffiusive regime. Moreover, we will consider the effect of the interplay of the EY spin relaxation and the ISGE in the presence of intrinsic Rashba-Dresselhaus SOC. Compared to what we did in the previous Chapter, here we show first how two spin-orbit split bands due to the intrinsic SOC modify the EY mechanism and then the frequency dependence of ISGE is considered. In particular, we will find that the size and form of the ISGE is greatly modified by the presence of the various sources of SOC. Indeed, SOC affects the spin relaxation time by adding the EY mechanism to the DP, and, furthermore, it changes the non-equilibrium value of the current-induced spin polarization by introducing a new spin generation torque. For this purpose, we will first formulate the ISGE (the SGE can be obtained similarly by using the Onsager relations) in terms of the Kubo linear response theory. Then we will derive an expression for the ISGE in the presence of the RSOC and extrinsic SOC. This case with no DSOC, which is important by itself, allows the understanding of the origin of the additional spin torque in a situation which is technically simpler to treat with respect to the general case when both RSOC and DSOC are different from zero. We will extend our results to the general case when the both RSOC and DSOC, as well as SOC from impurities, are present. We will show how our result can be seen as the stationary solution of the Bloch equations for the spin dynamics. These results have been published in [56].

5.1 Linear Response Theory at $\omega \neq 0$

In this section, we use the standard Kubo formula of linear response theory to derive the ISGE in the presence of extrinsic and intrinsic SOC. The in-plane spin polarization to linear order in the electric fields is given by

$$S^i = \sigma_{EC}^{ij} E_j, \ i,j = x,y, \tag{5.1}$$

where E_i is the external electric fields with frequency ω and σ_{EC}^{ij} is the frequency-dependent Edelstein conductivity [22] given by Eq. (3.122) for the Kubo formula [91]

$$\sigma_{EC}^{ij}(\omega) = \frac{(-e)}{2\pi}\sum_{\mathbf{p}} \mathrm{Tr}[G^A(\epsilon+\omega)\Upsilon_i(\epsilon,\omega))G^R(\epsilon)J_j], \tag{5.2}$$

where the trace symbol includes the summation over spin indices. We keep the frequency dependence of $\sigma_{EC}^{ij}(\omega)$ in order to obtain the Bloch equations for the spin dynamics. In Eq. (5.2), $\Upsilon_i(\epsilon,\omega)$ is the renormalized spin vertex relative to a polarization along the i-axis, required by the standard series of ladder diagrams of the impurity technique [72, 85], as shown in Fig. 3.4. In the above Eq. (5.2), J_j are the *bare* number current vertices. In the plane-wave basis, their matrix elements from state $\mathbf{p}'$ to state $\mathbf{p}$ read

$$J_x = \delta_{\mathbf{p},\mathbf{p}'}\left(\frac{p_x}{m} - \alpha\sigma_y + \beta\sigma_x\right) + \delta J_{x,\mathbf{pp}'}, \tag{5.3}$$

$$J_y = \delta_{\mathbf{p},\mathbf{p}'}\left(\frac{p_y}{m} + \alpha\sigma_x - \beta\sigma_y\right) + \delta J_{y,\mathbf{pp}'}. \tag{5.4}$$

The latter term $\delta J_{j,\mathbf{pp}'}$ in equations (5.3) and (5.4), which depends explicitly on disorder, is of order λ_0^2 and originates from the extrinsic SOC. Such a term gives rise to the side-jump contribution to the spin Hall effect [24, 26] due to the extrinsic SOC. The side-jump and skew-scattering contributions to the spin Hall effect in the presence of RSOC have been considered in [73–75]. In fact, we have already evaluated both contributions to the Edelstein conductivity in the previous Chapter 3 by using the standard Kubo formula diagrammatic methods. A similar analysis has been carried out within the SU(2) gauge theory formulation in Ref. [75]. For this reason, we will not repeat such an analysis here, where we concentrate instead on the contributions generated by the first term on the right-hand side of equations (5.3) and (5.4).

To examine the problem of the interplay of the EY spin relaxation and the ISGE, let us recall the self-energy derived in Eq. (4.21) within the Born approximation. The self-energy has two contributions due to the spin-independent and spin-dependent scattering [22, 89]

$$\begin{aligned}\Sigma_{tot}^R(\mathbf{p}) &\equiv \Sigma_0^R(\mathbf{p}) + \Sigma_{EY}^R(\mathbf{p}) \\ &= n_i v_0^2 \sum_{\mathbf{p}'} G_{\mathbf{p}'}^R + n_i v_0^2 \frac{\lambda_0^4}{16}\sum_{\mathbf{p}'}\sigma_z G_{\mathbf{p}'}^R \sigma_z (\mathbf{p}\times\mathbf{p}')_z^2,\end{aligned} \tag{5.5}$$

whereas the imaginary part of the first term gives rise to the standard elastic scattering time

$$Im\Sigma_0^R(\mathbf{p}) = -i2\pi N_0 n_i v_0^2 = -\frac{i}{2\tau_0}. \tag{5.6}$$

The second one is responsible for the EY spin relaxation, which can be a function of the Fermi surfaces. From the point of view of the scattering matrix introduced in the previous Chapter (cf. Eq. (3.125)), the two self-energy contributions correspond to the Born approximation for the $|\mathcal{A}|^2$ and $|\mathcal{B}|^2$, respectively. Given the self-energy (5.5), the retarded Green function is also diagonal in momentum space and has the same structure with Eq. (4.19) except that the $G_{\pm}^R(\epsilon) = (\epsilon - \frac{p^2}{2m} \mp \gamma p + \frac{i}{2\tau_{\pm}})^{-1}$ is the Green function corresponding to the two branches in which the energy spectrum splits due to the SOC. The factor $\gamma^2 = \alpha^2 + \beta^2 + 2\alpha\beta\sin(2\phi)$ with $\hat{p}_x = \cos(\phi)$ and $\hat{p}_y = \sin(\phi)$ describes the dependence in momentum space of the SOC, when both RSOC and DSOC are present. Notice that inversion in the two-dimensional

momentum space ($(p_x, p_y) \to (-p_x, -p_y)$) leaves the factor γ invariant, since it corresponds to $\phi \to \phi + \pi$. As a consequence, $G_{x,y} \to -G_{x,y}$, whereas G_0 is invariant. This observation will turn out to be useful later when evaluating the renormalization of the spin vertices. The advanced Green function is easily obtained via the relation $G^A_\pm = (G^R_\pm)^*$. In the expression for $G^R_\pm$, $\frac{1}{2\tau_\pm}$ is a band-dependent time relaxation and plays an important role in our analysis. In order to obtain this term, we note that, after momentum integration over $\mathbf{p}'$ in Eq. (5.5), the imaginary part of the retarded self-energy reads

$$\Sigma^R_\pm = -\mathrm{i}\frac{1}{2\tau_0} - \mathrm{i}\left(\frac{\lambda_0^2}{4}\right)^2 \frac{1}{4\tau_0} p_F^2 p_\pm^2 \equiv -\frac{\mathrm{i}}{2\tau_\pm}. \tag{5.7}$$

Above, we indicate with p_F the Fermi momentum without RSOC and DSOC and with $p_\pm$ the γ-dependent momenta of the two spin-orbit split Fermi surfaces. To the lowest order in the spin-orbit splitting, we have

$$p_\pm = p_F(1 \mp \frac{\gamma}{v_F}), \tag{5.8}$$

where $v_F = p_F/m$. The momentum factors originate from the square of the vector product in the second term of Eq. (5.5). The factor p_F^2 is due to the *inner* $\mathbf{p}'$ momentum, which, upon integration, is eventually fixed at the Fermi surface in the absence of RSOC and DSOC. More precisely, when evaluating the momentum integral, one ends up by summing the contributions of the two spin-orbit split bands in such a way that the α- and β-dependent shift of the two Fermi surfaces cancels out in the sum. However, the outer $\mathbf{p}$ momentum remains unfixed. Its value will be fixed by the poles of the Green function in a successive integration over the momentum. Then, the γ-dependent relaxation times of the two Fermi surfaces read

$$\frac{1}{\tau_\pm} = \frac{1}{\tau}(1 \mp \frac{\tau}{\tau_{EY}}\frac{\gamma}{v_F}), \tag{5.9}$$

where

$$\frac{1}{\tau} = \frac{1}{\tau_0} + \frac{1}{2\tau_{EY}}, \tag{5.10}$$

with the standard expression for the EY spin relaxation rates

$$\frac{1}{\tau_{EY}} = \frac{1}{\tau_0}\left(\frac{\lambda_0 p_F}{2}\right)^4. \tag{5.11}$$

In order to evaluate Eq. (5.2), we need the renormalized spin vertex Υ_i, whose explicit dependence on ϵ and ω has been dropped for simplicity's sake. In the absence of impurity scattering, this vertex has its *bare* form in terms of Pauli matrices as expected for spin operators $\Upsilon_i^{(0)} = \sigma_i$. The superscript "$(0)$" indicates the bare character of the vertex. As shown before, multiple impurity scattering taken into account by ladder diagrams yields the renormalized vertex Υ_i, which, in general, will be a matrix in spin space and can then be represented by an expansion in Pauli matrices,

$$\Upsilon_i = \sum_{\rho=0,1,2,3} \Upsilon_i^\rho \sigma_\rho.$$

For vanishing RSOC or DSOC, symmetry reveals that the renormalized spin vertices share the same matrix structure of the bare ones $\Upsilon_i \sim \sigma_i$, i.e., in this case, the renormalized vertex differs by the bare one just by a factor. This is the case in Eq. (5.16) below. However, when both RSOC and DSOC are present, symmetry arguments again indicate that Υ_x and Υ_y are not simply proportional to σ_x and

σ_y, but acquire both σ_x and σ_y components. By following the standard procedure in Eq. (5.12), after projecting over the Pauli matrix components, the vertex equation reads [89]

$$\Upsilon_i^\rho = \delta_{\rho i} + \frac{1}{2}\sum_{\mu\upsilon\lambda} I_{\mu\upsilon}\mathrm{Tr}[\sigma_\rho\sigma_\mu\sigma_\lambda\sigma_\upsilon]\Upsilon_i^\lambda + \frac{1}{2}\sum_{\mu\upsilon\lambda} J_{\mu\upsilon}\mathrm{Tr}[\sigma_\rho\sigma_z\sigma_\mu\sigma_\lambda\sigma_\upsilon\sigma_z]\Upsilon_i^\lambda, \tag{5.12}$$

where

$$I_{\mu\upsilon} = \frac{1}{2\pi N_0\tau_0}\sum_{\mathbf{p}'} G_\mu^A(\epsilon+\omega)G_\upsilon^R(\epsilon),\ J_{\mu\upsilon} = \frac{\tau_0}{2\tau_{EY}}I_{\mu\upsilon}. \tag{5.13}$$

Once the spin vertices are known, the Edelstein conductivities from Eq. (5.2) can be put in the form

$$\sigma_{EC}^{ij} = \Upsilon_i^\rho\Pi_{\rho j}, \tag{5.14}$$

with the *bare* Edelstein conductivities given by

$$\Pi_{\rho j} = \frac{(-e)}{2\pi}\sum_{\mathbf{p}}\mathrm{Tr}[G^A(\epsilon+\omega)\frac{\sigma_\rho}{2}G^R(\epsilon)J_j]. \tag{5.15}$$

The bare Edelstein conductivities are those one would obtain by neglecting the vertex corrections due to the ladder diagrams. It is useful to point that one could have adopted the alternative route to renormalize the number current vertices and use the bare spin vertices. Indeed, this was the route followed originally by Edelstein [22]. Since the renormalized number of current vertices in the DC zero-frequency limit vanish [72], the evaluation of the Edelstein conductivity reduces to a bubble with bare spin vertices and the current vertices in the absence of RSOC and DSOC.

5.2 Inverse spin-galvanic effect in the Rashba model

To keep the discussion as simple as possible, in this section, we confine first to the case when only RSOC is present. We will derive the spin polarization, S^y, when an external electric field is applied along the x direction. Then, in the next section, we will evaluate the Bloch equation in the more general case when both RSOC and DSOC are present. In the case $\beta = 0$, the renormalized spin vertex Υ^y is simply proportional to σ_y, which means that $\Upsilon^y = \Upsilon_y^y\sigma^y$. Upon the integration over momentum in Eq. (5.12), only I_{00} is non-zero and the other eight possibilities of (μ,ν) in $I_{\mu,\nu}$ are zero. The cases $(0, x/y)$, $(x/y, 0)$, (x, y) and (y, x) vanish because of angle integration, whereas the two other cases (x, x) and (y, y) cancel each other out after taking the trace in Eq. (5.12).

As a result, we finally obtain (in the diffusive approximation $\omega\tau \ll 1$)

$$\Upsilon_y = \Upsilon_y^y\sigma^y = \frac{1}{1 - I_{00} + J_{00}}\sigma^y = \frac{1 - 4i\omega\tau}{\frac{\tau}{\tau_s} - i\omega\tau}\sigma^y, \tag{5.16}$$

where the integral I_{00} has been evaluated in Appendix B

$$I_{00} = \left(\frac{1 - 3i\omega\tau - \frac{\tau}{\tau_\alpha}}{1 - 4i\omega\tau}\right)\left(\frac{\tau}{\tau_0}\right), \tag{5.17}$$

with the total spin relaxation rate being $\frac{1}{\tau_s} = \frac{1}{\tau_{EY}} + \frac{1}{\tau_\alpha}$. Here, $1/\tau_\alpha = (2m\alpha)^2 D$ defines the DP spin relaxation rate due to the RSOC. Notice that, in the absence of SOC, the vertex becomes singular by sending to zero the frequency, signaling the spin conservation in that limit. One sees that the EY and DP

relaxation rates simply add up. This then gives $\sigma^{yx} = \Upsilon_y^y \Pi_{yx}$. Physically, in the zero-frequency limit, the factor $\Upsilon_y^y = \tau_s/\tau$ counts how many impurity scattering events are necessary to relax the spin. In the diffusive regime $\tau_s \gg \tau$, i.e., many impurity scattering events are necessary to erase the memory of the initial spin direction.

By neglecting the contribution from the extrinsic SOC in Eq. (5.3) for the current vertex, the bare conductivity Π_{yx} naturally separates in two terms $\Pi_{yx}^{(A)}$ and $\Pi_{yx}^{(B)}$ due to the components p_x/m and $-\alpha\sigma^y$ of the number current vertex. The expression for $\Pi_{yx}^{(A)}$ reads

$$\begin{aligned}
\Pi_{yx}^{(A)} &= (-e)\frac{1}{2\pi}\sum_{\mathbf{p}} \mathrm{Tr}\left[G^A(\epsilon+\omega)\frac{\sigma^y}{2}G^R(\epsilon)\frac{p_x}{m}\right] \\
&= \frac{e}{4\pi m}\sum_{\mathbf{p}}\frac{p}{2}\left[G_+^A(\epsilon+\omega)G_+^R(\epsilon) - G_-^A(\epsilon+\omega)G_-^R(\epsilon)\right] \\
&= \frac{e}{4m}\left(\frac{p_+N_+}{-i\omega+\frac{1}{\tau_+}} - \frac{p_-N_-}{-i\omega+\frac{1}{\tau_-}}\right). \qquad (5.18)
\end{aligned}$$

In the above $p_\pm$, $N_\pm$ and $\tau_\pm$ refer to the Fermi momentum, density of states and quasiparticle time in the $\pm$-band. To order α/v_F, one has

$$p_\pm = p_F(1 \mp \alpha/v_F),\ N_\pm = N_0(1 \mp \alpha/v_F). \qquad (5.19)$$

By including the contribution of the quasiparticle time in the $\pm$-band from Eq. (5.9), one gets

$$\Pi_{yx}^{(A)} = S_0\left(\frac{1-\frac{\tau}{2\tau_{EY}} - i\omega\tau}{1-2i\omega\tau}\right), \qquad (5.20)$$

where $S_0 = -eN_0\alpha\tau$. The evaluation of $\Pi_{yx}^{(B)}$ is more direct. It gives

$$\begin{aligned}
\Pi_{yx}^{(B)} &= \frac{e\alpha}{2\pi}\sum_{\mathbf{p}}\mathrm{Tr}\left[G^A(\epsilon+\omega)\frac{\sigma^y}{2}G^R(\epsilon)\sigma^y\right] \\
&= \frac{e\alpha}{2\pi}\sum_{\mathbf{p}}\left(G_0^A(\epsilon+\omega)G_0^R(\epsilon)\right) \\
&= -S_0\left(\frac{1-\frac{\tau}{\tau_\alpha} - 3i\omega\tau}{1-4i\omega\tau}\right). \qquad (5.21)
\end{aligned}$$

Combining both contributions with accuracy up to order $\omega\tau$ gives

$$\Pi_{yx} = \Pi_{yx}^{(A)} + \Pi_{yx}^{(B)} = S_0\left(\frac{\frac{\tau}{\tau_\alpha} - \frac{\tau}{2\tau_{EY}}}{1-6i\omega\tau}\right). \qquad (5.22)$$

By combining the vertex correction Eq. (5.16) and the bare conductivity Π_{yx} in Eq. (5.14), we get the following contribution to the frequency-dependent spin polarization

$$(S^y)^{(1)} = \left(\frac{1}{\frac{\tau}{\tau_s} - i\omega\tau}\right)\left(\frac{1-4i\omega\tau}{1-6i\omega\tau}\right)S_\alpha^x\left(\frac{\tau}{\tau_\alpha} - \frac{\tau}{2\tau_{EY}}\right), \qquad (5.23)$$

with $S_\alpha^x = -eN_0\alpha\tau E_x$. This is not the full story yet, as we are going to explain. What we have learned up to now is that the momentum dependence of the EY self-energy on the two spin-split Fermi surfaces yields an extra term to the Edelstein polarization. Such a momentum dependence can also modify the vertex corrections–the integrals $J_{\mu\upsilon}$ in Eq. (5.13)–which lead to the renormalized spin vertex. To appreciate this aspect, we notice that, in evaluating such integrals in the absence of the RSOC, the moduli of $\mathbf{p}$ and $\mathbf{p}'$

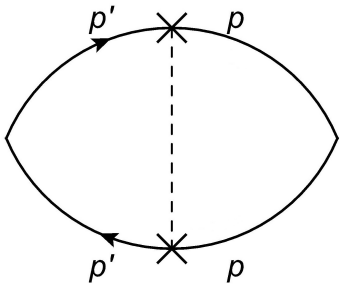

Figure 5.1: The diagram needed to evaluate the extra vertex correction to the ISGE due to extrinsic SOC. The left and right vertices denote the spin vertex S^y and the component (p_x/m) of the number current vertex J_x, whereas the crosses on the top and bottom Green functions line stand for $-i(\lambda_0^2/4)\mathbf{p}' \times \mathbf{p}$ and $-i(\lambda_0^2/4)\mathbf{p} \times \mathbf{p}'$, respectively.

are taken at the Fermi surface in the absence of spin splitting. We emphasize that taking into account the momentum dependence on the Rashba-split Fermi surfaces one instead gets an extra contribution. Consider the diagram of Fig. 5.1. After integration over $\mathbf{p}'$, the left side of the diagram gives

$$-\frac{(\lambda_0^2/4)^2 p_F^2 p^2}{2\tau_0}\tau = -\frac{\tau}{2\tau_{EY}}\frac{p^2}{p_F^2}.$$

If we set $p = p_F$, we would recover the standard diagrammatic calculation in the absence of intrinsic RSOC. By combining the above left side with the rest of the diagram, one gets an additional contribution to the bare conductivity

$$\begin{aligned}(\delta\Pi) &= -\frac{\tau}{2\tau_{EY}}\left(-\frac{e}{2\pi}\sum_{\mathbf{p}}\frac{p^2}{p_F^2}\mathrm{Tr}\left[G^A(\epsilon+\omega)\frac{\sigma^y}{2}G^R(\epsilon)\frac{p_x}{m}\right]\right) \\ &= \frac{-\tau}{2\tau_{EY}}\left(\frac{e}{4mp_F^2}\right)\left(\frac{p_+^3 N_+}{-i\omega+\frac{1}{\tau_+}} - \frac{p_-^3 N_-}{-i\omega+\frac{1}{\tau_-}}\right). \end{aligned} \tag{5.24}$$

To this expression, we must subtract the one obtained by replacing $p = p_F$, which is already accounted for in the ladder summation. Hence, the extra vertex part $(\delta\Pi)$ modifies the spin polarization to give the second contribution

$$(S^y)^{(2)} = \frac{1}{\left(\frac{\tau}{\tau_s} - i\omega\tau\right)}\left(\frac{1-4i\omega\tau}{1-6i\omega\tau}\right)S_\alpha^x\left(-\frac{\tau}{2\tau_{EY}}\right). \tag{5.25}$$

Hence, by summing the above result with Eq. (5.23), the total spin polarization reads

$$S^y = \frac{1}{\left(\frac{1}{\tau_s} - i\omega\right)}\left(1+\frac{2i\omega\tau}{1-6i\omega\tau}\right)S_\alpha^x\left(\frac{1}{\tau_\alpha}-\frac{1}{\tau_{EY}}\right) \approx \frac{1}{\left(\frac{1}{\tau_s} - i\omega\right)}S_\alpha^x\left(\frac{1}{\tau_\alpha}-\frac{1}{\tau_{EY}}\right). \tag{5.26}$$

In the diffusive regime, terms in $\omega\tau$ in the second round brackets on the right-hand side of Eq. (5.26), which are responsible for higher-order frequency dependence, can be neglected. In the zero-frequency limit, Eq. (5.26) has two main contributions described by the two terms in the last round brackets. The first term is responsible for the Edelstein result [22] due to the intrinsic SOC, whereas the second one, which arises to order λ_0^4, is an additional contribution to the spin polarization due to the extrinsic SOC. In the Rashba model without extrinsic SOC, only the first term is present, and, indeed, Eq. (5.26) reduces

to it when $\lambda_0 = \omega = 0$. After Fourier transforming, the above equation can be written in the form of the Bloch equation

$$\partial_t S^y = -\left(\frac{1}{\tau_\alpha} + \frac{1}{\tau_{EY}}\right) S^y + \left(\frac{1}{\tau_\alpha} - \frac{1}{\tau_{EY}}\right) S^x_\alpha. \tag{5.27}$$

The terms on the right-hand side describe the various torques controlling the spin dynamics. The first term, which includes DP and EY contributions, is the spin relaxation torque, whereas the second term represents the spin generation torque. The above result coincides with that obtained in Chapter 4 (cf. Eq. (4.36)) if the extra term $(-1/\tau_{EY})$ in the spin generation torque is not considered. In the next section, we will generalize this result to the more general case when both RSOC and DSOC are present.

5.3 Inverse spin-galvanic effect in the Rashba-Dresselhaus model

As we have seen in the previous Section, the size and form of the ISGE is greatly modified by the presence of the EY spin relaxation due to the extrinsic SOC. To analyze this fact more generally, we focus here on the model with RSOC and DSOC as well as SOC from impurities. In order to evaluate Eq. (5.2) for the Edelstein conductivity, we need the renormalized spin vertex Υ_i. For vanishing RSOC or DSOC, the renormalized spin vertices share the same matrix structure of the bare ones $\Upsilon_i \sim \sigma_i$. However, when both RSOC and DSOC are explicitly taken into account, Υ_x and Υ_y are not only simply proportional to σ_x and σ_y, but also acquire components on both σ_x and σ_y. By following the procedure shown in Eq. (5.12) and upon integration over momentum, the vertex equation for Υ_y reduces to

$$\begin{pmatrix} 1 - I_{00} + J_{00} & -2(I_{yx} - J_{yx}) \\ -2(I_{xy} - J_{xy}) & 1 - I_{00} + J_{00} \end{pmatrix} \begin{pmatrix} \Upsilon^y_y \\ \Upsilon^x_y \end{pmatrix} = \begin{pmatrix} 1 \\ 0 \end{pmatrix}, \tag{5.28}$$

while that forΥ_x is

$$\begin{pmatrix} 1 - I_{00} + J_{00} & -2(I_{xy} - J_{xy}) \\ -2(I_{yx} - J_{yx}) & 1 - I_{00} + J_{00} \end{pmatrix} \begin{pmatrix} \Upsilon^y_x \\ \Upsilon^x_x \end{pmatrix} = \begin{pmatrix} 0 \\ 1 \end{pmatrix}, \tag{5.29}$$

where

$$\begin{aligned} 1 - I_{00} + J_{00} &\simeq \left(\frac{-i\omega + \langle \frac{1}{\tau_\gamma} \rangle + \frac{1}{\tau_{EY}}}{1 - 4i\omega\tau}\right)\tau \\ -2(I_{xy} - J_{xy}) &\simeq \left(\frac{1 - i\omega\tau}{1 - 4i\omega\tau}\right)\left(1 - \frac{\tau}{\tau_{EY}}\right)\frac{2\tau}{\tau_{\alpha\beta}}, \end{aligned} \tag{5.30}$$

where $\langle \dots \rangle$ indicated the average over the momentum directions. The technical points of the calculation in Eq. (5.30) are given in Appendix B. In the diffusive regime, $\frac{1}{\tau_\gamma} = (2m\gamma)^2 D$ and $\frac{1}{\tau_{\alpha\beta}} = (2m)^2 \alpha\beta D$ are the DP relaxation rates due to the total intrinsic spin-orbit strength and the interplay of RSOC/DSOC, respectively. For vanishing DSOC, Eq. (5.30) reduces to the same expression in Eq. (5.16) as expected in the Rashba model. However, with both RSOC and DSOC, spin relaxation is anisotropic and one needs to diagonalize the matrix on the left-hand side of equations (5.28) and (5.29). Such a matrix then identifies the spin eigenmodes. Having in mind to derive the Bloch equations governing to spin dynamics, we rewrite Eq. (5.1) by using Eq. (5.14)

$$\begin{pmatrix} S^x \\ S^y \end{pmatrix} = \begin{pmatrix} \Upsilon^x_x & \Upsilon^y_x \\ \Upsilon^x_y & \Upsilon^y_y \end{pmatrix} \sum_j \begin{pmatrix} \Pi_{xj} \\ \Pi_{yj} \end{pmatrix} E_j, \tag{5.31}$$

where, by virtue of equations (5.28) and (5.29),

$$\begin{pmatrix} \Upsilon_x^x & \Upsilon_y^x \\ \Upsilon_x^y & \Upsilon_y^y \end{pmatrix}^{-1} = \frac{\tau}{1-4i\omega\tau} \begin{pmatrix} -i\omega + \langle \frac{1}{\tau_\gamma} \rangle + \frac{1}{\tau_{EY}} & \frac{2}{\tau_{\alpha\beta}}(1-i\omega\tau) \\ \frac{2}{\tau_{\alpha\beta}}(1-i\omega\tau) & -i\omega + \langle \frac{1}{\tau_\gamma} \rangle + \frac{1}{\tau_{EY}} \end{pmatrix}. \tag{5.32}$$

In the diffusive regime, we can safely neglect the factor $\omega\tau$ with respect to unity in the denominator in front of the matrix and in the off diagonal elements of the matrix. The quantities $\Pi_{\rho j}$ appearing on the right-hand side of Eq. (5.31) can be evaluated by standard techniques. However, some care is required when evaluating the momenta due to the extrinsic SOC at the spin-split Fermi surfaces. The final result for the bare conductivities reads

$$\Pi_{xx} = \frac{-\tau S_\beta^x}{1-6i\omega\tau} \langle \frac{1}{\tau_\gamma} - \frac{1}{\tau_{EY}} - \frac{2}{\tau_\gamma}\frac{\alpha^2}{\gamma^2} \rangle, \tag{5.33}$$

$$\Pi_{xy} = \frac{-\tau S_\alpha^y}{1-6i\omega\tau} \langle \frac{1}{\tau_\gamma} - \frac{1}{\tau_{EY}} - \frac{2}{\tau_\gamma}\frac{\beta^2}{\gamma^2} \rangle, \tag{5.34}$$

$$\Pi_{yx} = \frac{\tau S_\alpha^x}{1-6i\omega\tau} \langle \frac{1}{\tau_\gamma} - \frac{1}{\tau_{EY}} - \frac{2}{\tau_\gamma}\frac{\beta^2}{\gamma^2} \rangle, \tag{5.35}$$

$$\Pi_{yy} = \frac{\tau S_\beta^y}{1-6i\omega\tau} \langle \frac{1}{\tau_\gamma} - \frac{1}{\tau_{EY}} - \frac{2}{\tau_\gamma}\frac{\alpha^2}{\gamma^2} \rangle, \tag{5.36}$$

with

$$S_\beta^x = -eN_0\tau\beta E_x, \tag{5.37}$$

$$S_\alpha^y = -eN_0\tau\alpha E_y, \tag{5.38}$$

$$S_\alpha^x = -eN_0\tau\alpha E_x, \tag{5.39}$$

$$S_\beta^y = -eN_0\tau\beta E_y. \tag{5.40}$$

We take the angular average over the DP relaxation rates in Eqs. (5.32-5.36)

$$\int_0^{2\pi} \frac{d\phi}{2\pi}\frac{1}{\tau_\gamma} = \frac{1}{\tau_\alpha} + \frac{1}{\tau_\beta}, \tag{5.41}$$

$$(-2)(\alpha^2 \text{ or } \beta^2)\int_0^{2\pi} \frac{d\phi}{2\pi}\frac{1}{\tau_\gamma}\frac{1}{\gamma^2} = \frac{-2}{\tau_\alpha} \text{ or } \frac{-2}{\tau_\beta}, \tag{5.42}$$

where $\frac{1}{\tau_\alpha} = (2m\alpha)^2 D$, $\frac{1}{\tau_\beta} = (2m\beta)^2 D$ are the DP relaxation rates due to RSOC and DSOC in the diffusive approximation. By inserting the above expression into Eqs. (5.33-5.36) and vertex correction in Eq. (5.32) and using Eq. (5.31), we may write the expression of the ISGE components in a form reminiscent of the Bloch equations

$$\begin{pmatrix} -i\omega + \frac{1}{\tau_\alpha} + \frac{1}{\tau_\beta} + \frac{1}{\tau_{EY}} & \frac{2}{\tau_{\alpha\beta}} \\ \frac{2}{\tau_{\alpha\beta}} & -i\omega + \frac{1}{\tau_\alpha} + \frac{1}{\tau_\beta} + \frac{1}{\tau_{EY}} \end{pmatrix} \begin{pmatrix} S^x \\ S^y \end{pmatrix} = \begin{pmatrix} -S_\alpha^y(\frac{1}{\tau_\alpha} - \frac{1}{\tau_\beta} - \frac{1}{\tau_{EY}}) - S_\beta^x(\frac{-1}{\tau_\alpha} + \frac{1}{\tau_\beta} - \frac{1}{\tau_{EY}}) \\ S_\alpha^x(\frac{1}{\tau_\alpha} - \frac{1}{\tau_\beta} - \frac{1}{\tau_{EY}}) + S_\beta^y(\frac{-1}{\tau_\alpha} + \frac{1}{\tau_\beta} - \frac{1}{\tau_{EY}}) \end{pmatrix} \tag{5.43}$$

Indeed, by performing the anti-Fourier transform with respect to the frequency ω, Eq. (5.43) can be written as

$$\partial_t \mathbf{S} = -(\hat{\Gamma}_{DP} + \hat{\Gamma}_{EY})\mathbf{S} + (\hat{\Gamma}_{DP} - \hat{\Gamma}_{EY})\frac{N_0}{2}\mathbf{B}, \tag{5.44}$$

where $\mathbf{B}$ represents the internal SOC field induced by the electric current. The $\hat{\Gamma}_{DP}$ and $\hat{\Gamma}_{EY}$ are the DP and EY relaxation matrix

$$\mathbf{B} = 2e\tau \begin{pmatrix} \beta E_x + \alpha E_y \\ -(\alpha E_x + \beta E_y) \end{pmatrix}, \hat{\Gamma}_{DP} = \begin{pmatrix} \frac{1}{\tau_\alpha} + \frac{1}{\tau_\beta} & \frac{2}{\tau_{\alpha\beta}} \\ \frac{2}{\tau_{\alpha\beta}} & \frac{1}{\tau_\alpha} + \frac{1}{\tau_\beta} \end{pmatrix}, \hat{\Gamma}_{EY} = \begin{pmatrix} \frac{1}{\tau_{EY}} & 0 \\ 0 & \frac{1}{\tau_{EY}} \end{pmatrix}. \tag{5.45}$$

Equation (5.44) is the main result of the present Chapter. It shows that the intrinsic and extrinsic SOC act in parallel as far as relaxation to the equilibrium state is concerned, i.e., the DP and EY spin relaxation matrices add up. However, as far as the spin generation torques are concerned, DP and EY processes have opposite signs. One should notice that the spin generation torque due to SJ and SS processes discussed diagrammatically in Eqs. (4.53-4.54) must also be taken into account. This is simply obtained by multiplying the DP relaxation matrix $\hat{\Gamma}_{DP}$ in the second term on the right-hand side of Eq. (5.44) by the factor $1 + \theta^{sH}_{ext}/\theta^{sH}_{int}$, where θ^{sH}_{ext} and θ^{sH}_{int} are the spin Hall angles for extrinsic and intrinsic SOC.

The extrinsic spin Hall angle can be derived from Eq. (4.52) for the SJ and SS contributions. To develop some quick intuition, one may notice that again for $\beta = \lambda_0 = 0$ and $E_y = \omega = 0$, Eq. (5.43) reproduces the Edelstein result for the Rashba model obtained in Eq. (4.1). Furthermore, when also $\omega \neq 0$, it reproduces the frequency-dependent spin polarization for the Rashba model as shown in the previous section. When $\lambda_0 \neq 0$ and $\beta = 0$, we see that the ISGE, due to the interplay of the extrinsic and intrinsic SOC, gets an additional spin torque, suggesting that the EY spin-relaxation is detrimental to the Edelstein effect. The diagrammatic analysis reported here provides the following interpretation. The EY spin relaxation depends on the Fermi momentum. When there are two Fermi surfaces with different Fermi momenta, the one with the smaller momentum undergoes less spin relaxation of the EY type than the one with larger momentum. On the other hand, the ISGE arises precisely because there is an unbalance among the two Fermi surfaces with respect to spin polarization. For a given momentum direction, the larger Fermi surface contributes more to the Edelstein polarization than the smaller Fermi surface. Hence, the combination of these two facts suggests a negative effect from the interplay of Edelstein effect and EY spin relaxation. By neglecting the EY relaxation, one sees that the DP terms can cancel each other out if the RSOC and DSOC strengths are equal. This cancellation or anisotropy of the spin accumulation has been obtained in Eqs. (4.36-4.37) for the Bloch equations in the absence of the interplay of EY spin relaxation and the ISGE. As mentioned before, this cancellation could be used to determine the absolute values of the RSOC and DSOC strengths under spatial combination of spin dependent relaxation.

In accordance with the experimental observations of Ref. [65], our results show that the current-induced spin polarization does not align along the internal magnetic field $\mathbf{B}$ due to the SOC. According to Eq. (5.44), this may occur due to the presence of the extrinsic SOC both in the spin relaxation torque and in the spin generation torque. Indeed, when the extrinsic SOC is absent, the spin polarization must necessarily align along the $\mathbf{B}$ field. Hence, our theory could, in principle, provide a method to measure the relative strength of intrinsic and extrinsic SOC.

Chapter 6

Theory of current-induced spin polarizations in an electron gas: SU(2) approach

In this Chapter, the derivation is based on the SU(2) gauge-field formulation of the Rashba-Dresselhaus SOC. Our main goal is to identify a new spin-generation torque arising from EY scattering, which was already derived in the previous Chapter 5 by using the diagrammatic Kubo formula. One of the aims to use the SU(2) approach is to present the same physical phenomena from different view points. However this method has advantages with respect to the linear response theory by allowing the non-linear situation to be considered.

More precisely, according to our derivation in Chapter 3 concerning the kinetic equation in the presence of RSOC and DSOC, we derive the Bloch equations when only intrinsic SOC is present. Then we present a rigorous derivation of the Bloch equations, including the corrections arising from extrinsic effects. Here we obtain the crucial new spin-generation torque arising from the EY process, and discuss its implications for the ISGE/EE and SGE/IEE in specific experimental setups. Finer details concerning the calculation of the collision integral are provided in Appendix C. These results have been published in [37].

6.1 The "intrinsic" Bloch equations

As shown in [36], the spin density and spin current density defined by

$$\begin{aligned} S^a(\mathbf{r},t) &= \sum_{\mathbf{p}} \mathrm{Tr}\left[f(\mathbf{p},\mathbf{r},t)\frac{\sigma^a}{2}\right], \\ J_i^a(\mathbf{r},t) &= \sum_{\mathbf{p}} \frac{p_i}{m}\mathrm{Tr}\left[f(\mathbf{p},\mathbf{r},t)\frac{\sigma^a}{2}\right], \end{aligned} \tag{6.1}$$

obey a continuity-like equation

$$\tilde{\partial}_t S^a + \tilde{\partial}_i J_i^a = 0. \tag{6.2}$$

which was already derived in Eq. (3.55). After making explicit the covariant derivatives according to (3.50), the continuity-like equation (6.2) becomes

$$\partial_t S^a + \epsilon_{abc} e\Psi^b S^c + \nabla_i J_i^a - \epsilon_{abc} e\mathcal{A}_i^b J_i^c = 0. \tag{6.3}$$

Here ϵ_{abc} is the fully antisymmetric Ricci tensor. The second term in Eq. (6.3) is the standard *precession* term due to the Zeeman term (3.28). The last term of (6.3) can be made explicit by providing the expression for the spin current J_i^a, where the lower (upper) index indicates the space (spin) component. In Eq. (3.85) the expression of J_i^a was derived via a microscopic theory in the diffusive regime [36, 71]. The expression reads

$$J_i^a = v_i S^a - D(\nabla_i S^a - \epsilon_{abc} e\mathcal{A}_i^b S^c) - \frac{e\tau n}{4m}(\mathcal{E}_i^a + \epsilon_{ijk} v_j \mathcal{B}_k^a) \tag{6.4}$$

where $v_i = -\frac{e\tau}{m} E_i$ is the average drift velocity of electrons driven by the external electric field. As explained in Chapter 3, all the terms in Eq. (6.4) have a specific physical origin. The first is a *drift* term, containing the spin density S^a carried by the electrons drifted by the electric field E_i. The second is a *diffusion* term that contains two contributions: (i) the standard diffusion current proportional to $\nabla_i S^a$, and (ii) the contribution originating from the gauge-field part of the covariant derivative (3.50) acting on the spin density. The third term corresponds the *SU(2) drift* current driven by the spin-dependent force of Eq. (3.53). In particular the second contribution in this term yields the spin *Hall* coupling due to the SU(2) magnetic field $\mathcal{B}_i^a$.

Because of non Abelian nature of the SU(2) gauge group the corresponding magnetic and electric fields can be nonzero even for spatially homogeneous potentials provided their components are not commuting. In this important special case the SU(2) magnetic and electric fields are determined by the commutator term in Eq. (3.51) (cf., also Eqs. (25-30) in [36])

$$\epsilon_{ijk}\mathcal{B}_k^a = -\epsilon_{abc} e\mathcal{A}_i^b \mathcal{A}_j^c, \tag{6.5}$$

$$\mathcal{E}_i^a = \epsilon_{abc} e\mathcal{A}_i^b \Psi^c. \tag{6.6}$$

Using this representation for the fields and recalling the Einstein relation $\frac{\tau n}{m} = D\frac{\partial n}{\partial \mu} \equiv 4D\chi$ one can combine the gauge potential-dependent terms in Eq. (6.4) into a single item, and rewrite the expression for the spin current in the following compact form

$$J_i^a = v_i S^a - D\nabla_i S^a + D\epsilon_{abc} e\mathcal{A}_i^b (S^c - \chi\Omega^c) \tag{6.7}$$

where $\mathbf{\Omega}$ is the total magnetic field introduced by

$$\Omega^a = e\Psi^a - e\mathcal{A}_k^a v_k \equiv \Delta^a + B^a. \tag{6.8}$$

Here $\mathbf{\Delta}$ is the usual Zeeman field defined after Eq. (3.28) for the external magnetic field and $\mathbf{B}$ represents the internal SOC field induced by the electric current (electric field)

$$B^a = -e\mathcal{A}_k^a v_k = \frac{e\tau}{m} e\mathcal{A}_k^a E_k. \tag{6.9}$$

Now the Bloch equation describing the global spin dynamics in the presence of intrinsic SOC can be derived by assuming a homogeneous spin density ($\nabla_i \mathbf{S} = 0$) and substituting the spin current of Eq. (6.7)

into Eq. (6.3). The resulting equation reads

$$\partial_t S^a = -(\mathbf{\Omega} \times \mathbf{S})^a - \hat{\Gamma}^{ab}_{DP} \left(S^b - \chi \Omega^b \right), \tag{6.10}$$

where Ω^a is given by Eq. (6.8) and the DP relaxation tensor $\hat{\Gamma}^{ab}_{DP}$ is defined as follows

$$\hat{\Gamma}^{ab}_{DP} = e^2 D \epsilon_{afc} \epsilon_{bdc} \mathcal{A}^d_i \mathcal{A}^f_i = e^2 D \left(\delta^{ab} \mathcal{A}^c_i \mathcal{A}^c_i - \mathcal{A}^a_i \mathcal{A}^b_i \right). \tag{6.11}$$

Equation (6.10) generalizes Eq. (4.7) of Section 4.2 to the case of arbitrary intrinsic SOC. It is worth noticing that in the present formalism the DP relaxation arises as the *second order* covariant derivative (the covariant Laplacian). One needs to act twice with the gauge field to get the quadratic dependence on the SOC in the spin relaxation matrix.

The second term on the right hand side of the Bloch equation (6.10) corresponds to the intrinsic torque $\mathcal{T}^a_{int}$ for generic SOC. The part of $\mathcal{T}^a_{int}$ proportional to the internal SO field $\mathbf{B}$ (6.9) can be recognized as the spin generation torque

$$\mathcal{T}^a_{int,sg} = \hat{\Gamma}^{ab}_{DP} B^b = e^4 D \frac{\tau}{m} \mathcal{A}^b_i (\mathcal{A}^b_i \mathcal{A}^a_k - \mathcal{A}^b_k \mathcal{A}^a_i) E_k. \tag{6.12}$$

The intrinsic spin generation torque $\mathcal{T}^a_{int,sg}$ is given by the covariant divergence of the spin Hall current, that is the very last term proportional to $\mathcal{B}_k$ in Eq. (6.4). Therefore the spin generation torque vanishes for the configurations of the gauge potentials with vanishing SU(2) magnetic field. These configurations correspond to a so-called pure gauge SOC for which different space components of the SU(2) potential are commuting and the intrinsic spin Hall effect is absent. Our results imply that in this situation the current-induced spin polarization is also absent.

It is instructive to write explicitly the above general formulas for the specific form of the vector potential of Eq. (3.27) corresponding to the Rashba-Dresselhaus SOC. In this case the SU(2) magnetic field has only one nonzero component

$$e\mathcal{B}^z_z = -e\mathcal{F}^a_{xy} = (2m\beta)^2 - (2m\alpha)^2. \tag{6.13}$$

As the SU(2) magnetic field determines the spin Hall coupling it can be expressed in terms of the spin Hall angle for the intrinsic SOC defined by

$$\theta^{int}_{SH} = m\tau(\beta^2 - \alpha^2) = \frac{e\tau \mathcal{B}^z_z}{4m}. \tag{6.14}$$

The expression for the spin Hall angle has a suggestive interpretation by recalling the classical Hall effect where the coupling between the mutually orthogonal charge currents is given by the product of the cyclotron frequency and the scattering time $\omega_c \tau = eB_{exter}\tau/m$. In the present case to get the spin Hall angle (6.14) one needs to combine the SU(2) cyclotron frequency $e\mathcal{B}^z_z/(4m)$ with the scattering time τ. An intuitive way to understand the origin of the factor of 4 in the denominator of the SU(2) cyclotron frequency is the following. Let us imagine that spin up and spin down particles undergo the ordinary Hall effect in opposite directions with a spin-dependent magnetic field, $j^{\uparrow}_y = (\tau/m) B^{\uparrow} j^{\uparrow}_x$ and $j^{\downarrow}_y = -(\tau/m) B^{\downarrow} j^{\downarrow}_x$. By defining the spin current as $J^z_y = (j^{\uparrow}_y - j^{\downarrow}_y)/2$ and identifying $B^{\uparrow} = -B^{\downarrow} = \mathcal{B}^z_z/2$, one immediately finds the "SU(2)" cyclotron frequency $e\mathcal{B}^z_z/(4m)$.

By introducing further an in-plane Zeeman field $e\Psi^x \equiv \Delta^x$ and $e\Psi^y \equiv \Delta^y$, we find that the only nonzero components of the SU(2) electric field are

$$e\mathcal{E}_x^z = \Delta_x 2m\alpha + \Delta_y 2m\beta \tag{6.15}$$

$$e\mathcal{E}_y^z = \Delta_x 2m\beta + \Delta_y 2m\alpha. \tag{6.16}$$

In this case the total magnetic field $\mathbf{\Omega}$ of Eq. (6.8) also has only in-plane components

$$\Omega^x = \Delta^x + B^x \tag{6.17}$$

$$\Omega^y = \Delta^y + B^y \tag{6.18}$$

with the internal SO field $\mathbf{B}$ (6.9) of the form

$$B^x = 2e\tau(\beta E_x + \alpha E_y) \tag{6.19}$$

$$B^y = -2e\tau(\alpha E_x + \beta E_y). \tag{6.20}$$

The general DP relaxation matrix $\hat{\Gamma}_{DP}$ of Eq. (6.11) entering Eq. (6.10) simplifies as follows

$$\hat{\Gamma}_{DP} = \begin{pmatrix} \tau_\alpha^{-1} + \tau_\beta^{-1} & 2\tau_{\alpha\beta}^{-1} & 0 \\ 2\tau_{\alpha\beta}^{-1} & \tau_\alpha^{-1} + \tau_\beta^{-1} & 0 \\ 0 & 0 & 2(\tau_\alpha^{-1} + \tau_\beta^{-1}) \end{pmatrix} \tag{6.21}$$

where $\tau_\alpha^{-1} = (2m\alpha)^2 D$, $\tau_\beta^{-1} = (2m\beta)^2 D$ and $\tau_{\alpha\beta}^{-1} = (2m)^2 \alpha\beta D$. One should remember that the above equation has the same form with Eq. (5.45) for the DP spin relaxation rates.

Notice that for $\beta = 0$ the matrix $\hat{\Gamma}_{DP}$ becomes diagonal, and τ_α reduces to the DP relaxation time introduced in Eq. (4.6). Finally, the spin generation torque reads

$$\begin{aligned} \boldsymbol{\mathcal{T}}_{int,sg} &\equiv \hat{\Gamma}_{DP}\chi\mathbf{B} \\ &= -2m\theta_{SH}^{int}(-2eN_0D) \begin{pmatrix} -\alpha E_y + \beta E_x \\ -\beta E_y + \alpha E_x \\ 0 \end{pmatrix}. \end{aligned} \tag{6.22}$$

The above equation generalizes the spin generation torque introduced in Eq. (4.8) to the case of RSOC and DSOC for arbitrary direction of the electric field.[1] In agreement with the general discussion after Eq. (6.12) the spin generation torque is proportional to the spin Hall angle. Therefore, it vanishes for SOC giving $\theta_{SH}^{int} = 0$ which in the present case corresponds to the compensated RSOC and DSOC with $\alpha = \pm\beta$.

The meaning of Eq. (6.10) is that, under stationary conditions, $\mathbf{S} = \chi\mathbf{\Omega}$, provided the spin Hall angle is nonzero. This implies that the spin polarization follows the total magnetic field and (for an energy-independent scattering time [36]) there can be no out-of-plane spin polarization since $\mathbf{\Omega}$ lays in the xy plane. This is no longer the case when one considers the extrinsic SOC as will be shown in the following Section.

[1]Notice that $\boldsymbol{\mathcal{T}}_{int,sg}$ corresponds to γ in the notations of Ref. [65], however we will consider it in the next Chapter.

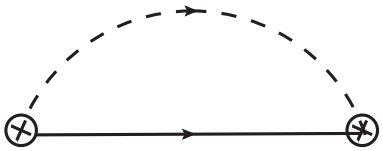

Figure 6.1: Self-energy diagram in second order in the spin-orbit impurity potential, shown as a crossed empty dot, contributing to the EY spin relaxation.

6.2 The effects of extrinsic SOC

The interplay of intrinsic and extrinsic SOC was investigated previously in [71, 73, 74, 89]. According to the analysis therein Eq. (6.10) acquires two modifications. The first, to order λ_0^2, is an additional contribution to the spin Hall coupling in the third term in expression (6.4) for the spin current. This arises from the inclusion of side-jump and skew-scattering effects due to the extrinsic SOC, as derived in Chapter 4 and leads to a renormalization of the spin Hall angle in the expression of the spin generation torque in Eq. (6.22)

$$\theta_{SH}^{int} \to \theta_{SH} = \theta_{SH}^{int} + \theta_{SH}^{ext}. \tag{6.23}$$

The second term, which arises to order λ_0^4, is an additional contribution to the spin relaxation matrix (the EY spin relaxation). In fact, there exists, to the same order λ_0^4, a third *new* contribution, which will be derived in detail in the following way.

To see how the new contribution arises, we focus on the term of order λ_0^4 in the self-energy, whose Feynman diagram is shown in Fig. 6.1 and whose expression reads

$$\check{\Sigma}_{EY}(\mathbf{p}) \quad = \quad n_i \sum_{\mathbf{p}'} \hat{V}_{\mathbf{p},\mathbf{p}'} \check{G}_{\mathbf{p}'} \hat{V}_{\mathbf{p}',\mathbf{p}}, \tag{6.24}$$

where $\hat{V}_{\mathbf{p},\mathbf{p}'}$ is the spin-dependent part of the impurity scattering amplitude

$$\hat{V}_{\mathbf{p},\mathbf{p}'} = iv_0(\lambda_0/2)^2(\mathbf{p}\times\mathbf{p}')\cdot\boldsymbol{\sigma}. \tag{6.25}$$

Shifting the self-energy of Eq. (6.24) according to SU(2) shifts (3.44-3.45) yields the locally covariant EY self-energy

$$\tilde{\check{\Sigma}}_{EY} = \tilde{\check{\Sigma}}_{EY}^{(0)} + \tilde{\check{\Sigma}}_{EY}^{(1)}. \tag{6.26}$$

In Eq. (6.26), we separated the term responsible for the EY relaxation

$$\tilde{\check{\Sigma}}_{EY}^{(0)} = n_i \sum_{\mathbf{p}'} \hat{V}_{\mathbf{p},\mathbf{p}'} \tilde{\check{G}}_{\mathbf{p}'} \hat{V}_{\mathbf{p}',\mathbf{p}} \tag{6.27}$$

from that giving rise to the new contribution

$$\tilde{\check{\Sigma}}_{EY}^{(1)} = \frac{n_i}{2} \sum_{\mathbf{p}'} (\hat{V}_{\mathbf{p},\mathbf{p}'} \{\mathcal{A}_k, \partial_{p_k'} \tilde{\check{G}}_{\mathbf{p}'}\} \hat{V}_{\mathbf{p}',\mathbf{p}} - \{\mathcal{A}_k, \partial_{p_k} \hat{V}_{\mathbf{p},\mathbf{p}'} \tilde{\check{G}}_{\mathbf{p}'} \hat{V}_{\mathbf{p}',\mathbf{p}}\}). \tag{6.28}$$

In the last equation the summation over the repeated index k is understood. Correspondingly, the Keldysh collision kernel acquires two contributions to order λ_0^4 and reads

$$\delta I_K \equiv -i\left[\tilde{\tilde{\Sigma}}_{EY}, \tilde{\tilde{G}}\right] = -i\left[\tilde{\tilde{\Sigma}}^{(0)}_{EY}, \tilde{\tilde{G}}\right] - i\left[\tilde{\tilde{\Sigma}}^{(1)}_{EY}, \tilde{\tilde{G}}\right]. \tag{6.29}$$

The first term on the right hand side gives rise to the EY spin relaxation [74], and contributes an extra relaxation channel on the right hand side of Eq. (6.10)

$$-\frac{1}{\tau_{EY}}\begin{pmatrix} 1 & 0 & 0 \\ 0 & 1 & 0 \\ 0 & 0 & d-2 \end{pmatrix}(\mathbf{S} - \chi\mathbf{\Delta}) \equiv -\hat{\Gamma}_{EY}(\mathbf{S} - \chi\mathbf{\Delta}) \tag{6.30}$$

where we have introduced the dimensionality-dependent EY spin relaxation rate given by

$$\frac{1}{\tau_{EY}} = \frac{4(d-1)}{d^2}\frac{1}{\tau}\left(\frac{\lambda_0 p_F}{2}\right)^4. \tag{6.31}$$

In the above $d = 2, 3$ is the dimensionality of the space where particles move. The $d = 2$ case corresponds to the 2-dimensional electron gas case, where we have concentrated our attention until now. The z component of the spin is a constant of the motion and does not undergo relaxation in this case. However, the peculiarity of the new term we are going to derive appears also, and more remarkably, in the $d = 3$ case. For this reason we keep the dependence on the dimensionality from now on.

The Keldysh (K) component of the second term in (6.29) reads

$$\begin{aligned} \delta I^K_K &= -i\left(\tilde{G}^R - \tilde{G}^A\right)\tilde{\Sigma}^{(1),K}_{EY} - i\left(\tilde{\Sigma}^{(1),R}_{EY}\tilde{G}^K - \tilde{G}^K\tilde{\Sigma}^{(1),A}_{EY}\right) \\ &\equiv \delta I^{(1)} + \delta I^{(2)}, \end{aligned} \tag{6.32}$$

having used that $\tilde{G}^{R,A} \sim \sigma^0$. In order to obtain the Bloch equation we need to sum over the momentum as done for obtaining the continuity equation (6.2). The summation over momentum of the Boltzmann collision integral[2] is obtained as

$$\sum_{\mathbf{p}} \int \frac{\mathrm{d}\epsilon}{2\pi i}\, \delta I^K_K \equiv \Delta I^{(1)} + \Delta I^{(2)}. \tag{6.33}$$

By replacing $\tilde{G}^R$, $\tilde{G}^A$ and $\tilde{G}^K$ with the expressions (3.47-3.48), one obtains

$$\Delta I^{(1)} = \frac{n_i \pi}{2}\sum_{\mathbf{p}'\mathbf{p}} \delta(\epsilon_{\mathbf{p}} - \epsilon_{\mathbf{p}'})\Big(\partial_{p'_k}\hat{V}_{\mathbf{p},\mathbf{p}'}\{\mathcal{A}_k, (1-2f_{\mathbf{p}'})\}\hat{V}_{\mathbf{p}',\mathbf{p}} + \partial_{p_k}\{\mathcal{A}_k, \hat{V}_{\mathbf{p},\mathbf{p}'}(1-2f_{\mathbf{p}'})\hat{V}_{\mathbf{p}',\mathbf{p}}\Big), \tag{6.34}$$

and

$$\Delta I^{(2)} = -\frac{n_i \pi}{2}\sum_{\mathbf{p}'\mathbf{p}} \delta(\epsilon_{\mathbf{p}} - \epsilon_{\mathbf{p}'})\frac{1}{2}\Big\{(\partial_{p'_k}\hat{V}_{\mathbf{p},\mathbf{p}'}2\mathcal{A}_k\hat{V}_{\mathbf{p}',\mathbf{p}} + \partial_{p_k}\{\mathcal{A}_k, \hat{V}_{\mathbf{p},\mathbf{p}'}\hat{V}_{\mathbf{p}',\mathbf{p}}\}), (1-2f_{\mathbf{p}})\Big\}. \tag{6.35}$$

In both of the above equations, the first term, after the delta function, has been obtained by an integration by parts with respect to the momentum $\mathbf{p}'$. As a result, the derivatives with respect to p'_k and p_k act on the $\hat{V}_{\mathbf{p},\mathbf{p}'}$ factors only. In Eq. (6.34) the dependence on the directions of the momentum $\mathbf{p}$ is restricted to the $\hat{V}_{\mathbf{p},\mathbf{p}'}$ factors only, so that one can perform at once the integration over the solid angle of $\mathbf{p}$ and then

[2]The Boltzmann collision integral is the Keldysh collision intgeral (6.29) integrated over the energy

take the derivative with respect to $\mathbf{p}'$. Appendix C provides some useful identities (see Eqs. (C.2-C.4)) on how to carry out these operations. Notice also that the second term in round brackets of Eq. (6.34) vanishes, because the derivative with respect to $\mathbf{p}$ yields a linear dependence on $\mathbf{p}$ so that the solid angle integral gives zero.

By reasoning in the same way, one sees that the first term in round brackets within the anticommutator of Eq. (6.35) also vanishes. In the second term one can make at once the integration over the solid angle of $\mathbf{p}'$, again by using the results of Appendix C. As a result, after working out the Pauli algebra, one gets

$$\Delta I = \pi n_i v_0^2 \left(\frac{\lambda_0}{2}\right)^4 \frac{d-1}{d} \sum_{\mathbf{p}'\mathbf{p}} \delta(\epsilon_{\mathbf{p}} - \epsilon_{\mathbf{p}'}) p^2 \Big[\frac{d-2}{d-1} \left(\sigma^k \left\{ e\mathcal{A}_k, p'_l f(\epsilon_{\mathbf{p}'}) \right\} \sigma^l + \sigma^l \left\{ e\mathcal{A}_k, p'_l f(\epsilon_{\mathbf{p}'}) \right\} \sigma^k \right) - \sigma^i \left\{ e\mathcal{A}_k, p'_k f(\epsilon_{\mathbf{p}'}) \right\} \sigma^i + 2p'^2 \left\{ e\mathcal{A}_k, p_k f(\epsilon_{\mathbf{p}}) \right\} \Big]. \quad (6.36)$$

In Eq. (6.36) the summation over repeated indices runs over x, y, z for $d = 3$. For $d = 2$, the last two lines of Eq. (6.36) survive and only the $i = z$ term remains. Then the sum over momentum of the Boltzmann collision integral is [3]

$$\begin{aligned} \Delta I^a &= \frac{1}{2}\mathrm{Tr}[\sigma^a \Delta I] \\ &= \frac{1}{\tau}\left(\frac{\lambda_0}{2}\right)^4 p_F^2 \frac{(d-1)}{2d} \sum_{\mathbf{p}} f^0(\epsilon_{\mathbf{p}}) p_i \Big(e\mathcal{A}_i^a + \frac{d-2}{d-1}(e\mathcal{A}_a^i + e\mathcal{A}_n^n \delta_{ai}). \Big) \end{aligned} \quad (6.37)$$

This is *zero* as long as $f^0(\epsilon_{\mathbf{p}})$ is isotropic, which is the case in a homogeneous system at equilibrium. Things change as soon as an electric field is switched on and carriers have a finite drift velocity $\mathbf{v} = -e\tau\mathbf{E}/m$. We then have the spin generation torque due to the interplay of intrinsic and extrinsic SOCs $\mathcal{T}^a_{ext,sg} \equiv \Delta I^a$

$$\begin{aligned} \mathcal{T}^a_{ext,sg} &= -\frac{N_0}{2\tau_{EY}} \Big(e\mathcal{A}_i^a + \frac{d-2}{d-1}(e\mathcal{A}_a^i + e\mathcal{A}_n^n \delta_{ai}) \Big) v_i \\ &= \mathcal{C}_i^a v_i \end{aligned} \quad (6.38)$$

where we have introduced the extrinsic SOC torque tensor $\mathcal{C}_i^a$. In $d = 3$ it is instructive to represent this tensor as follows

$$\mathcal{C}_i^a = -\frac{eN_0}{2\tau_{EY}} \left[\mathcal{A}_n^n \delta_{ia} + \frac{3}{2}\left(\frac{1}{2}\left(\mathcal{A}_i^a + \mathcal{A}_a^i\right) - \frac{1}{3}\mathcal{A}_n^n \delta_{ia} \right) + \frac{1}{2}\left(\mathcal{A}_i^a - \mathcal{A}_a^i\right) \right] \quad (6.39)$$

by separating explicitly all irreducible tensor parts - the unit, the traceless symmetric, and antisymmetric contributions. Comparing this with the similar representation for the plain $\mathcal{A}_k^a$ we see that the symmetric ("Dresselhaus") part has a contribution 3 times as large relative to the antisymmetric ("Rashba") part. Hence Eq. (6.39) shows that the value at which the spin polarization would like to relax to by EY processes has a form different from the SOC internal field defined in Eq. (6.9) due to DP processes. The latter has the same structure as the first term in the brackets of Eq. (6.38) but with an opposite sign. Three-dimensional motion adds an entirely new term to the internal SOC field induced by the electric field. Although when going to $d = 3$ the linear DSOC may not be appropriate anymore, the overall message is that the interplay of extrinsic SOC and SU(2) intrinsic SOC is extremely rich. The exploration of the consequences of this are however beyond the scope of the present subject.

[3] The corrections to the charge collision integral ΔI^0, relevant for the reciprocal SGE/IEE case in e.g. spin pumping setups, require considering higher-order terms and are discussed in [99].

For $d = 2$ only the first term in the brackets of Eq. (6.38) survives, so that, by considering $a = y$ for RSOC ($e\mathcal{A}_x^y = -2m\alpha$), we have

$$\mathcal{T}_{ext,sg}^y = -\frac{1}{\tau_{EY}} N_0 \alpha m v_x. \tag{6.40}$$

Hence, the spin generation torque due to the interplay of RSOC and extrinsic SOC has the opposite sign with respect to the corresponding term originating by the Dyakonov-Perel precessional relaxation $\mathcal{T}_{int,sg}^y = 1/\tau_{DP}(N_0 \alpha m v_x)$. We name this new term the Elliott-Yafet torque (EYT).

We can then write the Bloch equation in the final form

$$\partial_t \mathbf{S} = -\boldsymbol{\Omega} \times \mathbf{S} - (\hat{\Gamma}_{DP} + \hat{\Gamma}_{EY})(\mathbf{S} - \chi \boldsymbol{\Delta}) + \boldsymbol{\mathcal{T}}_{sg}, \tag{6.41}$$

where the spin generation torque $\boldsymbol{\mathcal{T}}_{sg}$, in the presence of extrinsic SOC is given by

$$\boldsymbol{\mathcal{T}}_{sg} = \boldsymbol{\mathcal{T}}_{int,sg} + \delta\boldsymbol{\mathcal{T}}_{int,sg} + \boldsymbol{\mathcal{T}}_{ext,sg}, \tag{6.42}$$

where

$$\boldsymbol{\mathcal{T}}_{int,sg} = \hat{\Gamma}_{DP} \chi \mathbf{B} \tag{6.43}$$

$$\delta\boldsymbol{\mathcal{T}}_{int,sg} = \frac{\theta_{SH}^{ext}}{\theta_{SH}^{int}} \hat{\Gamma}_{DP} \chi \mathbf{B} \tag{6.44}$$

$$\boldsymbol{\mathcal{T}}_{ext,sg} = -\hat{\Gamma}_{EY} \chi \mathbf{B}. \tag{6.45}$$

Hence, the extrinsic SOC yields two additional spin generation torques (6.44) and (6.45) associated to spin Hall effect (to order λ_0^2) and Elliott-Yafet processes (to order λ_0^4), respectively. The second torque has the same form but opposite sign of the intrinsic torque, indicating that the EY spin-relaxation is detrimental to the ISGE/EE as anticipated in Section 4.2. The Bloch equations (6.41) together with the expressions of the various torques (6.42-6.45), the DP ($\hat{\Gamma}_{DP}$) and EY ($\hat{\Gamma}_{EY}$) spin relaxation matrices (6.21) and (6.30) and the definition of the total magnetic field $\boldsymbol{\Omega}$ (6.17-6.18) are the main result of this Chapter. In accordance with the experimental observations of Ref. [65], Eq. (6.41) shows that, in general, the static non-equilibrium spin polarization will not be aligned along the internal effective magnetic field $\boldsymbol{\Omega}$. To analyze the effect of this new spin generation torque in detail, in the following Chapter, we will solve the Bloch equation (6.41) numerically.

Chapter 7

The current-induced spin polarization: Remarks on experiments and theory

We now discuss some applications of the formalism developed in Chapters 5-6. To show how these results can be manifest in the experiments, the Bloch equations for spin dynamics derived in the previous Chapters solve numerically in the regime of the diffusive limit and then the relevant experiments present.

7.1 The inverse spin-galvanic effect in an anisotropic spin-orbit field

Up to now, we have derived the ISGE by using the SU(2) gauge-field formulation of the Rashba-Dresselhaus SOC and diagrammatic Kubo approach. We have derived the Bloch equations which govern the spin dynamics of the carriers in the diffusive approximation. According to our results in the previous Chapter 6, the Bloch equations for the vector of the spin components $\mathbf{S} = (S^x, S^y, S^z)$ can be written in the form

$$\partial_T \mathbf{S} = -(\hat{\Gamma}_{DP} + \hat{\Gamma}_{EY}) \left(\mathbf{S} - \frac{N_0}{2} \mathbf{\Delta} \right) - (\mathbf{\Delta} + \mathbf{B}) \times \mathbf{S} + (\hat{\Gamma}_{DP} - \hat{\Gamma}_{EY}) \frac{N_0}{2} \mathbf{B} + \frac{\theta_{SH}^{ext}}{\theta_{SH}^{int}} \hat{\Gamma}_{DP} \frac{N_0}{2} \mathbf{B} \qquad (7.1)$$

where at zero temperature the Pauli spin susceptibility reduces to $\chi = N_0/2$ with N_0 as the density of states per spin at the Fermi levels. In the above equation, $\mathbf{\Delta}$ is an in-plane externally magnetic field coupling to the carriers via the Zeeman effect. The external in-plane electric field $\mathbf{E} = (E_x, E_y, 0)$ induces the in-plane magnetic field $\mathbf{B} = (B_x, B_y, 0)$ via the SOC, as one derived in Eqs. (6.19-6.20). The matrices $\hat{\Gamma}_{DP}$ and $\hat{\Gamma}_{EY}$ describe the spin relaxation due to the intrinsic Rashba-Dresselhaus SOC and extrinsic SOC, respectively. In a 2DEG, the intrinsic DP spin relaxation $\hat{\Gamma}_{DP}$ has been carried out in Eq. (6.21),

while the $\hat{\Gamma}_{EY}$ in the 2D can be derived via Eq. (6.31) as

$$\hat{\Gamma}_{EY} = \frac{1}{\tau_{EY}} \begin{pmatrix} 1 & 0 & 0 \\ 0 & 1 & 0 \\ 0 & 0 & 0 \end{pmatrix}, \quad \frac{1}{\tau_{EY}} = \frac{1}{\tau_0} \left(\frac{\lambda p_F}{2} \right)^4 \tag{7.2}$$

In the equation (7.1), the first two terms describe the total relaxation towards the precession and the applied external magnetic field around the total magnetic field, whereas the last two terms describe the Rashba-Edelstein effect [4, 21, 40] due to the magnitude of SO splitting. In order to gain some physical intuition, consider a case with zero extrinsic SOC and with zero external magnetic field. This leads to a stationary solution for the Bloch equations (7.1) according to $\mathbf{S} = (N_0/2)\mathbf{B}$, i.e. the non-equilibrium spin polarization aligns, via susceptibility $N_0/2$ with the internal magnetic field $\mathbf{B}$. In this case, the DP relaxation matrix becomes irrelevant, because the Γ_{DP} appears in front of the spin vectors cancels with the Γ_{DP} in front of the internal field.

Such symmetry can be broken when the extrinsic SOC is present, as reviewed in the previous Chapters. The EY mechanism affects the Bloch equation via the two ways. First, the EY mechanism appears in the diagonal element of the spin relaxation rates, hence the total relaxation rate read $\hat{\Gamma}_{EY} + \hat{\Gamma}_{DP}$. The second way is that the EY mechanism affects the Bloch equation via the term $-\hat{\Gamma}_{EY}(N_0\mathbf{B})/2$. One should notice that this term describes the interplay between EY relaxation and the ISGE. It arises because the EY mechanism, which depends on the forth power of the momentum, is sensitive to the splitting of the Fermi surface induced by the RSOC and DSOC. Its minus sign is appeared because the spins belonging to the carriers at the larger Fermi surface are relaxed more efficiently than the spin of carriers at the smaller Fermi surface. Finally the last term in Eq. (7.1) describes the contribution of the extrinsic spin Hall effect to the Rashba-Edelstein effect. The extrinsic spin Hall angle θ_{SH}^{ext} contains the side-jump and skew-scattering, whose specific structure has been carried out in Chapter 4. One should remember that the introduction of the extrinsic SOC makes the ISGE and SO magnetic field non parallel, a feature seen in experiments [55, 65]. In the rest of this section, we will analyze the consequences of the Bloch equations (7.1) in some details.

7.1.1 Analysis of the Bloch equations in a 2DEG

The final form of the Bloch equations for the spin dynamics according to Eq. (7.1) can be written as

$$\partial_t \mathbf{S} = -\hat{\Gamma}_{tot} \left(\mathbf{S} - \frac{N_0}{2} \mathbf{\Omega}_{rel} \right) - \mathbf{\Omega}_{pre} \times \mathbf{S}, \tag{7.3}$$

where

$$\hat{\Gamma}_{tot} = \hat{\Gamma}_{DP} + \hat{\Gamma}_{EY} \tag{7.4}$$

describe the total relaxation matrix include both the DP and EY mechanisms, and the spin polarization relaxes according to the effective total relaxation magnetic field

$$\mathbf{\Omega}_{rel} = \mathbf{\Delta} + \hat{\Gamma}_{tot}^{-1} \left(\frac{\theta_{SH}}{\theta_{SH}^{int}} \hat{\Gamma}_{DP} - \hat{\Gamma}_{ext} \right) \mathbf{B}, \tag{7.5}$$

whereas the precession is controlled by the total precessional magnetic field $\mathbf{\Omega}_{pre} \equiv \mathbf{\Omega} = \mathbf{\Delta} + \mathbf{B}$. Finally we have introduced the total spin Hall angle $\theta_{SH} = \theta_{SH}^{int} + \theta_{SH}^{ext}$. To proceed further, it is sufficient to

introduce the reduced units. We can use the inverse Dresselhaus DP time $\tau_{DP}^{-1} = (2m\beta)^2 D$ as a unit of energy. We measure also the spin polarization in the units of $S_0 = (N_0/2)/\tau_{DP}$. We then define the following dimensionless parameters

$$\begin{aligned} r &= \frac{\alpha}{\beta} \\ \delta &= |\boldsymbol{\Delta}|\tau_{DP} \\ q &= \frac{\tau_{DP}}{\tau_{EY}} \\ b &= 2e\tau\beta E\tau_{DP} = \frac{eE}{k_F^2\beta} \\ s_H &= \frac{\theta_{SH}}{\theta_{SH}^{int}} = \frac{\theta_{SH}^{ext} + \theta_{SH}^{int}}{\theta_{SH}^{int}} \end{aligned} \tag{7.6}$$

and dimensionless matrices

$$\hat{\gamma}_{tot} = \begin{pmatrix} 1+r^2+q & 2r & 0 \\ 2r & 1+r^2+q & 0 \\ 0 & 0 & 2(1+r^2) \end{pmatrix}, \quad \hat{\gamma}_{rel} = \begin{pmatrix} s_H(1+r^2)-q & 2r & 0 \\ 2r & s_H(1+r^2)-q & 0 \\ 0 & 0 & 2s_H(1+r^2) \end{pmatrix}$$

and dimensionless vector

$$\boldsymbol{\delta} = \begin{pmatrix} \hat{\delta}_x \\ \hat{\delta}_y \\ 0 \end{pmatrix}, \ \mathbf{b} = \begin{pmatrix} \hat{E}_x + r\hat{E}_y \\ -(r\hat{E}_x + \hat{E}_y) \\ 0 \end{pmatrix}$$

with $\boldsymbol{\delta}$ as the unit vectors along the direction of the applied magnetic field and $(\hat{E}_x, \hat{E}_y, 0)$ corresponding to the unit vector along the applied electric field. In reduced units, the Bloch equations reads

$$\partial_t \mathbf{S} = -\hat{\gamma}_{tot}(\mathbf{S} - \delta\boldsymbol{\delta} - b\hat{\gamma}_{tot}^{-1}\hat{\gamma}_{rel}\mathbf{b}) - (\delta\boldsymbol{\delta} + b\mathbf{b}) \times \mathbf{S}. \tag{7.7}$$

We define for convenience

$$\boldsymbol{\omega} = \delta\boldsymbol{\delta} + b\mathbf{b}. \tag{7.8}$$

In the absence of extrinsic SOC, when $q = 0$, $\hat{\gamma}_{tot} = \hat{\gamma}_{rel}$ and $s_H = 1$, one has $\mathbf{S} = \delta\boldsymbol{\delta} + b\mathbf{b}$, i.e. the ISGE is always parallel to the total (internal plus external) magnetic field. Hence, there is no S^z component even for finite applied magnetic field in the plane. In the general case, the static solution satisfies the system

$$\begin{aligned} &\left[\begin{pmatrix} 1+r^2+q & 2r & 0 \\ 2r & 1+r^2+q & 0 \\ 0 & 0 & 2(1+r^2) \end{pmatrix} + \begin{pmatrix} 0 & 0 & \omega_y \\ 0 & 0 & -\omega_x \\ -\omega_y & \omega_x & 0 \end{pmatrix} \right] \begin{pmatrix} S^x \\ S^y \\ S^z \end{pmatrix} \\ &= \delta \begin{pmatrix} 1+r^2+q & 2r & 0 \\ 2r & 1+r^2+q & 0 \\ 0 & 0 & 2(1+r^2) \end{pmatrix} \begin{pmatrix} \hat{\delta}_x \\ \hat{\delta}_y \\ 0 \end{pmatrix} + b \begin{pmatrix} s_H(1+r^2)-q & 2r & 0 \\ 2r & s_H(1+r^2)-q & 0 \\ 0 & 0 & 2s_H(1+r^2) \end{pmatrix} \begin{pmatrix} b_x \\ b_y \\ 0 \end{pmatrix}. \end{aligned} \tag{7.9}$$

The third row of the system gives the expression for S^z

$$S^z = \frac{1}{2(1+r^2)}(\omega_y S^x - \omega_x S^y). \tag{7.10}$$

By inserting the above expression in the first two rows, one obtains

$$\left[\begin{pmatrix} 1+r^2+q & 2r \\ 2r & 1+r^2+q \end{pmatrix} + \frac{1}{2(1+r^2)} \begin{pmatrix} \omega_y^2 & -\omega_x\omega_y \\ -\omega_x\omega_y & \omega_x^2 \end{pmatrix}\right] \begin{pmatrix} S^x \\ S^y \end{pmatrix}$$
$$= \delta \begin{pmatrix} 1+r^2+q & 2r \\ 2r & 1+r^2+q \end{pmatrix} \begin{pmatrix} \hat{\delta}_x \\ \hat{\delta}_y \end{pmatrix} + b \begin{pmatrix} s_H(1+r^2)-q & 2r \\ 2r & s_H(1+r^2)-q \end{pmatrix} \begin{pmatrix} b_x \\ b_y \end{pmatrix}. \quad (7.11)$$

In the absence of the external magnetic field ($\delta = 0$), one has in compact form

$$\left(\hat{\mu} + \frac{b^2}{2(1+r^2)}\hat{\omega}\right) \mathbf{S}_{xy} = b\hat{\nu}\mathbf{b}, \quad (7.12)$$

where

$$\mathbf{S}_{xy} = \begin{pmatrix} S^x \\ S^y \end{pmatrix}, \quad \mathbf{b} = \begin{pmatrix} b_x \\ b_y \end{pmatrix}$$

and

$$\hat{\mu} = \begin{pmatrix} 1+r^2+q & 2r \\ 2r & 1+r^2+q \end{pmatrix}, \quad \hat{\omega} = \begin{pmatrix} b_y^2 & -b_xb_y \\ -b_xb_y & b_x^2 \end{pmatrix}, \quad \hat{\nu} = \begin{pmatrix} s_H(1+r^2)-q & 2r \\ 2r & s_H(1+r^2)-q \end{pmatrix}.$$

The solution of (7.12) can be found in powers of b. Then

$$\begin{aligned} \mathbf{S}_{xy} &= \mathbf{S}_{xy}^{(1)} + \mathbf{S}_{xy}^{(3)} + \dots \\ \mathbf{S}_{xy}^{(1)} &= b\hat{\mu}^{-1}\hat{\nu}\mathbf{b} \\ \mathbf{S}_{xy}^{(3)} &= -\frac{b^2}{2(1+r^2)}\hat{\mu}^{-1}\hat{\omega}\mathbf{S}_{xy}^{(1)} \\ \mathbf{S}_{xy}^{(2n+1)} &= -\frac{b^2}{2(1+r^2)}\hat{\mu}^{-1}\hat{\omega}\mathbf{S}_{xy}^{(2n-1)}, \end{aligned} \quad (7.13)$$

hence $\mathbf{S}_{xy}$ is an odd function of b.

When the extrinsic SOC dominates, we can observe $s_H \sim \beta^{-2}$. Furthermore, $q \sim \beta^{-2}$ and $b \sim \beta^{-1}$. Since the physical ISGE must be multiplied by $N_0\tau_{DP}^{-1} \sim \beta^2$, so that $\mathbf{S}_{xy}^{(1)} \sim \beta^{-1}$ a feature seen in the experiments [65]. Then S^z is an even function of b, starting with a term b^2. In Fig. 7.1 we plot S^z as function of the external magnetic field for different values of the ratio q between the DP and EY relaxation times and fixed ratio of the total spin Hall angle to the intrinsic spin Hall angle $s_H = 5$. Notice that in principle when $q = 0$, the spin Hall angle should be $s_H = 1$. However, in the top left Fig. 7.1, we left $s_H = 5$ even though $q = 0$ to emphasize the role of the extrinsic SOC in the spin relaxation and in the spin Hall effect. When there is no EY relaxation, the S^z curve as function of the applied magnetic field is odd and passes thorough the origin. When EY relaxation is present, the S^z curve has a finite intercept that scales as the square of the applied electric field. In Fig. 7.2, we present the vector plot of the ISGE (blue) and the internal SO field (yellow) for different values of the extrinsic SOC. In the top right panel we have $q = 0$ and $s_H = 1$, i.e. there is no extrinsic SOC. As expected from the equations, the ISGE is parallel to the SO internal field, which is maximum along the $[1, 1]$ axis. By increasing the EY relaxation, the ISGE is no longer parallel to the SO internal field. When $q = 4.5$, the ISGE is maximum along the direction $[1, -1]$, a feature that seems to agree with the data [55]. In Fig. 7.3, we present the vector plot of the ISGE (blue) and the internal SO field (yellow) for different values of the extrinsic SOC

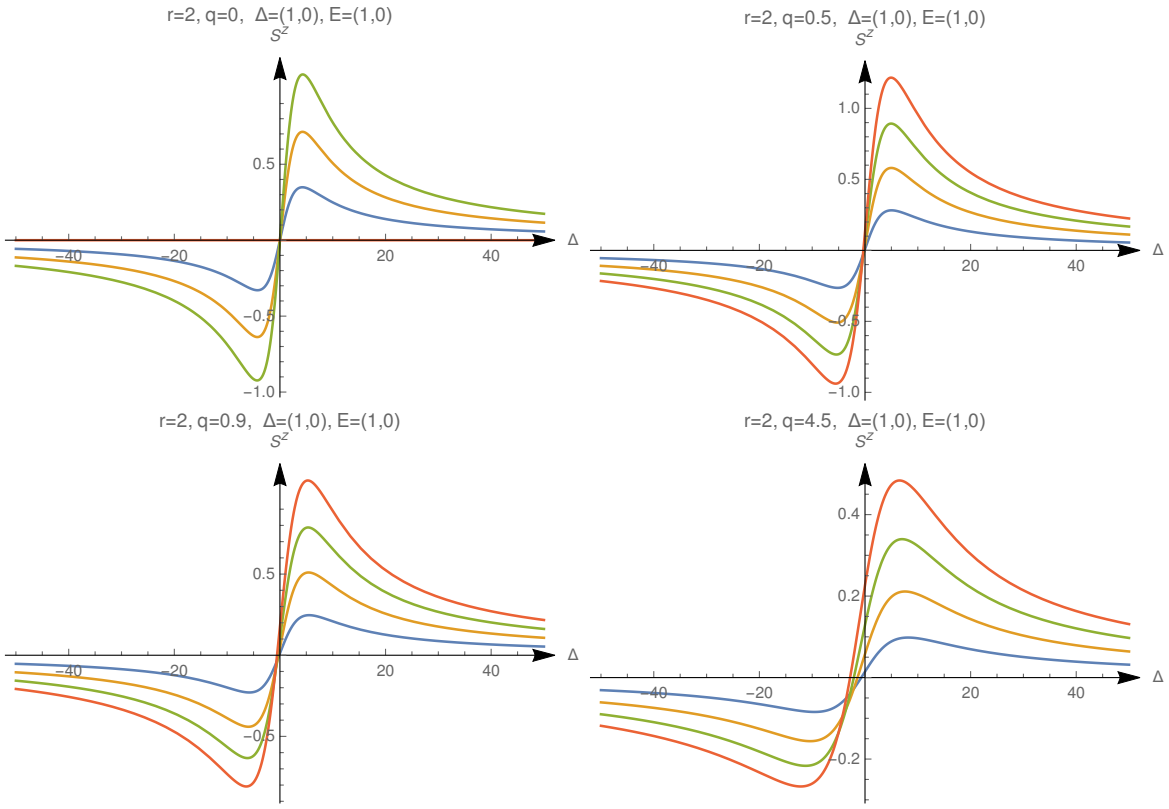

Figure 7.1: S^z as a function of the external magnetic field (applied along the $[1,0]$ axis) for $r = 2$, $s_H = 5$, $E = 0.2$ (blue), $E = 0.4$ (yellow), $E = 0.6$ (green), $E = 0.8$ (red). The DP-EY ratio is $q = 0$ (top left) and $q = 0.5$ (top right), $q = 0.9$ (bottom left) and $q = 4.5$ (bottom right). Notice that the plots do not pass through the origin. The intercept depends on the applied electric field along the $[1,0]$ direction.

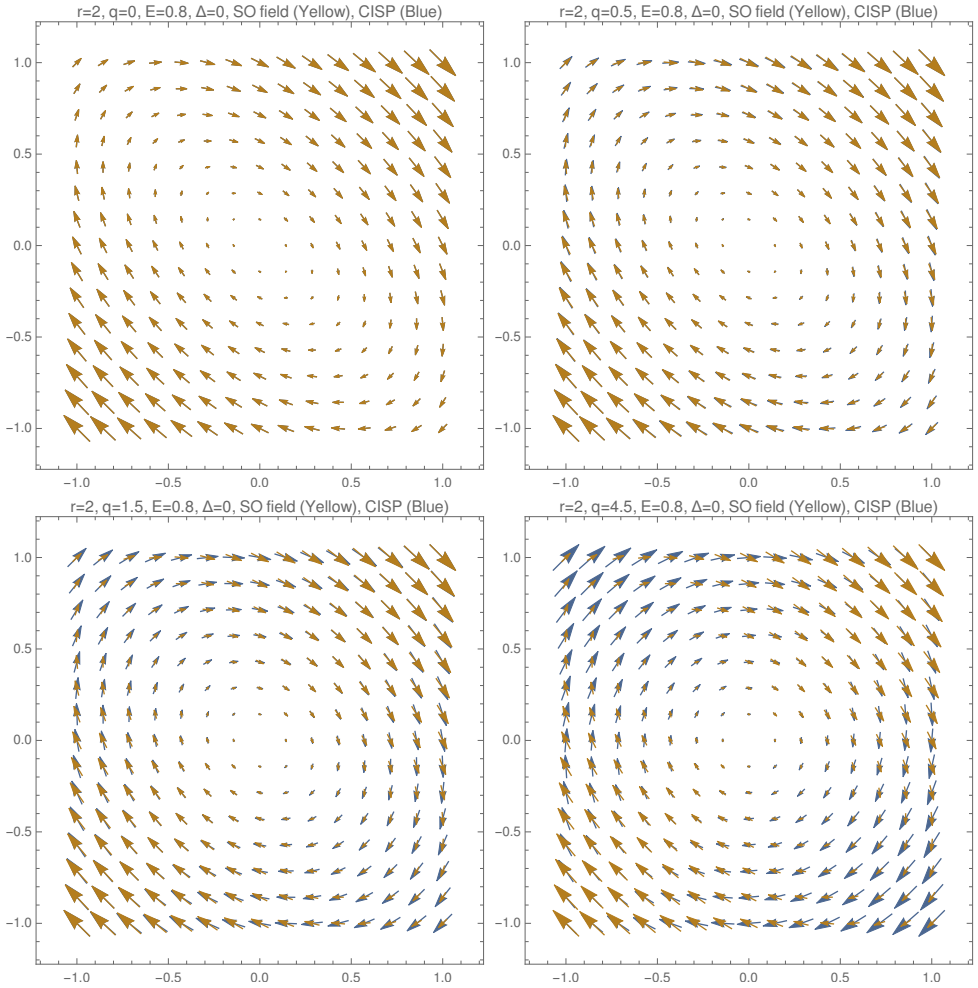

Figure 7.2: Vector plot of the in-plane polarization (S^x, S^y) (Blue) and (B^x_{so}, B^y_{so}) (Yellow) for $q = 0$ (top left) and $q = 0.5$ (top right), $q = 1.5$ (bottom left) and $q = 4.5$ (bottom right). The external magnetic field $\Delta = 0$, the applied electric field $E = 0.8$ along the $[1, 0]$ direction and $r = 2$.

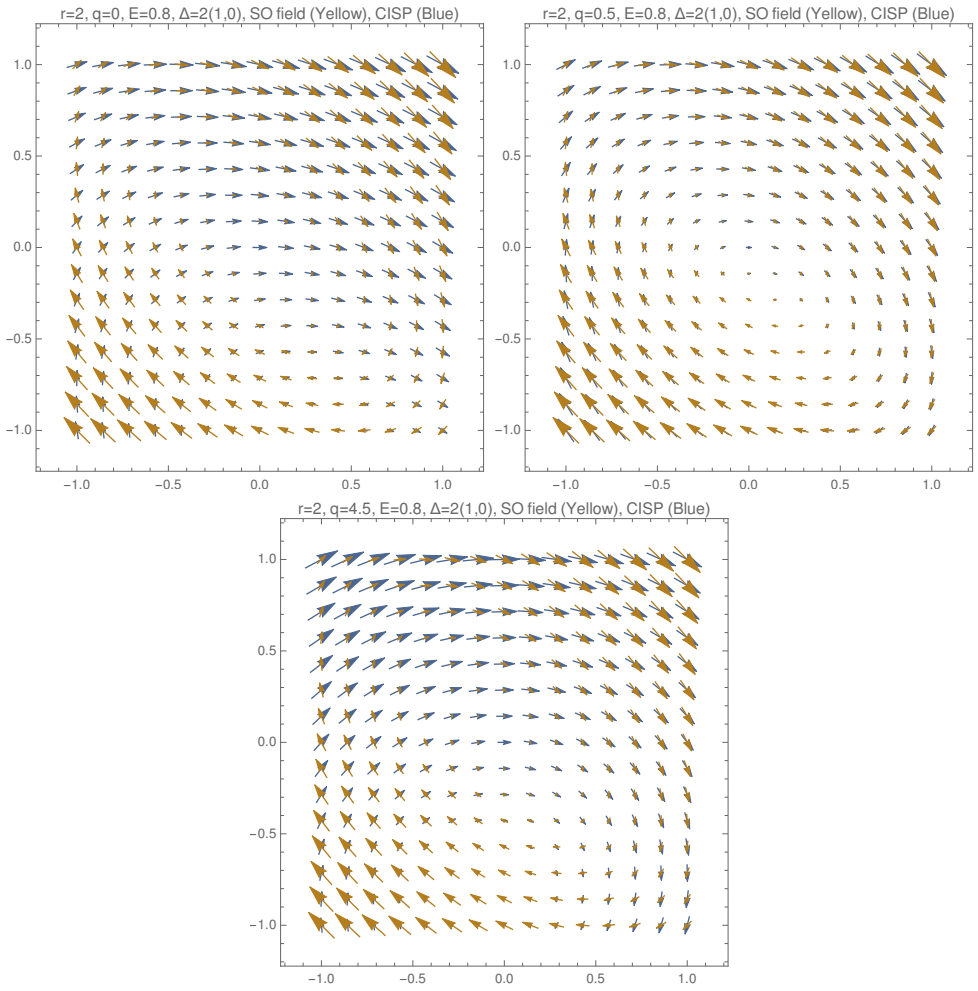

Figure 7.3: Vector plot of the in-plane polarization (S^x, S^y) (Blue) and (B^x_{so}, B^y_{so}) (Yellow) for $q = 0$ (left), $q = 0.5$ (center) and $q = 4.5$ (right). The external magnetic field $\Delta = 2$ along the $[1, 0]$ direction, the applied electric field $E = 0.8$ along the $[1, 0]$ axis and $r = 2$.

at fixed external magnetic field $\delta = 2$ along the $[1, 0]$ axis. Clearly the ISGE (blue) tends to align along the direction of the external field. This is especially true when the SO internal field is lower. Whereas in the previous Chapters we have considered the theory of the effect for a 2DEG, in the next section we will concentrate on the relevant experiments.

7.2 Experiments

The first experimental demonstration of the ISGE was in quantum wells by measuring the current produced by absorption of polarized light (IEE or SGE) [30, 32, 33]. By using spin pumping from a ferromagnet, it has been shown that non-equilibrium spin polarization at a metallic Ag/Bi interface yields an electrical current [83]. In this latter case, which is a manifestation of the inverse effect, one refers also to the inverse Rashba-Edelstein effect. The latter has been also observed in ferromagnet-topological insulator interfaces[59, 92] and in LAO/STO systems [51].

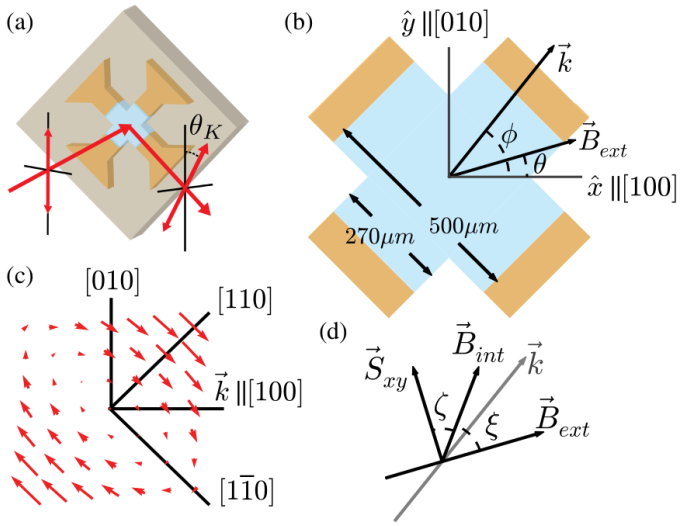

Figure 7.4: Kerr rotation measures the component of SGE along the laser axis $\hat{z}$ (a) InGaAs epilayer (blue) is etched into cross shape with four electrical contacts on the GaAs substrate. (b) The direction of applied electric field determine the drift momentum $\mathbf{k}$ at the angle ϕ with respect to the [100] crystal direction. (c) The internal magnetic field due to the intrinsic SOC as a function of $\mathbf{k}$ with relative strength $(\frac{\alpha}{\beta})$ with $\alpha > 0$. (d) the angles between spin polarization and magnetic field.
(Taken from [65], © 2014 American physical society)

In semiconducting structures, the direct effect is measured via the optical detection of the ISGE [14, 42, 65, 93, 109]. The Faraday rotation spectroscopy has been used to determine the magnitude and direction of the k-dependent spin splitting in strained InGaAs epilayers [64, 65]. In this way, the circular polarized photons are oriented under the electron spins in the samples, which are controlled by the in-plane external and spin-orbit (SO) magnetic fields. The experimental geometry is shown in Fig. 7.4(b), where the InGaAs epilayer is etched into the cross-shaped channel with the four electrical contacts on the GaAs substrate. When an electric voltage applies to the contacts, the electron drifted momentum varies along each channel. Hence the electron spin precesses about the axis along the direction of the effective magnetic field arising from the SO and external fields. Such a situation has been measured in Ref. [55] for GaAs and InGaAs epilayers with varying Indium concentration and doping the densities, where a pump-probe probe optical setup has been used for measuring the non-equilibrium spin polarizations. According to this observation samples with higher Indium and carrier concentrations and lower mobilities were measured to have larger the ISGE. Furthermore the crystal axis with the largest SO splitting had the smallest ISGE and vise versa. This is consist with Fig. 7.2 where the spin polarization is completely opposed to the internal magnetic field if the EY spin relaxation is strong enough. For different material parameters, the relation between the ISGE and SO magnetic field can be either positive or negative depending on the relative strength values of the SOCs. More precisely, a negative differential relation between the magnitude of the ISGE and SO fields has been measured when the extrinsic SHE dominates. However the positive one arises when the extrinsic effect is not strong enough. This observation is qualitatively consist with our theory obtained in the previous Chapters (5-6) via the SU(2) gauge theory formalism and diagrammatic Kubo formula approach.

Chapter 8

The inverse spin galvanic effect in quantum wells

As its title suggests, in this present Chapter we will evaluate the ISGE in a quantum well. In a 2DEG, we consider the intrinsic SOC due to the structure inversion asymmetry (RSOC) and/or bulk inversion asymmetry (DSOC). In this system, the mechanism is developed for the case when both the cubic and linear parts of the Rashba-Dresselhaus SOC are present. To describe this system, we first derive the Eilenberger equation in terms of a generic SOC. Then we use it to derive the Bloch equations governing the spin dynamics of carriers in the linear Rashba-Dresselhaus SOC. One of the advantages of this method is to show how the ISGE can be derived beyond the diffusive approximation. Then we analyze the Bloch equations analytically and also numerically in the two different models, the simplest case of the Rashba model and then the Rashba-Dresselhaus model. We extend our model to the case when the cubic Rashba and Dresselhaus SOCs are present. In this case, we will find that the ISGE does not appear. However when both the linear and cubic SOC are present, several new terms can arise from the interplay between the linear and cubic SOC.

8.1 The Eilenberger equation

The model Hamiltonian in the presence of a generic intrinsic SOC has the form

$$H = \frac{p^2}{2m} + \mathbf{b}\cdot\sigma + V(\mathbf{r}), \tag{8.1}$$

where $V(\mathbf{r})$ and $\mathbf{p} = (p_x, p_y, 0)$ represent the impurity potential and the vector of the momentum operator confined to the xy plane. In a 2DEG, the $\mathbf{b}$ can be defined as the effective magnetic field due to the Rashba-Dresslhaus SOC. By following the standard procedure used in Ref. [78], the equation of the motion for the Green function $\check{G}$ has the form

$$\partial_t \check{G} + \frac{1}{2}\{\frac{p}{m} + \frac{\partial}{\partial \mathbf{p}}(\mathbf{b}\cdot\sigma), \frac{\partial}{\partial x}\check{G}\} + i[\mathbf{b}\cdot\sigma, \check{G}] = -i[\check{\Sigma}, \check{G}], \tag{8.2}$$

where $\check{G}$ is the dressed Green function by including the disorder and SOC effect. In the Wigner coordinates, the Green function is described as $\check{G} = G(\mathbf{p}, x)$, where $\mathbf{p}$ is the Fourier transform of the relative

coordinate and x is the centre of mass coordinate. We dropped the explicit dependence $G(\mathbf{p}, x)$ for simplicity's sake. The quasiclassical Green function is given by

$$\check{g} = \frac{i}{\pi} \int d\xi \check{G}, \tag{8.3}$$

with $\xi = p^2/2m - \mu$ as the energy with respect to the chemical potential μ in the absence of SOC. The above equation guarantees that the $\check{g}$ does not depend on the modulus of the momentum $\mathbf{p}$, but just depends on the momentum direction $\hat{\mathbf{p}}$. For the Green function, following [70] we make the ansatz

$$\check{G} = \begin{pmatrix} G^R & G^K \\ 0 & G^A \end{pmatrix} = \frac{1}{2} \left\{ \begin{pmatrix} G_0^R & 0 \\ 0 & -G_0^A \end{pmatrix}, \begin{pmatrix} \tilde{g}^R & \tilde{g}^K \\ 0 & \tilde{g}^A \end{pmatrix} \right\} \tag{8.4}$$

where G_0^R and g^k are the retarded Green function in the absence of external perturbation and the equilibrium Keldysh component of the Green function, i.e.

$$G_0^R = \frac{1}{\epsilon + \xi - \mathbf{b} \cdot \sigma - \Sigma^R} \tag{8.5}$$

$$g^K = tanh(\frac{\epsilon}{2T})(g^R - g^A) \tag{8.6}$$

with Σ^R the retarded self-energy due to the impurity potential, and the curly brackets in Eq. (8.4) denote the anticommutator properties. The advanced Green function is obtained via $G_0^A = (G_0^R)^\star$. Since the main contribution to the ξ-integral is related to the region near to zero, it is sufficient to expand $\mathbf{b}$ around the small values of ξ. As a result, the Green function can be shifted according to

$$\check{\tilde{g}} = \check{g} + \frac{1}{2}\{\partial_\xi \mathbf{b_0} \cdot \sigma, \check{g}\} \tag{8.7}$$

$$\check{g} = \check{\tilde{g}} - \frac{1}{2}\{\partial_\xi \mathbf{b_0} \cdot \sigma, \check{\tilde{g}}\}. \tag{8.8}$$

where ∂_ξ is the partial derivative taken with respect to ξ. In the limit of the small $|\mathbf{b}|$ compared to the Fermi energy, we have

$$b \approx b_0 - \xi \frac{\partial b_0}{\partial \xi} \tag{8.9}$$

$$|p_\pm| \approx p_F \mp \frac{|b_0|}{v_F}, \tag{8.10}$$

where the subscript "0" denotes the evaluation at the Fermi surface and the $p_\pm$ refers to the Fermi momentum in the $\pm$-bands. Assuming again that $|\mathbf{b}| \ll \epsilon_F$, we can easily show

$$\check{g}_\pm = \frac{1}{2}\{\frac{1}{2} \pm \frac{1}{2}\mathbf{b}_0 \cdot \sigma, \check{g}\}, \quad \check{g} = \check{g}_+ + \check{g}_-. \tag{8.11}$$

Notice that the locally covariant $\tilde{g}^{R/A}$ do not depend on the SOC and so have no spin structure, i.e. $\tilde{g}^R = 1$. Then, by using Eq. (8.8), we can easily show that $g^R = 1 - \partial_\xi(\mathbf{b}_0 \cdot \sigma)$. Hence in equilibrium we have

$$g^K = tanh(\frac{\epsilon}{2T})(g^R - g^A) = 2tanh(\frac{\epsilon}{2T})(1 - \partial_\xi(\mathbf{b}_0 \cdot \sigma)) = g_{eq}(1 - \partial_\xi(\mathbf{b}_0 \cdot \sigma)). \tag{8.12}$$

By integrating over energy and retaining terms up to the first order in $|\mathbf{b}|/\epsilon_F$, the Eilenberger equation (8.2) can be rewritten as follows [70]

$$\sum_{\nu=\pm} \left(\partial_t \check{g}_\nu + \frac{1}{2}\{\frac{p_\nu}{m} + \frac{\partial}{\partial \mathbf{p}}(\mathbf{b}_\nu \cdot \sigma), \frac{\partial}{\partial x}\check{g}_\nu\} + i[\mathbf{b} \cdot \sigma, \check{g}_\nu]\right) = -i[\check{\Sigma}, \check{g}] \tag{8.13}$$

where ±-labels stand for the Fermi surfaces of the two spin subbands due to the effective magnetic field. Finally, the self-energy $\check{\Sigma}$ appears in the collision integral (on the right hand side of the Eilenberger Eq. (8.13)) and describes the spin independent scattering by disorder. The standard self-energy in the limit of the self consistent Born approximation has the form

$$\check{\Sigma} = -\frac{i}{2\tau}\langle \check{g} \rangle, \frac{1}{\tau} = 2\pi N_0 n_i v_0^2, \tag{8.14}$$

where $N_0 = m/2\pi$ and n_i are the density of states in the absence of the SOC and impurity concentration. $\langle \cdots \rangle$ denotes the angular average over the momentum direction. Finally the τ is the elastic scattering time at the level of the Fermi's golden rule. The Keldysh (K) component of the collision kernel can be placed into the form

$$[\Sigma, g]^K = (g^R - g^A)\Sigma^K + (\Sigma^R g^K - g^K \Sigma^A). \tag{8.15}$$

Then the Keldysh components of the linearized Eilenberger equation according to Eq. (8.13) can be written as [70]

$$(M_0 + M_1)g^K = (N_0 + N_1)\langle g^K \rangle, \tag{8.16}$$

where

$$\begin{aligned}
M_0 &= g^K + \tau \partial_t g^K + v_F \tau \hat{p} \cdot \partial_x g^K + i\tau[\mathbf{b}_0 \cdot \sigma, g^K], \\
\frac{1}{\tau} M_1 &= -\frac{1}{2}\{\frac{\mathbf{b}_0 \cdot \sigma}{p_F}\hat{p} - \partial_{\mathbf{p}}(\mathbf{b}_0 \cdot \sigma), \partial_x g^K\} - i[\partial_\xi(\mathbf{b}_0 \cdot \sigma), \{\mathbf{b}_0 \cdot \sigma, g^K\}] - \frac{1}{2\tau}\{\partial_\xi(\mathbf{b}_0 \cdot \sigma), g^K\}, \\
N_0\langle g^K \rangle &= \langle g^K \rangle, \\
N_1\langle g^K \rangle &= \{\partial_\xi(\mathbf{b}_0 \cdot \sigma), g^K\}.
\end{aligned} \tag{8.17}$$

In the presence of SOC, $\langle g^K \rangle$ can be written as a system of four equations according to the spin structure of the quasiclassical Keldysh Green function, i.e.

$$g^K = g_0^K \sigma^0 + g_i^K \sigma^i, i = x, y, z. \tag{8.18}$$

The internal magnetic fields arising from the intrinsic Rashba-Dresselhaus SOC are obtained by the expansion in the power series of the momentum as [44]

$$\mathbf{b} = \mathbf{b}_R^{(N)} + \mathbf{b}_D^{(N)} = (b_x^{(N)}, b_y^{(N)}, 0) = p^N \begin{pmatrix} \alpha_N sin(N\phi) - \beta_N cos(N\phi) \\ -(\alpha_N cos(N\phi) + \beta_N sin(N\phi)) \end{pmatrix} = b_0 \hat{\mathbf{b}} \tag{8.19}$$

with the $N = 1, 3, 5, \cdots$ corresponding to the linear, cubic and higher order of the k-dependent SOC. In the above equation, the $\hat{\mathbf{b}}$ does not depend on the modulus of the momentum. Hence, the retarded and Keldysh components of the Green function according to Eqs. (8.11-8.12) are derived by

$$g^R = 1 - \frac{N}{2}\frac{b_0}{E_F}\hat{\mathbf{b}} \cdot \sigma, \tag{8.20}$$

$$g^K = \big(1 - \frac{N}{2}\frac{b_0}{E_F}\hat{\mathbf{b}} \cdot \sigma\big) 2\tanh(\frac{\epsilon}{2T}). \tag{8.21}$$

Now we will consider the Eilenberger equation in the presence of the external electric fields. In order to evaluate an infinite system under the uniform condition but time-dependent electric fields, we can use the minimal substitution

$$\partial_r \to \partial_r - |e| E \hat{E}_{\mathbf{r}} \partial_\epsilon, \quad \text{with } r = x, y \tag{8.22}$$

where $|e|$ and E are the absolute values of electron charge and the applied electric fields, while $\hat{E}_r = (\hat{E}_x, \hat{E}_y) = (cos(\theta), sin(\theta))$ with θ the angle of the applied electric fields. Hence, we can go back to Eq. (8.16) and solve it for the system under the influence of a uniform but time-dependent electric field along the $\mathbf{r}$ direction as

$$M_0 g^K = (N_0 + N_1)\langle g^K \rangle + S_{\mathbf{E}}, \tag{8.23}$$

where, by using equations (8.17) and after some simple algebra, we obtain

$$M_0 = \begin{pmatrix} L & 0 & 0 & 0 \\ 0 & L & 0 & -a\hat{b}_y \\ 0 & 0 & L & a\hat{b}_x \\ 0 & a\hat{b}_y & -a\hat{b}_x & L \end{pmatrix},\ N_0 + N_1 = \begin{pmatrix} 1 & -c\hat{b}_x & -c\hat{b}_y & 0 \\ -c\hat{b}_x & 1 & 0 & 0 \\ -c\hat{b}_y & 0 & 1 & 0 \\ 0 & 0 & 0 & 1 \end{pmatrix},\ S_{\mathbf{E}} = \tilde{E} \begin{pmatrix} \hat{\mathbf{E}} \cdot \hat{\mathbf{p}} \\ \hat{\mathbf{E}} \cdot \hat{\mathbf{p}} \frac{N+1}{2} \frac{b_0}{E_F} \hat{b}_x - \frac{\hat{\mathbf{E}} \cdot \partial_{\mathbf{p}}}{v_F} b_x \\ \hat{\mathbf{E}} \cdot \hat{\mathbf{p}} \frac{N+1}{2} \frac{b_0}{E_F} \hat{b}_y - \frac{\hat{\mathbf{E}} \cdot \partial_{\mathbf{p}}}{v_F} b_y \\ 0 \end{pmatrix} \tag{8.24}$$

with the terms

$$L = 1 + \tau \partial_t, \quad a = 2\tau b_0, \quad c = (N/2)(b_0/E_F), \quad \tilde{E} = -|e| v_F \tau E \partial \epsilon g_{eq}. \tag{8.25}$$

Hence, the equation (8.23) can be rewritten as

$$g^K = M_0^{-1} S_{\mathbf{E}} + M_0^{-1}(N_0 + N_1)\langle g^K \rangle, \tag{8.26}$$

where

$$M_0^{-1} S_{\mathbf{E}} = \frac{\tilde{E}}{L^3 + L a^2 b^2} \begin{pmatrix} \frac{\hat{E} . \hat{p}}{L}(L^3 + L a^2 b^2) \\ (L^2 + a^2 \hat{b}_x^2)(\hat{\mathbf{E}} \cdot \hat{\mathbf{p}} \frac{N+1}{2} \frac{b_0}{E_F} \hat{b}_x - \frac{\hat{\mathbf{E}} \cdot \partial_{\mathbf{p}}}{v_F} b_x) + a^2 \hat{b}_x \hat{b}_y (\hat{\mathbf{E}} \cdot \hat{\mathbf{p}} \frac{N+1}{2} \frac{b_0}{E_F} \hat{b}_y - \frac{\hat{\mathbf{E}} \cdot \partial_{\mathbf{p}}}{v_F} b_y) \\ a^2 \hat{b}_x \hat{b}_y (\hat{\mathbf{E}} \cdot \hat{\mathbf{p}} \frac{N+1}{2} \frac{b_0}{E_F} \hat{b}_x - \frac{\hat{\mathbf{E}} \cdot \partial_{\mathbf{p}}}{v_F} b_x) + (L^2 + a^2 \hat{b}_y^2)(\hat{\mathbf{E}} \cdot \hat{\mathbf{p}} \frac{N+1}{2} \frac{b_0}{E_F} \hat{b}_y - \frac{\hat{\mathbf{E}} \cdot \partial_{\mathbf{p}}}{v_F} b_y) \\ -\hat{b}_y (\hat{\mathbf{E}} \cdot \hat{\mathbf{p}} \frac{N+1}{2} \frac{b_0}{E_F} \hat{b}_x - \frac{\hat{\mathbf{E}} \cdot \partial_{\mathbf{p}}}{v_F} b_x) + \hat{b}_x (\hat{\mathbf{E}} \cdot \hat{\mathbf{p}} \frac{N+1}{2} \frac{b_0}{E_F} \hat{b}_y - \frac{\hat{\mathbf{E}} \cdot \partial_{\mathbf{p}}}{v_F} b_y) \end{pmatrix} \tag{8.27}$$

$$M_0^{-1}(N_0 + N_1) = \frac{1}{L^3 + L a^2 b^2} \begin{pmatrix} \frac{1}{L}(L^3 + L a^2 b^2) & \frac{-c\hat{b}_x}{L}(L^3 + L a^2 b^2) & \frac{-c\hat{b}_y}{L}(L^3 + L a^2 b^2) & 0 \\ -c(\hat{b}_x(L^2 + a^2 \hat{b}_x^2) + a^2 \hat{b}_y^2 \hat{b}_x) & L^2 + a^2 \hat{b}_x^2 & a^2 \hat{b}_x \hat{b}_y & a\hat{b}_y L \\ -c(\hat{b}_y(L^2 + a^2 \hat{b}_y^2) + a^2 \hat{b}_y \hat{b}_x^2) & a^2 \hat{b}_x \hat{b}_y & L^2 + a^2 \hat{b}_y^2 & -a\hat{b}_x L \\ 0 & -a\hat{b}_y L & a\hat{b}_x L & 1 \end{pmatrix}. \tag{8.28}$$

where $b^2 = b_x^2 + b_y^2$. To obtain the spin polarizations, we have to use

$$S^i = -\frac{N_0}{4} \int d\epsilon \langle g_i^K \rangle, \quad \int d\epsilon \partial_\epsilon g_{eq} = 4 \tag{8.29}$$

Hence the equation (8.26) with the terms derived in Eqs. (8.27-8.28) represents the Eilenberger equation in terms of a generic intrinsic SOC. In the following section, we will solve it in terms of the linear Rashba-Dresselhaus SOC. One of the advantages of Eq. (8.26) is its ability to describe the ISGE beyond the diffusive approximation.

8.2 The inverse spin-galvanic effect: Beyond the diffusive regime

In this section, we will formulate the ISGE in the presence of the linear RSOC and DSOC. Compared to our treatment in the previous Chapters, we will evaluate the Bloch equations beyond the diffusive approximation. After deriving the Bloch equations, we will then solve them numerically in the different strength values of the SOC. In a 2DEG, the effective magnetic field due to the combination of the linear Rashba-Dresselhaus SOC reads [37]

$$\mathbf{b^{(1)}} = p \begin{pmatrix} \alpha\hat{p}_y + \beta\hat{p}_x \\ -\alpha\hat{p}_x - \beta\hat{p}_y \\ 0 \end{pmatrix}, \tag{8.30}$$

where α and β describe the strength values of the linear Rashba and Dresselhaus SOC, respectively. The spin generations $\mathbf{S_E}$ due to the uniform electric field are derived by using Eq. (8.24)

$$S_{E_x} = -eE_x\tau\partial_\epsilon g_{eq} \begin{pmatrix} v_F\hat{p}_x \\ -2\alpha\hat{p}_x\hat{p}_y - 2\beta\hat{p}_x^2 + \beta \\ 2\alpha\hat{p}_x^2 + 2\beta\hat{p}_x\hat{p}_y - \alpha \\ 0 \end{pmatrix} \tag{8.31}$$

$$S_{E_y} = -eE_y\tau\partial_\epsilon g_{eq} \begin{pmatrix} v_F\hat{p}_y \\ -2\alpha\hat{p}_y^2 - 2\beta\hat{p}_x\hat{p}_y + \alpha \\ 2\alpha\hat{p}_x\hat{p}_y + 2\beta\hat{p}_y^2 - \beta \\ 0 \end{pmatrix}. \tag{8.32}$$

By performing the angular average of Eq. (8.26) and under the uniform conditions, one gets

$$(1 - \langle M_0^{-1}\rangle)\langle g^K\rangle = \langle M_0^{-1}(S_{E_x} + S_{E_y})\rangle. \tag{8.33}$$

To evaluate the above equation, we have to identify the several integrals with respect to the momentum direction, which are given in Appendix D. Under the uniform but time-dependent electric field, we have

$$\langle M_0^{-1}\rangle = \frac{1}{L^3 + L(2\tau p_F)^2(\alpha^2+\beta^2)} \begin{pmatrix} M_{11} & M_{12} \\ M_{21} & M_{22} \end{pmatrix}, \tag{8.34}$$

where

$$M_{11} = M_{22} = \left(L^2 + \frac{(2\tau p_F)^2}{2}(\alpha^2+\beta^2)\right)\left(\frac{1}{\sqrt{1-\mathcal{C}^2}}\right) - \frac{(2\tau p_F)^2\alpha\beta}{\mathcal{C}}\left(-1 + \frac{1}{\sqrt{1-\mathcal{C}^2}}\right) \tag{8.35}$$

$$M_{12} = M_{21} = (2\tau p_F)^2\Big(\frac{\alpha^2+\beta^2}{2\mathcal{C}}\Big)\Big(-1 + \frac{1}{\sqrt{1-\mathcal{C}^2}}\Big) - (2\tau p_F)^2\frac{\alpha\beta}{\sqrt{1-\mathcal{C}^2}} \tag{8.36}$$

with $L = 1 + \tau\partial_t$. The generation torques, $\langle M_0^{-1}S_{E_x}\rangle$ and $\langle M_0^{-1}S_{E_y}\rangle$, are given by

$$\langle M_0^{-1}S_{E_x}\rangle = \frac{-eE\tau\partial_\epsilon g_{eq}(\beta^2-\alpha^2)\hat{E}_x}{L^3 + L(2\tau p_F)^2(\alpha^2+\beta^2)} \begin{pmatrix} -\frac{\beta(2\tau p_F)^2}{2}\frac{1}{\sqrt{1-\mathcal{C}^2}} - \frac{\alpha}{2}\delta \\ -\frac{\alpha(2\tau p_F)^2}{2}\frac{1}{\sqrt{1-\mathcal{C}^2}} - \frac{\beta}{2}\delta \end{pmatrix} \tag{8.37}$$

$$\langle M_0^{-1}S_{E_y}\rangle = \frac{-eE\tau\partial_\epsilon g_{eq}(\beta^2-\alpha^2)\hat{E}_y}{L^3 + L(2\tau p_F)^2(\alpha^2+\beta^2)} \begin{pmatrix} \frac{\alpha(2\tau p_F)^2}{2}\frac{1}{\sqrt{1-\mathcal{C}^2}} + \frac{\beta}{2}\delta \\ \frac{\beta(2\tau p_F)^2}{2}\frac{1}{\sqrt{1-\mathcal{C}^2}} + \frac{\alpha}{2}\delta \end{pmatrix}, \tag{8.38}$$

where

$$\delta = L^2\big(\frac{1}{(\alpha^2+\beta^2)\mathcal{C}-2\alpha\beta}\big)\big(-1+\frac{1}{\sqrt{1-\mathcal{C}^2}}\big), \tag{8.39}$$

$$\mathcal{C} = (2\tau p_F)^2\frac{2\alpha\beta L}{L^3+L(2\tau p_F)^2(\alpha^2+\beta^2)}. \tag{8.40}$$

Finally, by using Eq. (8.29), we can rewrite Eq. (8.33) in the new form as follows

$$\begin{aligned}\big(1-\langle M_0^{-1}\rangle\big)\begin{pmatrix}S^x\\S^y\end{pmatrix} &= \frac{eE\tau N_0(\beta^2-\alpha^2)\hat{E}_x}{L^3+L(2\tau p_F)^2(\alpha^2+\beta^2)}\begin{pmatrix}-\frac{\beta(2\tau p_F)^2}{2}\frac{1}{\sqrt{1-\mathcal{C}^2}}-\frac{\alpha}{2}\delta\\-\frac{\alpha(2\tau p_F)^2}{2}\frac{1}{\sqrt{1-\mathcal{C}^2}}-\frac{\beta}{2}\delta\end{pmatrix} \\ &+ \frac{eE\tau N_0(\beta^2-\alpha^2)\hat{E}_y}{L^3+L(2\tau p_F)^2(\alpha^2+\beta^2)}\begin{pmatrix}\frac{\alpha(2\tau p_F)^2}{2}\frac{1}{\sqrt{1-\mathcal{C}^2}}+\frac{\beta}{2}\delta\\\frac{\beta(2\tau p_F)^2}{2}\frac{1}{\sqrt{1-\mathcal{C}^2}}+\frac{\alpha}{2}\delta\end{pmatrix}.\end{aligned} \tag{8.41}$$

By inserting all the terms in the above equation as shown before in Eq. (8.34) for the DP spin relaxation $(1-\langle M_0^{-1}\rangle)$ and also the terms in Eqs. (8.39-8.40), we may derive the Bloch equations beyond the diffusive regime, when the k-linear Rashba-Dresselhaus SOC are present. To compare to the previous results derived in the diffusive regime, as presented in the previous Chapters in Eq. (6.41) and Eq. (5.43), we found the extra components, δ and $\mathcal{C}$, which appear only when the interplay of the Rashba-Dresselhaus SOC is considered beyond the diffusive approximation. To keep the discussion as simple as possible, we will first solve Eq. (8.41) numerically for the case when only RSOC is present. The extension to the DSOC is straightforward.

8.2.1 The inverse spin galvanic effect in the linear Rahsba model

In this section, we will solve the Bloch equations (8.41) numerically for the different strength values of RSOC. After setting $\beta = 0$ in Eq. (8.41), the Bloch equations in the 2DEG Rashba model read

$$\begin{pmatrix}S^x\\S^y\end{pmatrix} = \frac{1}{2}\frac{S_0^\alpha(2\tau p_F\alpha)^2}{L^3-L^2+(L-\frac{1}{2})(2\tau p_F\alpha)^2}\begin{pmatrix}\hat{E}_y\\\hat{E}_x\end{pmatrix} \tag{8.42}$$

with $S_0^\alpha = -eE\tau N_0\alpha$. The spin-charge interconversion can be readily seen from Eq. (8.42), where the coupling between $J_x \sim E_x$ and S^y or between $J_y \sim E_y$ and S^x are clear. Such spin-charge conversion can be understood phenomenologically by symmetry arguments. As mentioned in the first Chapter, the electric current and spin polarization are polar and axial vectors. In centro-symmetric systems, the axial and polar vector transform differently and the result has no spin polarization, however in the restricted symmetry conditions the polar and axial vector transform similarly. Under such symmetry operation, one can expect a coupling between J_x and S^y or between J_y and S^x. In the static limit when the frequency is zero, i.e. $L = 1$, the spin polarization becomes

$$\begin{pmatrix}S^x\\S^y\end{pmatrix} = S_0^\alpha\begin{pmatrix}\hat{E}_y\\\hat{E}_x\end{pmatrix}, \tag{8.43}$$

which is in the full agreement with the Edelstein result [21]. In the following equation, we will consider the frequency-dependent ISGE by inserting $L = 1 - i\omega\tau$ inside Eq. (8.42). Hence, one gets

$$\begin{pmatrix}S^x\\S^y\end{pmatrix} = \big(\frac{S_0^\alpha(2\tau p_F\alpha)^2}{2}\big)\begin{pmatrix}\frac{\frac{1}{2}(2\tau p_F\alpha)^2-2\omega^2\tau^2+i\omega\tau(1+(2\tau p_F\alpha)^2+\omega^2\tau^2)}{(-2\omega^2\tau^2+\frac{1}{2}(2\tau p_F\alpha)^2)^2+\omega^2\tau^2(1+(2\tau p_F\alpha)^2-\omega^2\tau^2)^2}\end{pmatrix}\begin{pmatrix}\hat{E}_y\\\hat{E}_x\end{pmatrix}, \tag{8.44}$$

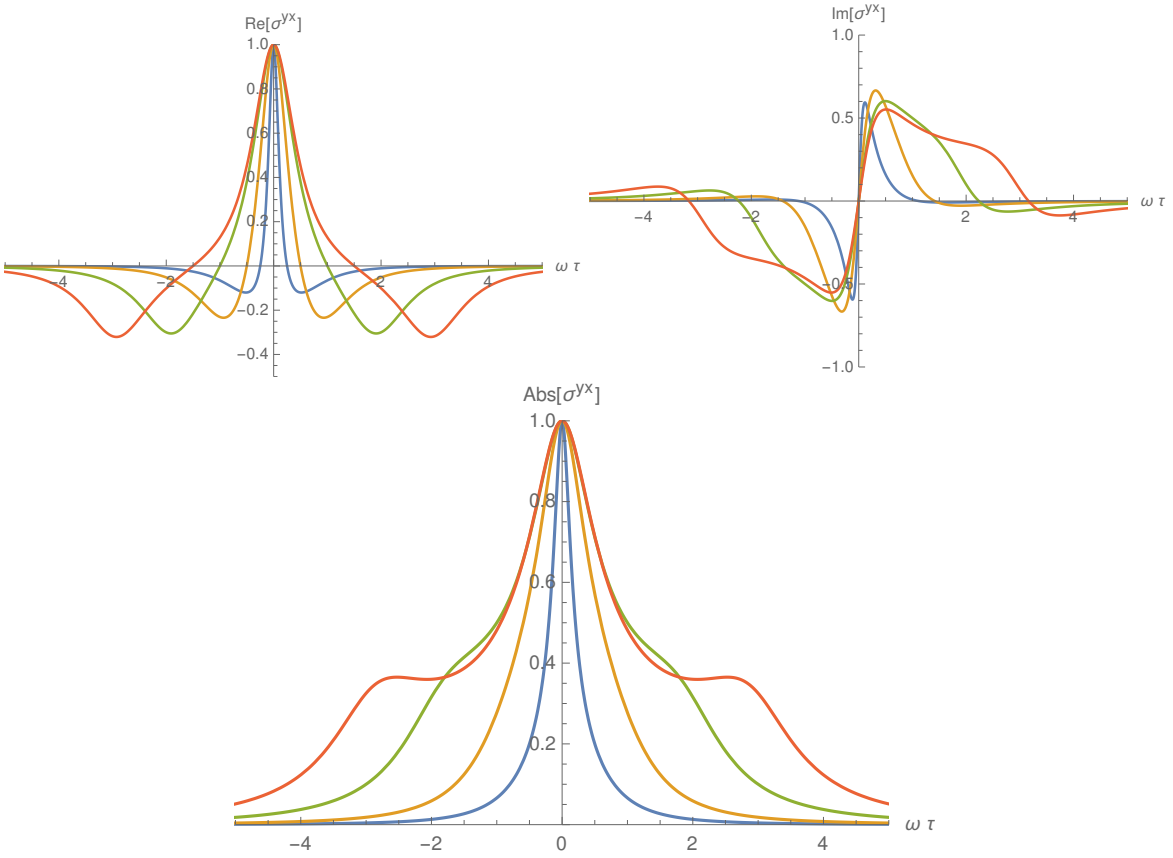

Figure 8.1: Real (top right), imaginary (top left) and absolute values (bottom panel) of Edelstein conductivity σ^{yx} as a function of the frequency for different values of $(2\tau p_F) = 0.1$, $\alpha = 5$ (blue), and $(2\tau p_F) = 1$, $\alpha = 1$ (yellow), and $(2\tau p_F) = 1$, $\alpha = 2$ (green), and $(2\tau p_F) = 1$, $\alpha = 3$ (red). The results are given in the units of S_0^{α}.

which means that the ISGE can be divided into the real and imaginary components, however the imaginary one vanishes when the frequency is zero. To analyze some aspects of the frequency behavior of the ISGE, we will consider both of them. The real and imaginary components become zero, respectively, when

$$|\omega\tau| = \frac{1}{2}(2\tau\alpha p_F), \tag{8.45}$$

$$|\omega\tau| = 0, i\sqrt{1+(2\tau\alpha p_F)^2}. \tag{8.46}$$

Since the imaginary part of the ISGE vanishes, the real part dominates, and vice versa. Hence, in the different values of the frequency, one can expect the different behavior of the ISGE. To examine the transient response of the time, we can use

$$S^i(t) = \int_{-\infty}^{t} \frac{d\omega}{2\pi} e^{-i\omega t} S^i(\omega) \tag{8.47}$$

where

$$S^i(\omega) = \sigma^{ij}_{EC}(\omega) E_j(\omega), \ i/j = x, y \tag{8.48}$$

with $\sigma^{ij}_{EC}(\omega)$ as the frequency-dependent Edelstein conductivity [21], which can be found easily from Eq. (8.42). As we saw from Eq. (8.44), the real and imaginary terms of the ISGE are odd and even

functions with respect to $\omega\tau$. Hence, from Eq. (8.47), we have

$$S(t) = \int_0^\infty \frac{d\omega}{2\pi}[2cos(\omega t)S_r(\omega) + 2sin(\omega t)S_i(\omega)] \tag{8.49}$$

where $S_r(\omega)$ and $S_i(\omega)$ are the real and imaginary parts of the spin polarization (8.44). Notice that when $t = 0$ just the real part of the spin polarization remains. In Fig. 8.1, we show the real, imaginary and absolute components of the Edelstein conductivity σ^{yx} as a function of the frequency in the units of $S_0 = -|e|\tau N_0$ for the different strength values of the Rashba SOC. In the early evolution of the frequency, the σ^{yx} decreases from S_0, as we expected from Eq. (8.48). By increasing the frequency, the real and imaginary components become zero according to equation (8.45) and the significant amplitude of the conductivity oscillation compared with its value at zero frequency happens when the frequency is close to $x = 2\tau\alpha p_F$. One should notice that the values of the both real and imaginary of the spin polarization depend on the strength values of SOC and by increasing the frequency, the spin polarization has a significant amount if the strength values of x is big enough. This is because in the relation of x^2 there are two different regimes which are responsible for the different physical results. If we assume $x^2 \ll 1$, i.e. the Rashba SO splitting is small compared to disorder broadening. This limit is called the diffusive regime and describes the regime of high impurity concentration. Eqs. (8.45-8.46) show that the conductivity can increase when $\omega\tau$ is close to x. In this regime the Rashba strength is not strong and hence the frequency evaluation of Edelstein conductivity decreases by increasing the frequency. However in the case of beyond the diffusive regime when $x^2 \gg 1$, the frequency behavior of Edelstein conductivity shows that the conductivity can increase by increasing the SOC strength. In this case, the conductivity has a significant amount when x is near to $\omega\tau$. In the next section, we will extend our results to the case when the Rashba and Dresselhaus SOCs are present.

8.2.2 The inverse spin-galvanic effect in the linear Rashba-Dresslhaus SOC

As we obtained in the previous section, the ISGE has different behavior with respect to the parameter $x = 2\tau\alpha p_F$. In the beginning, we assumed that the Fermi energy ϵ_F is the largest energy scale as

$$\epsilon_F >> \frac{1}{\tau},\ \epsilon_F >> 2\gamma p_F \tag{8.50}$$

where γ is the total SO strength due to the combination of the RSOC and DSOC, and depends on the direction of the momentum. The above equations show that the SO splitting and the disorder broadening are much smaller than the Fermi energy ϵ_F. In terms of the two small parameters γ/v_F and $1/\epsilon_F\tau$, we can rewrite x as

$$x = 2\tau\gamma p_F = (\frac{4\gamma}{v_F})\epsilon_F\tau. \tag{8.51}$$

In relation to x, there are two different regimes that can be used to give the physical meaning to our results. The first is the so-called diffusive regime, which describes the regime of high impurity concentration, i.e. $x^2 \ll 1$. On the other hand the second one is called beyond diffusive regime, with $x^2 \gg 1$ and sketches out the opposite situation, i.e. low concentration of impurities. To analyze this fact more generally, we focus here on a model with the linear DSOC as well as the linear RSOC. We will evaluate the ISGE in the two different regimes based on the diffusive and beyond the diffusive regime. Then we show their numerical

results in these two limits. In diffusive regime, we can assume $(2\tau\alpha p_F)^2 \ll 1$ and $(2\tau\beta p_F)^2 \ll 1$, which means that many impurity scattering are needed to erase the initial condition of the spin direction, hence the impurity scattering variations are small. In this limit, we can neglect the terms with higher order of the Rashba-Dresselhaus SOC, i.e.,

$$\mathcal{C}^2 = \frac{4L^2(2\alpha\tau p_F)^2(2\beta\tau p_F)^2}{(L^3 + L(2\tau p_F)^2(\alpha^2+\beta^2))^2} \to 0 \Longrightarrow (1 - \frac{1}{\sqrt{1+\mathcal{C}^2}}) \approx 0. \tag{8.52}$$

However, when one of the Rashba and Dresslhaus SOC is absent, the $\mathcal{C}$ is automatically zero. Then the terms in the Eilenberger equation (8.33) can be simplified as

$$\delta \approx 0 \tag{8.53}$$

$$\langle M_0^{-1} \rangle \approx \frac{1}{L^3 + L(2\tau p_F)^2(\alpha^2+\beta^2)} \begin{pmatrix} 1 - 2i\omega\tau + \frac{1}{2}(2\tau p_F)^2(\alpha^2+\beta^2) & -(2\tau p_F)^2(\alpha\beta) \\ -(2\tau p_F)^2(\alpha\beta) & 1 - 2i\omega\tau + \frac{1}{2}(2\tau p_F)^2(\alpha^2+\beta^2) \end{pmatrix}. \tag{8.54}$$

Notice that we kept the denominator of Eq. (8.54), because it will compensate with the numerator of $\langle M_0^{-1} S_{E_x} \rangle$. By inserting the above equations inside Eq. (8.41), we may find the spin polarization in a form of Bloch equations in the diffusive limit

$$(-i\omega\tau + \hat{\Gamma})\mathbf{S} = \hat{\mathcal{T}}\mathbf{E}, \tag{8.55}$$

where the DP spin relaxation $\hat{\Gamma}$ and the spin generation torque $\hat{\mathcal{T}}$ are given by

$$\hat{\Gamma} = \frac{(2\tau p_F)^2}{2} \begin{pmatrix} \alpha^2+\beta^2 & 2\alpha\beta \\ 2\alpha\beta & \alpha^2+\beta^2 \end{pmatrix}, \quad \hat{\mathcal{T}} = S_0 \frac{(2\tau p_F)^2}{2}(\beta^2-\alpha^2) \begin{pmatrix} -\beta & \alpha \\ -\alpha & \beta \end{pmatrix}, \tag{8.56}$$

with $S_0 = -eE\tau N_0$. Notice that in the diffuse approximation $\omega\tau \ll 1$, we kept just the first order of $\omega\tau$. The above equation is exactly in agreement with the result of the previous Chapters in Eq. (5.43) and Eq. (6.41), when the extrinsic effect does not consider in the Bloch equations. To develop some quick intuitions, for $\beta = 0$, the equation (8.55) reproduces the results for the Rashba model in Eq. (8.42). Furthermore, when also $\omega = \beta = 0$, Eq. (8.55) reproduces the Edelstein result [21], as shown in Eq. (8.43).

Now we solve Eq. (8.55) numerically for the Edelstein conductivities (σ^{yx} and σ^{yx}) when the Rashba and Dresselhaus are present. Fig. 8.2 shows the frequency evaluation of σ^{yx} and σ^{xx} in the diffusive regime. In this limit, there is no peak in the frequency evolution of the conductivities, because the real and imaginary parts of the Edelstein conductivities, as shown before in Eq. (8.44) for the Rashba model, highly depends on the strength values of x and in diffusive regime, the Rashba and Dresselhaus SOC are not strong enough. To evaluate the Bloch equations beyond the diffusive approximation, we have to keep all the orders of x and $\omega\tau$. As we shown before in Eq. (8.41), in this regime the contribution to the Bloch equations is highly modified by introducing several new terms. Fig. 8.3 shows the components of Edelstein conductivities numerically as a function of the frequency beyond the diffusive regime. Compared with diffusive regime, we found that the Edeldtein conductivities can be increased in the frequency by increasing the strength of SOCs. Hence the Edelstein conductivity is found to have different behavior with respect to the frequency. In the diffusive regime the conductivity rapidly decreased by increasing

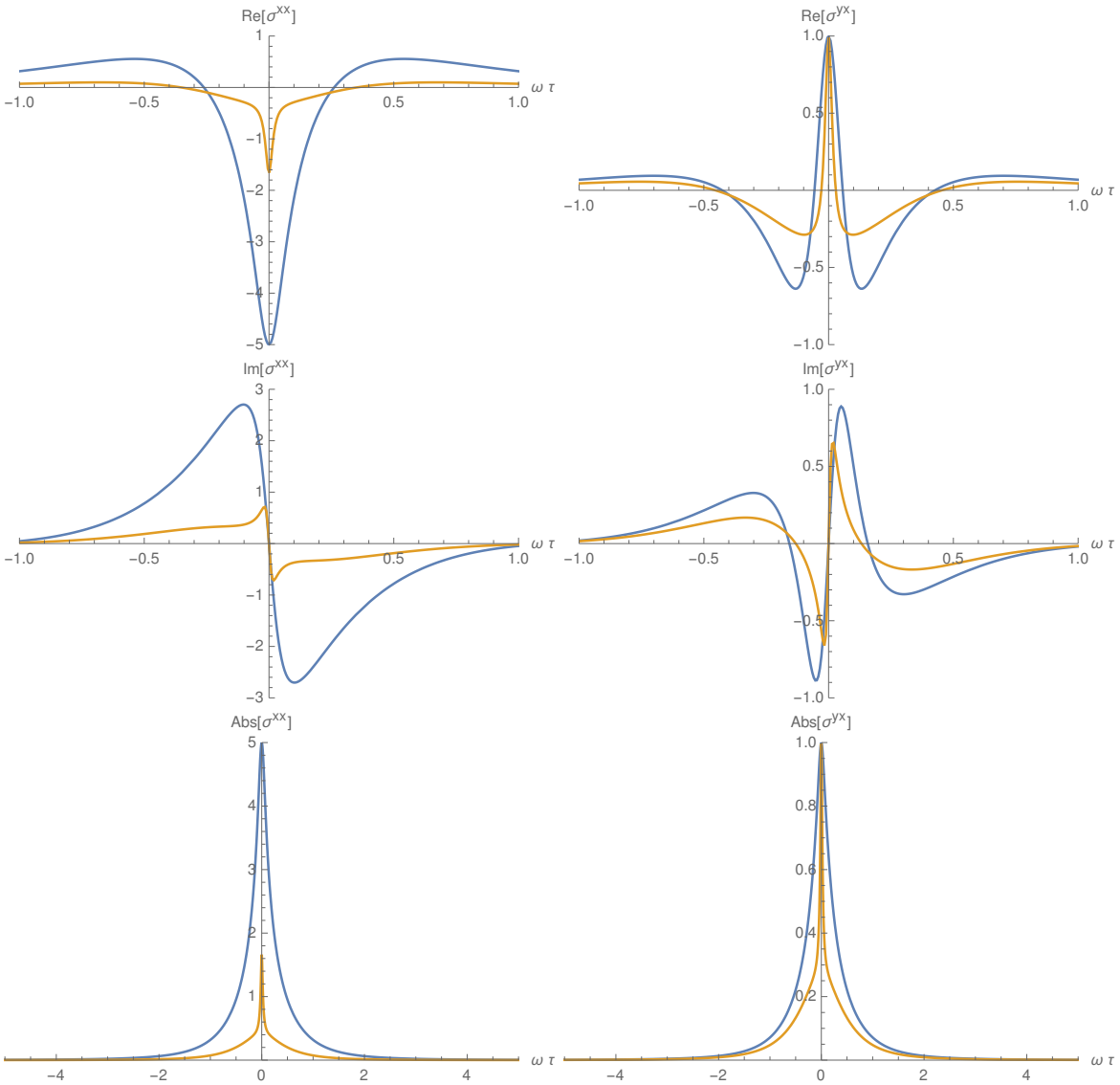

Figure 8.2: Different parts of the Edelstein conductivity $(\sigma^{xx}, \sigma^{yx})$ as a function of the frequency for different values of $\alpha = 1$ and $\beta = 5$ (yellow), $\alpha = 3$ and $\beta = 5$ (blue), where $(2\tau p_F) = 0.1$ is fixed for all values. The results are given in the units of S_0^α.

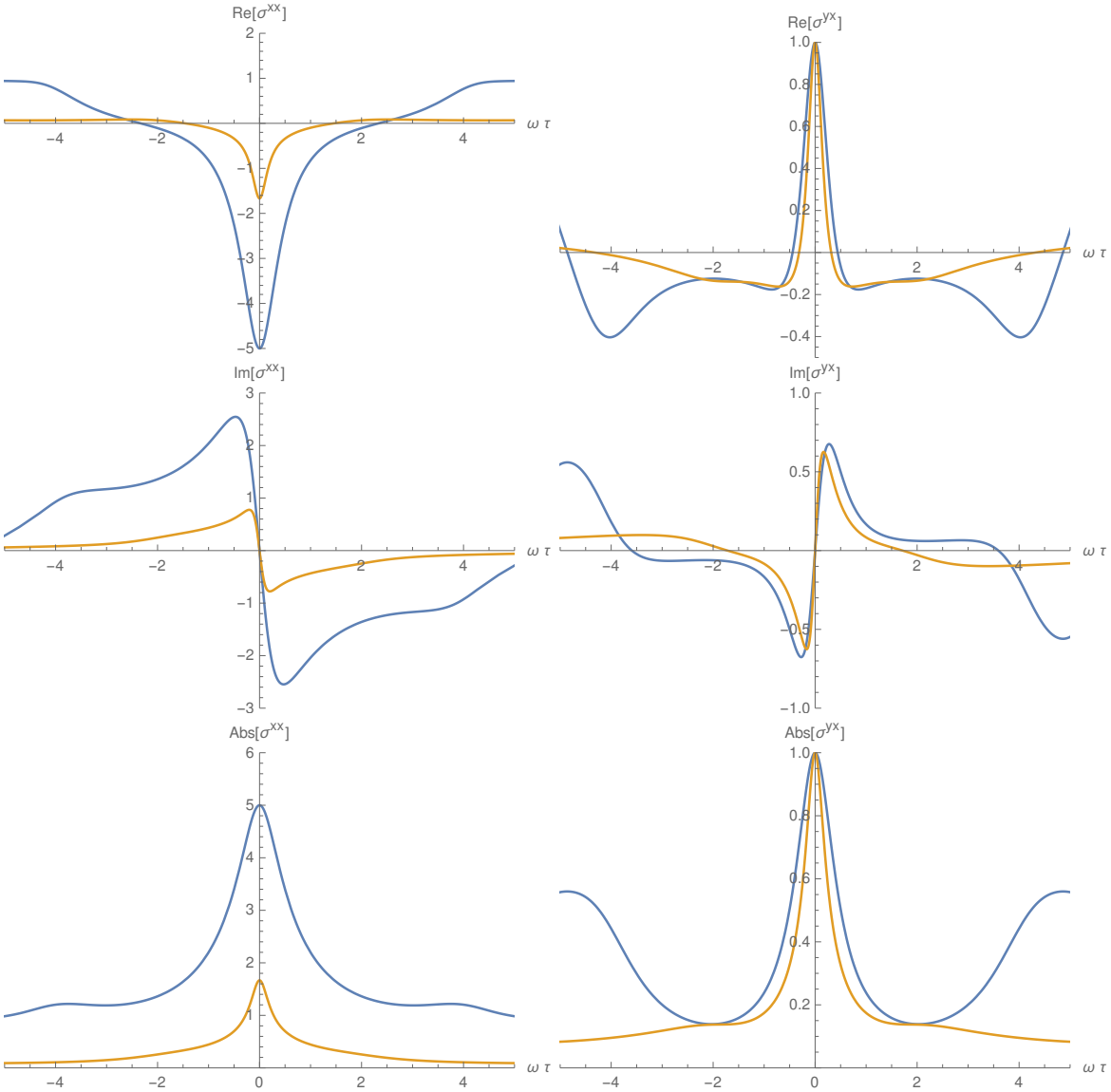

Figure 8.3: The Edelstein conductivity (σ^{xx},σ^{yx}) as a function of the frequency for different values of $\alpha = 1$ and $\beta = 5$ (yellow), $\alpha = 3$ and $\beta = 5$ (blue), where $(2\tau p_F) = 1$ is fixed for all values. The results are given in the units of S_0^{α}.

frequency, however beyond the diffusive approximation the conductivity can increase when x is close to $\omega\tau$. One should notice that in the case of the strong SOC, the cubic Rashba and Dresselhaus SOC become important as well as the linear ones. In the following section, we will evaluate the ISGE in the presence of the cubic Rashba and Dresselhaus SOC. We find that the cubic SOC does not have any effect in the ISGE.

8.3 The cubic Rashba-Dresselhaus terms in a 2DEG

For the quantum well model the Hamiltonian contains p-cubic intrinsic SOC in addition to p-linear intrinsic SOC [45, 68]. According to Eq. (2) from Ref. [63], the effective Hamiltonian of the structural inverse asymmetry for the cubic order of the wave vector $\mathbf{p}$ yields

$$H_R^{(3)} = i\alpha_3 \begin{pmatrix} 0 & (p_x - ip_y)^3 \\ -(p_x + ip_y)^3 & 0 \end{pmatrix} = b_R^{(3)} \cdot \sigma \tag{8.57}$$

with $b_R^{(3)}$ as the internal magnetic field due to the cubic Rashba SOC. From Eq. (8.57), it is sufficient to rewrite the effective magnetic field in the following alternative form

$$b_R^{(3)} = \alpha_3 p^3 \begin{pmatrix} 3\hat{p}_y\hat{p}_x^2 - \hat{p}_y^3 \\ 3\hat{p}_x\hat{p}_y^2 - \hat{p}_x^3 \\ 0 \end{pmatrix} = \alpha_3 p^3 \begin{pmatrix} sin(3\phi) \\ -cos(3\phi) \\ 0 \end{pmatrix}. \tag{8.58}$$

The spin splitting given by Eq. (8.58) represents the cubic Rashba SOC in the plane of the quantum wells. In asymmetric quantum wells, the Hamiltonian also contains the terms of the different symmetry due to the bulk inversion asymmetry, i.e. the cubic Dresslhaus SOC [45]

$$H_D^{(3)} = \beta_3 \begin{pmatrix} 0 & -(p_x - ip_y)^3 \\ -(p_y + ip_x)^3 & 0 \end{pmatrix} = b_D^{(3)} \cdot \sigma \tag{8.59}$$

where

$$b_D^{(3)} = \beta_3 p^3 \begin{pmatrix} 3\hat{p}_x\hat{p}_y^2 - \hat{p}_x^3 \\ -(3\hat{p}_y\hat{p}_x^2 - \hat{p}_y^3) \\ 0 \end{pmatrix} = \beta_3 p^3 \begin{pmatrix} -cos(3\phi) \\ -sin(3\phi) \\ 0 \end{pmatrix} \tag{8.60}$$

with $\mathbf{p} = p(\hat{p}_x, \hat{p}_y) = p(cos(\phi), sin(\phi), 0)$. Hence, the internal magnetic field due to the combination of the cubic Rashba-Dresslhaus SOC is described by

$$\mathbf{b}^{(3)} = \mathbf{b}_R^{(3)} + \mathbf{b}_D^{(3)} = (\mathbf{b}_x^{(3)}, \mathbf{b}_y^{(3)}, 0) = p^3 \begin{pmatrix} \alpha_3 sin(3\phi) - \beta_3 cos(3\phi) \\ -(\alpha_3 cos(3\phi) + \beta_3 sin(3\phi)) \end{pmatrix} = b_0^{(3)} \hat{\mathbf{b}}^{(3)} \tag{8.61}$$

where $\hat{\mathbf{b}}$ does not depend on the modulus of the momentum direction. To linear order in the external electric field, the spin generation torque $S_{\mathbf{E}}$ according to Eq. (8.24) reads

$$S_{\mathbf{E}} = \tilde{E} \begin{pmatrix} \hat{\mathbf{E}} \cdot \hat{\mathbf{p}} \\ \frac{4}{3} c_3 \hat{\mathbf{E}} \cdot \hat{\mathbf{p}} \hat{b}_x^{(3)} - c_3 \hat{\mathbf{E}} \cdot \hat{\mathbf{s}} \\ \frac{4}{3} c_3 \hat{\mathbf{E}} \cdot \hat{\mathbf{p}} \hat{b}_y^{(3)} - c_3 \hat{\mathbf{E}} \cdot \hat{\mathbf{z}} \times \mathbf{s} \\ 0 \end{pmatrix} \tag{8.62}$$

with the unit vector $\hat{s} = (2\hat{p}_x\hat{p}_y, \hat{p}_x^2 - \hat{p}_y^2, 0) = (sin(2\phi), cos(2\phi), 0)$ and $c_3 = (3/2)(b_0^{(3)}/E_F)$. As it was obtained in Eq. (8.26), the Eilenberger equation has the form

$$g^K = M_0^{-1} S_{\mathbf{E}} + M_0^{-1}(N_0 + N_1)\langle g^K \rangle \tag{8.63}$$

where

$$M_0^{-1} S_{\mathbf{E}} = \frac{\tilde{E}}{L^3 + La_3^2} \begin{pmatrix} \frac{\hat{E}.\hat{p}}{L}(L^3 + La_3^2) \\ c_3[(L^2 + a_3^2\hat{b}_x^2)(\frac{4}{3}\hat{E}\cdot\hat{p}\hat{b}_x - \hat{s}\cdot\hat{E}) + a_3^2\hat{b}_x\hat{b}_y(\frac{4}{3}\hat{E}\cdot\hat{p}\hat{b}_y - \hat{z}\times\hat{s}\cdot\hat{E})] \\ c_3[a_3^2\hat{b}_x\hat{b}_y(\frac{4}{3}\hat{E}\cdot\hat{p}\hat{b}_x - \hat{s}\cdot\hat{E}) + (L^2 + a_3^2\hat{b}_y^2)(\frac{4}{3}\hat{E}\cdot\hat{p}\hat{b}_y - \hat{z}\times\hat{s}\cdot\hat{E})] \\ c_3 a_3 L[-\hat{b}_y(\frac{4}{3}\hat{E}\cdot\hat{p}\hat{b}_x - \hat{s}\cdot\hat{E}) + \hat{b}_x(\frac{4}{3}\hat{E}\cdot\hat{p}\hat{b}_y - \hat{z}\times\hat{s}\cdot\hat{E})] \end{pmatrix} \tag{8.64}$$

$$M_0^{-1}(N_0 + N_1) = \frac{1}{L^3 + La_3^2} \begin{pmatrix} \frac{1}{L}(L^3 + La_3^2) & \frac{-c_3\hat{b}_x}{L}(L^3 + La_3^2) & \frac{-c_3\hat{b}_y}{L}(L^3 + La_3^2) & 0 \\ -c_3[\hat{b}_x(L^2 + a_3^2\hat{b}_x^2) + a_3^2\hat{b}_y^2\hat{b}_x] & L^2 + a_3^2\hat{b}_x^2 & a_3^2\hat{b}_x\hat{b}_y & a\hat{b}_y L \\ -c_3[\hat{b}_y(L^2 + a_3^2\hat{b}_y^2) + a_3^2\hat{b}_y\hat{b}_x^2] & a_3^2\hat{b}_x\hat{b}_y & L^2 + a_3^2\hat{b}_y^2 & -a_3\hat{b}_x L \\ 0 & -a_3\hat{b}_y L & a\hat{b}_x L & 1 \end{pmatrix} \tag{8.65}$$

with $a_3^2 = \alpha_3^2 + \beta_3^2$. By taking the integration over the momentum direction in Eq. (8.63), one gets

$$\langle g^K \rangle = (1 - \langle M_0^{-1}(N_0 + N_1)\rangle)^{-1}\langle M_0^{-1} S_E \rangle \tag{8.66}$$

Under the uniform conditions and after inserting Eqs. (8.64-8.65) inside Eq. (8.66) and taking all the integrals, we find

$$\langle M_0^{-1}(N_0 + N_1)\rangle = \begin{pmatrix} \frac{1}{L} & 0 & 0 & 0 \\ 0 & \frac{L^2 + \frac{1}{2}a_3^2}{L^3 + La_3^2} & 0 & 0 \\ 0 & 0 & \frac{L^2 + \frac{1}{2}a_3^2}{L^3 + La_3^2} & 0 \\ 0 & 0 & 0 & \frac{L^2}{L^3 + La_3^2} \end{pmatrix}, \ \langle M_0^{-1} S_E \rangle = 0 \tag{8.67}$$

which means that the ISGE due to the cubic Rashba-Dresselhaus SOC does not exist. Notice that this result also follows trivially from the diagrammatic approach. In this way, the vertex correction is exactly zero because of a very simple reason. The vertex correction contains the first harmonics, while the Green functions contain the only third one. Hence, the angle average is a product of different harmonics and their overlap becomes zero as it has been noticed first by Murakami [62]. In the following section, we will derive the ISGE in a general case when both the linear and cubic RSOC are present. We will find the new terms caused by the interface between the linear and cubic RSOC.

8.4 The inverse galvanic effect in the presence of linear and cubic Rashba SOC

As we have seen in the previous section, the ISGE does not exist in the cubic SOC case, indeed the effect only happens in linear SOC case. In this section, we will evaluate ISGE in the presence of both the linear and cubic RSOC. The main goal of this section is to see how the effect of the interplay between

linear and cubic SOC modifies the ISGE. To keep the discussion as simple as possible, we limit ourselves to the case when only Rashba SOC present. We will derive the spin polarization S^y when the external electric field is applied along the x direction, indeed the spin polarization S^x goes to zero after integration over momentum. In the case $\beta = 0$, the internal magnetic field in the presence of linear and cubic Rashba SOC reads

$$\mathbf{b}_{\mathcal{R}} = \begin{pmatrix} p(\alpha_1 sin(\phi) + \alpha_3 p^2 sin(3\phi)) \\ -p(\alpha_1 cos(\phi) + \alpha_3 p^2 cos(3\phi)) \\ 0 \end{pmatrix} \tag{8.68}$$

where α_1 and α_3 are the strengths of the linear and cubic Rashba SOC, respectively. By replacing the internal magnetic field $\mathbf{b}_{\mathcal{R}}$ in Eq. (8.13) for the Eilenberger equation, one gets

$$Mg^K = N\langle g^K\rangle + S_{E_x} \tag{8.69}$$

where

$$\begin{aligned} M &= \begin{pmatrix} L & 0 & 0 & 0 \\ 0 & L & 0 & -2\tau b_y \\ 0 & 0 & L & 2\tau b_x \\ 0 & 2\tau b_y & -2\tau b_x & L \end{pmatrix}, \; S_{E_x} = \tilde{E} \begin{pmatrix} v_F cos(\phi) \\ 2p_F^2\alpha_3 sin(4\phi) - (p_F^2\alpha_3 + \alpha_1) sin(2\phi) \\ -2p_F^2\alpha_3 cos(4\phi) + (p_F^2\alpha_3 + \alpha_1) cos(2\phi)) \\ 0 \end{pmatrix} \\ N &= \begin{pmatrix} 1 & -c_{13}\alpha_3 sin(3\phi) - \frac{\alpha_1 sin(\phi)}{v_F} & c_{13}\alpha_3 cos(3\phi) + \frac{\alpha_1 cos(\phi)}{v_F} & 0 \\ -c_{13}\alpha_3 sin(3\phi) - \frac{\alpha_1 sin(\phi)}{v_F} & 1 & 0 & 0 \\ c_{13}\alpha_3 cos(3\phi) + \frac{\alpha_1 cos(\phi)}{v_F} & 0 & 1 & 0 \\ 0 & 0 & 0 & 1 \end{pmatrix} \end{aligned} \tag{8.70}$$

with $c_{13} = 3p_F m$ and $\tilde{E} = |e|\tau E \partial\epsilon g_{eq}$. After taking the integrals in Eq. (8.69), we have

$$(1 - \langle M^{-1}N\rangle)\langle g^K\rangle = \langle M_0^{-1} S_{E_x}\rangle, \tag{8.71}$$

where the terms $\langle M^{-1}N\rangle$ and $\langle g^K\rangle$ have the form

$$\langle M^{-1}N\rangle = \frac{1}{L^3 + L(a_1^2 + a_3^2)} \begin{pmatrix} \langle M^{-1}N\rangle_{11} & 0 & 0 \\ 0 & \langle M^{-1}N\rangle_{22} & 0 \\ 0 & 0 & \langle M^{-1}N\rangle_{33} \end{pmatrix}, \; \langle g^K\rangle = \begin{pmatrix} \langle g_x^K\rangle \\ \langle g_y^K\rangle \\ \langle g_z^K\rangle \end{pmatrix} \tag{8.72}$$

with

$$\begin{aligned} \langle M^{-1}N\rangle_{11} &= (L^2 + \frac{1}{2}(a_1^2 + a_3^2))\langle \frac{1}{1 + \Gamma cos(2\phi)}\rangle + \frac{1}{2}(-a_1^2 + 2a_1a_3)\langle \frac{cos(2\phi)}{1 + \Gamma cos(2\phi)}\rangle \qquad (8.73) \\ &- \frac{1}{2}a_3^2\langle \frac{cos(6\phi)}{1 + \Gamma cos(2\phi)}\rangle - a_1a_3\langle \frac{cos(4\phi)}{1 + \Gamma cos(2\phi)}\rangle \\ \langle M^{-1}N\rangle_{22} &= (L^2 + \frac{1}{2}(a_1^2 + a_3^2))\langle \frac{1}{1 + \Gamma cos(2\phi)}\rangle + \frac{1}{2}(a_1^2 + 2a_1a_3)\langle \frac{cos(2\phi)}{1 + \Gamma cos(2\phi)}\rangle \qquad (8.74) \\ &+ \frac{1}{2}a_3^2\langle \frac{cos(6\phi)}{1 + \Gamma cos(2\phi)}\rangle + a_1a_3\langle \frac{cos(4\phi)}{1 + \Gamma cos(2\phi)}\rangle \\ \langle M^{-1}N\rangle_{33} &= L^2\langle \frac{1}{1 + \Gamma cos(2\phi)}\rangle \qquad (8.75) \end{aligned}$$

where $a_1 = 2\tau p_F \alpha_1$ and $a_3 = 2\tau p_F^3 \alpha_3$. In the above equations, the Γ is defined as

$$\Gamma = \frac{2La_1a_3}{L^3 + L(a_1^2 + a_3^2)}. \tag{8.76}$$

Finally, the $\langle M^{-1} S_{E_x} \rangle$ has the form

$$\langle M^{-1} S_{E_x} \rangle = \frac{\tilde{E}}{L^3 + L(a_1^2 + a_3^2))} \begin{pmatrix} 0 \\ \langle M^{-1} S_{E_x} \rangle_y \\ 0 \end{pmatrix} \tag{8.77}$$

with

$$\begin{aligned} \langle M^{-1} S_{E_x} \rangle_y &= \frac{\alpha_1}{2}\Big(a_1^2 - 3a_3^2 + 2a_1a_3\Big)\langle \frac{1}{1+\Gamma cos(2\phi)} \rangle \\ &+ \Big(L^2(\alpha_1 + p_F^2\alpha^2) + \frac{1}{2}(a_1^2\alpha_1 - a_3^2 p_F^2 \alpha_3) + \frac{a_1a_3}{2}(\alpha_1 + p_F^2\alpha_3)\Big)\langle \frac{cos(2\phi)}{1+\Gamma cos(2\phi)} \rangle \\ &+ p_F^2\alpha_3\Big(-2L^2 + a_1a_3 - \frac{1}{2}(a_1^2 + a_3^2)\Big)\langle \frac{cos(4\phi)}{1+\Gamma cos(2\phi)} \rangle + \alpha_1 a_1 a_3 \langle \frac{cos(6\phi)}{1+\Gamma cos(2\phi)} \rangle \end{aligned} \tag{8.78}$$

where $L = 1 - \omega\tau$ and the results of each integrals provided in Appendix D. Notice that when the cubic Rashba SOC goes to zero, it reproduces the result of ISGE in the linear Rashba model, as derived in Eq. (8.43). More precisely, when the cubic RSOC is absent, from Eq. (8.71) one gets

$$\Big(1 - \frac{L^2 + \frac{1}{2}a_1^2}{L^3 + La_1^2}\Big)\langle g_y^K \rangle = \frac{|e|\tau E \partial\epsilon g_{eq}}{L^3 + La_1^2}(\frac{\alpha_1}{2}a_1^2). \tag{8.79}$$

In the zero limit of the frequency $L = 1$, we get

$$\langle g_y^K \rangle = |e|\tau\alpha_1 \partial\epsilon g_{eq} E_x. \tag{8.80}$$

One should remember that the spin polarization S^y is related to the Keldysh component of $\langle g_y^K \rangle$ via the relation

$$S^y = -\frac{1}{4}N_0 \int d\epsilon \langle g_y^K \rangle = -\frac{1}{4}N_0 \int d\epsilon e\tau\alpha_1 E_x \partial\epsilon g_{eq} = -|e|\tau\alpha_1 E_x \tag{8.81}$$

To evaluate the above equation, we used

$$\int_{-\infty}^{\infty} d\epsilon \partial_\epsilon g_{eq} = \int d\epsilon \partial_\epsilon (2tanh(\frac{\epsilon}{2T})) = \int d\epsilon \partial_\epsilon (2(1 - 2f(\epsilon))) = 4 \tag{8.82}$$

with $f(\epsilon)$ as the distribution function. The above result is in agreement with the Edelstein results derived in Eq. (8.43). However, the cubic RSOC does not have effect in the ISGE by itself, but when the linear RSOC is considered as well, the ISGE is highly modified by introducing several new terms first in the relaxation rates (DP spin relaxation matrix) and then in the spin generation torques.

Chapter 9

Epilogue

To summarize, in this work we have considered the phenomenon of spin orientation induced by current by analyzing the interplay of intrinsic (Rashba and Dresselhaus) and extrinsic SOC. This phenomenon, known as the inverse spin galvanic effect or Edelstein effect, is the consequence of the coupling between spin polarization and electric current due to the SOC. To do so, we have derived the Bloch equations governing the spin dynamics by identifying the various relaxation mechanisms and spin generation torques. The results are valid at the level of the Born approximation and to first order beyond the Born approximation. They were obtained first by the standard diagrammatic techniques and then by the SU(2) gauge-field formulation of the Rashba-Dresselhaus SOC. We have shown how the interplay of intrinsic and extrinsic mechanisms modifies the ISGE in the 2DEG cases. We have also extended our results to the 3D electron gas, which can be useful to the interpretation of experiments in thin films.

When we only consider the intrinsic Rashba-Dresselhaus SOC, the spin relaxation mechanism is just the anisotropic DP spin relaxation rate, whose anisotropy is obtained by the relative strength between the RSOC and DSOC. In Chapter 4, we have shown that the contributions due to the RSOC and DSOC can cancel each other for equal RSOC and DSOC strengths and this leads to the cancellation or anisotropy of the spin accumulation. In the presence of purely intrinsic SOC, the spin polarization follows the internal effective magnetic field, whereas this no longer happens when the extrinsic spin-orbit is present. More precisely, the extrinsic SOC affects the spin relaxation time by adding the EY mechanism to the DP. Furthermore, it changes the non-equilibrium value of the ISGE by introducing an additional spin torque. This additional spin torque has been derived in the context of the diagrammatic approach in Chapter 5 and the SU(2) gauge-field formulation in Chapter 6. It describes the interplay between the EY mechanism and the ISGE. The diagrammatic approach was very useful to understand the physical origin of this new term. This new term shows that the precise relation between the spin polarization and the Rashba-Dresselhaus internal field depends on the relative magnitude of the DP and EY spin relaxation rates, as well as on the spin Hall angle. We have also investigated the side-jump and skew scattering contributions due to the extrinsic SOC to the ISGE by using the standard Kubo formula diagrammatic method in Chapter 4. These lead to the renormalization of the spin Hall angle in the expression of the spin generation torque.

In Chapters 5 and 6, we have shown that the behavior of the ISGE turns out to be more complex than expected from the consideration of the internal Rashba and Dresselhaus fields alone. When the extrinsic SOC is present, the symmetry of the ISGE does not necessarily coincide with that of the internal Rashba-Dresselhaus field, and an out-of-plane component of the ISGE appears. The derivation of this component has been shown in Chapter 7, which is in agreement with the recent experimental results [55, 65].

These results can be very useful in analyzing existing experiments on the ISGE/EE. They suggested that the spin polarization and internal magnetic field may not be aligned if the EY is strong enough. Motivated by recent experiments [55, 65], in Chapter 7 we have evaluated the ISGE numerically in order to make the comparison between the theory and experimental results. Our theory, which is able to show a negative differential relation between the ISGE and spin-orbit field, has been found to qualitatively agree well with the recent experimental results [55].

In Chapter 6, we have shown that this new term in 3D is even more remarkable. In fact, in 3D the linear SOC may not be appropriate anymore and one needs to consider the cubic SOC as well as the linear one. We have proven that in 3D the interplay of extrinsic SOC and intrinsic Rashba-Dresselhaus SOC is extremely complex. The exploration of the consequences of this have not been considered in this work.

In Chapter 8, we have evaluated the ISGE in a quantum well. In this system, the mechanism is developed for the case when the cubic and linear SOC are present. For this purpose, in Chapter 8 we have investigated the ISGE in the presence of both the linear and cubic SOCs by using the method of quasiclassical Green functions. We have derived the Eilenberger equation in the presence of a generic spin-orbit field. Compared with our results in the previous Chapters 4-7, the results have been derived beyond the diffusive regime. In this regime, we have found several new terms due to the interplay of the RSOC and DSOC. By extending to the cubic SOC, we have found that all the spin generation torques arising from the SOCs and electric fields become zero and there is no effect, while the cubic effect only appears in the DP spin relaxation rate. Hence, when the linear and cubic SOCs are present, we can expect the cubic and linear terms control the spin relaxation, whereas the linear SOC just provides the effect. In this case, we have found several new terms due to the interplay of the linear and cubic SOCs. However in the presence of the extrinsic SOC, the effect becomes more complex and still needs to be considered.

Appendix A

The extended Kane model and matrix elements

In this appendix, the various quantities needed for evaluating the matrix element of Eq. (2.20) are tabulated. In general, the form of the Kane Hamiltonian are described by the symmetries of system. In this system, some linear combinations of $\tilde{u_i}$ with the different u_{vo} can be used as a basis. These new basis transfer some particular symmetries to the Hamiltonian H, for instance the total angular momentum $\mathbf{J} = \mathbf{L} + \mathbf{S}$. In the language of group theory, $\tilde{u}_i$ transform according to a certain irreducible representation of the symmetry group of H, call Γ_i. By choosing a basis as $|J, m_j\rangle$, shown in Table A.1, the 8×8 Kane Hamiltonian reads [17]

$$H = \begin{pmatrix} [H_c]_{2\times 2} & [H_{cv}]_{2\times 6} \\ [H^{\dagger}_{6\times 2}] & [H_v]_{6\times 6} \end{pmatrix} \tag{A.1}$$

yields

$$[H_c]_{2\times 2} = \begin{pmatrix} V & 0 \\ 0 & V \end{pmatrix} \tag{A.2}$$

$$[H_{cv}]_{2\times 6} = \begin{pmatrix} \frac{-1}{\sqrt{2}}Pk_+ & \sqrt{\frac{2}{3}}Pk_z & \frac{1}{\sqrt{6}}Pk_- & 0 & \frac{-1}{\sqrt{3}}Pk_z & \frac{-1}{\sqrt{2}}Pk_- \\ 0 & \frac{1}{\sqrt{6}}Pk_+ & \frac{2}{\sqrt{3}}Pk_z & \frac{1}{\sqrt{2}}Pk_- & \frac{-1}{\sqrt{3}}Pk_+ & \frac{1}{\sqrt{3}}Pk_z \end{pmatrix} \tag{A.3}$$

$$[H_{cv}]_{6\times 6} = \begin{pmatrix} (V - E_0)\hat{1}_{6\times 6} & \hat{1}_{4\times 2} \\ \hat{0}_{2\times 4} & (V - E_g - \Delta)\hat{1}_{2\times 2} \end{pmatrix} \tag{A.4}$$

where

$$P = \frac{-i}{m_0}\langle S|p_x|X\rangle = \frac{-i}{m_0}\langle S|p_y|Y\rangle = \frac{-i}{m_0}\langle S|p_z|Z\rangle \tag{A.5}$$

$$\Delta = \frac{3}{4m_0^2}\langle X|[\partial_y U \partial_x - \partial_x U \partial_y]|Y\rangle \tag{A.6}$$

with $k_\pm = k_x \pm ik_y$. In the above equation, U represents crystal potential, and V is the perturbing potential. With these matrices, the renormalized mass $m^\star$, g-factor $g^\star$, and the SOC constant λ, as shown in Chapter 2, read

$$\frac{1}{2m^\star} = \left(\frac{1}{E_0 + \Delta} + \frac{2}{E_0}\right), \tag{A.7}$$

$$g^\star = \frac{2e}{\mu_B}\frac{P^2}{3}\left(\frac{1}{E_g} - \frac{1}{E_g + \Delta}\right), \tag{A.8}$$

$$\lambda = \frac{P^2}{3}\left(\frac{1}{E_g^2} - \frac{1}{(E_g + \Delta)^2}\right). \tag{A.9}$$

with μ_B Bohr magneton.

$\tilde{u}_i$	Γ	$\lvert J, m_j\rangle$	u_{j,m_j}
$\tilde{u}_1$	Γ_6	$\lvert\frac{1}{2},+\frac{1}{2}\rangle$	$i\lvert S\rangle\rvert+\frac{1}{2}\rangle$
$\tilde{u}_2$	Γ_6	$\lvert\frac{1}{2},-\frac{1}{2}\rangle$	$i\lvert S\rangle\rvert-\frac{1}{2}\rangle$
$\tilde{u}_3$	Γ_8	$\lvert\frac{3}{2},+\frac{3}{2}\rangle$	$-\frac{1}{\sqrt{2}}(\lvert X\rangle + i\lvert Y\rangle)\rvert+\frac{1}{2}\rangle$
$\tilde{u}_4$	Γ_8	$\lvert\frac{3}{2},+\frac{1}{2}\rangle$	$-\frac{1}{\sqrt{6}}(\lvert X\rangle + i\lvert Y\rangle)\rvert-\frac{1}{2}\rangle + \sqrt{\frac{2}{3}}\lvert Z\rangle\rvert+\frac{1}{2}\rangle$
$\tilde{u}_5$	Γ_8	$\lvert\frac{3}{2},-\frac{1}{2}\rangle$	$\frac{1}{\sqrt{6}}(\lvert X\rangle - i\lvert Y\rangle)\rvert+\frac{1}{2}\rangle + \sqrt{\frac{2}{3}}\lvert Z\rangle\rvert-\frac{1}{2}\rangle$
$\tilde{u}_6$	Γ_8	$\lvert\frac{3}{2},-\frac{3}{2}\rangle$	$+\frac{1}{\sqrt{2}}(\lvert X\rangle - i\lvert Y\rangle)\rvert-\frac{1}{2}\rangle$
$\tilde{u}_7$	Γ_7	$\lvert\frac{1}{2},+\frac{1}{2}\rangle$	$-\frac{1}{\sqrt{3}}(\lvert X\rangle + i\lvert Y\rangle)\rvert-\frac{1}{2}\rangle - \frac{1}{\sqrt{3}}\lvert Z\rangle\rvert+\frac{1}{2}\rangle$
$\tilde{u}_8$	Γ_7	$\lvert\frac{1}{2},-\frac{1}{2}\rangle$	$-\frac{1}{\sqrt{3}}(\lvert X\rangle - i\lvert Y\rangle)\rvert+\frac{1}{2}\rangle + \frac{1}{\sqrt{3}}\lvert Z\rangle\rvert-\frac{1}{2}\rangle$

Table A.1: Basis of the 8×8 Kane model. $|S\rangle$ represents the s-like orbital, and $|X\rangle$, $|Y\rangle$, $|Z\rangle$ are three p-like orbitals. $|\pm\frac{1}{2}\rangle$ are two-component spinors corresponding to the spin-up and spin-down. Here, Γ is the irreducible representation of the symmetry group of the zincblende crystal.

Appendix B

The integral of products of Green functions

In this appendix, we evaluate the integral of products involving pairs of retarded and advanced Green functions. To perform the calculations of the renormalized spin vertex in equation (5.30) and also in all of the analysis, we encounter the following kinds of integrals, which are evaluated to the first order in (γ/v_F) and $\omega\tau$ as

$$\sum_{\mathbf{p}} p^n G^R_{\pm}(\epsilon+\omega)G^A_{\pm}(\epsilon) \approx 2\pi N_{\pm} p^n_{\pm} \frac{1}{-i\omega+\frac{1}{\tau_{\pm}}}, \tag{B.1}$$

$$\sum_{\mathbf{p}} p^n G^R_{\pm}(\epsilon+\omega)G^A_{\mp}(\epsilon) \approx 2\pi N_0 p^n_{\pm} \frac{1}{-i\omega\pm 2i\gamma p_F+\frac{1}{\tau}}, \tag{B.2}$$

where $n=0,1$. We can then evaluate the I_{00} integral as

$$\begin{aligned} I_{00} &= \frac{1}{2\pi N_0\tau_0}\sum_{\mathbf{p}'} G^A_0(\epsilon+\omega)G^R_0(\epsilon) \qquad (B.3)\\ &= \frac{1}{2\pi N_0\tau_0}\sum_{\mathbf{p}'}\frac{1}{4}\left(G^A_+(\epsilon+\omega)G^R_+(\epsilon)+G^A_+(\epsilon+\omega)G^R_-(\epsilon)+G^A_-(\epsilon+\omega)G^R_+(\epsilon)+G^A_-(\epsilon+\omega)G^R_-(\epsilon)\right)\\ &= \frac{1}{4N_0\tau_0}\langle\frac{N_+}{-i\omega+\frac{1}{\tau_+}}+\frac{N_-}{-i\omega+\frac{1}{\tau_-}}+\frac{N_0}{-i\omega+2ip_F\gamma+\frac{1}{\tau}}+\frac{N_0}{-i\omega-2ip_F\gamma+\frac{1}{\tau}}\rangle\\ &\approx (\frac{\tau}{\tau_0})\left(\frac{1-3i\omega\tau-\langle\frac{\tau}{\tau_\gamma}\rangle}{1-4i\omega\tau}\right), \end{aligned}$$

and the same calculations for $2I_{xy}=2I_{yx}$ yields

$$\begin{aligned} 2I_{xy} &= \frac{2}{2\pi N_0\tau_0}\sum_{\mathbf{p}'} G^A_x(\epsilon+\omega)G^R_y(\epsilon) \qquad (B.4)\\ &= \frac{2}{2\pi N_0\tau_0}\left(\frac{-\alpha\beta}{4\gamma^2}\right)\sum_{\mathbf{p}'}\left(G^A_+(\epsilon+\omega)G^R_+(\epsilon)-G^A_+(\epsilon+\omega)G^R_-(\epsilon)-G^A_-(\epsilon+\omega)G^R_+(\epsilon)+G^A_-(\epsilon+\omega)G^R_-(\epsilon)\right)\\ &\approx (\frac{4\tau}{\tau_0})(\frac{2\tau}{\tau_\gamma})\left(\frac{-\alpha\beta}{4\gamma^2}\right)(\frac{1-i\omega\tau}{1-4i\omega\tau})\\ &= -\frac{2\tau}{\tau_{\alpha\beta}}(\frac{1-i\omega\tau}{1-4i\omega\tau}). \end{aligned}$$

Appendix C

An identity concerning angular integration

In the text, we need to perform the integration over the solid angle of $\mathbf{p}$

$$\int \left(\frac{\sin(\theta_{\mathbf{p}})\mathrm{d}\theta_{\mathbf{p}}}{2}\right)^{d-2} \frac{\mathrm{d}\phi_{\mathbf{p}}}{2\pi} \hat{V}_{\mathbf{p},\mathbf{p}'} \dots \hat{V}_{\mathbf{p}',\mathbf{p}} \equiv \langle \hat{V}_{\mathbf{p},\mathbf{p}'} \dots \hat{V}_{\mathbf{p}',\mathbf{p}} \rangle. \tag{C.1}$$

In the above the dots indicate any operator acting on the spin indices, but not depending on the momenta $\mathbf{p}$ and $\mathbf{p}'$. By writing explicitly the cross products in the $\hat{V}_{\mathbf{p},\mathbf{p}'}$ factors one has

$$\begin{aligned} -v_0^2 \left(\frac{\lambda_0}{2}\right)^4 \langle \sum_{ijklmn} \epsilon_{ijk}\epsilon_{lmn} p_i p'_j \sigma^k \dots p_l p'_m \sigma^n \rangle &= -v_0^2 \left(\frac{\lambda_0}{2}\right)^4 \sum_{ijklmn} \epsilon_{ijk}\epsilon_{lmn} \langle p_i p_l \rangle p'_j p'_m \sigma^k \dots \sigma^n \\ &= -v_0^2 \left(\frac{\lambda_0}{2}\right)^4 \frac{p^2}{d} \sum_{ijklmn} \epsilon_{ijk}\epsilon_{lmn}\delta_{il} p'_j p'_m \sigma^k \dots \sigma^n \\ &= -v_0^2 \left(\frac{\lambda_0}{2}\right)^4 \frac{p^2}{d} \left(p'^2 \sigma^i \dots \sigma^i - (d-2)\mathbf{p}' \cdot \boldsymbol{\sigma} \dots \mathbf{p}' \cdot \boldsymbol{\sigma}\right) \end{aligned} \tag{C.2}$$

where in $d = 3$ it is understood a summation over $i = x, y, z$ and in $d = 2$, $i = z$. If the dots are replaced by the identity in the spin space

$$\langle \hat{V}_{\mathbf{p},\mathbf{p}'} \dots \hat{V}_{\mathbf{p}',\mathbf{p}} \rangle = -v_0^2 \left(\frac{\lambda_0}{2}\right)^4 \frac{2p^2 p'^2}{d} \sigma^0. \tag{C.3}$$

Then the derivative with respect to p'_k yields

$$\partial_{p'_k} \langle \hat{V}_{\mathbf{p},\mathbf{p}'} \dots \hat{V}_{\mathbf{p}',\mathbf{p}} \rangle = -v_0^2 \left(\frac{\lambda_0}{2}\right)^4 \frac{p^2}{d} \left(2p'_k \sigma^i \dots \sigma^i - \sigma^k \dots \mathbf{p}' \cdot \boldsymbol{\sigma} - \mathbf{p}' \cdot \boldsymbol{\sigma} \dots \sigma^k\right) \tag{C.4}$$

Appendix D

Integrals over the momentum direction

In this appendix, we evaluate the integral of products involving the momentum direction arising beyond the diffusive regime. In order to evaluate these integrals, we encounter the following kind of angle integrals, which are evaluated to the first order in $(\mathbf{b}/v_F)$ as follows

$$\langle\frac{1}{1+\mathcal{C}sin(2\phi)}\rangle = \frac{1}{\sqrt{1-\mathcal{C}^2}} \tag{D.1}$$

$$\langle\frac{sin(2\phi)}{1+\mathcal{C}sin(2\phi)}\rangle = -\frac{1}{\mathcal{C}}(-1+\frac{1}{\sqrt{1-\mathcal{C}^2}}) \tag{D.2}$$

$$\langle\frac{cos(2\phi)}{1+\mathcal{C}sin(2\phi)}\rangle = \langle\frac{sin(4\phi)}{1+\mathcal{C}sin(2\phi)}\rangle = 0 \tag{D.3}$$

$$\langle\frac{cos(4\phi)}{1+\mathcal{C}sin(2\phi)}\rangle = -\frac{1}{\sqrt{1-\mathcal{C}}}+\frac{2}{\mathcal{C}^2}(-1+\frac{1}{\sqrt{1-\mathcal{C}^{\in}}}) \tag{D.4}$$

In the presence of both the linear and cubic Rashba SOC, we have the following integrals

$$\langle\frac{sin(2n\phi)}{1+\Gamma cos2\phi}\rangle = \langle\frac{sin((2n+1)\phi)}{1+\Gamma cos2\phi}\rangle = \langle\frac{cos((2n+1)\phi)}{1+\Gamma cos2\phi}\rangle = 0,\ n=0,1,2,\cdots \tag{D.5}$$

$$\langle\frac{1}{1+\Gamma cos2\phi}\rangle = \frac{1}{\sqrt{1-\Gamma^2}} \tag{D.6}$$

$$\langle\frac{cos(2\phi)}{1+\Gamma cos2\phi}\rangle = \frac{1}{\Gamma}(1-\frac{1}{\sqrt{1-\Gamma^2}}) \tag{D.7}$$

$$\langle\frac{cos(4\phi)}{1+\Gamma cos2\phi}\rangle = \frac{\left(-2\frac{1}{\sqrt{1-\Gamma^2}}+\Gamma\left(\Gamma\frac{1}{\sqrt{1-\Gamma^2}}-2\right)+2\right)}{(\Gamma-1)\Gamma^2} \tag{D.8}$$

$$\langle\frac{cos(6\phi)}{1+\Gamma cos2\phi}\rangle = \frac{\left(4\left(\frac{1}{\sqrt{1-\Gamma^2}}-1\right)+\Gamma\left(4-\Gamma\left(\Gamma+3\frac{1}{\sqrt{1-\Gamma^2}}-1\right)\right)\right)}{(\Gamma-1)\Gamma^3} \tag{D.9}$$

$$\langle\frac{cos(8\phi)}{1+\Gamma cos2\phi}\rangle = -\frac{\left(8\left(\frac{1}{\sqrt{1-\Gamma^2}}-1\right)+\Gamma\left(\Gamma\left(-8\frac{1}{\sqrt{1-\Gamma^2}}+\Gamma\left(\Gamma\frac{1}{\sqrt{1-\Gamma^2}}-4\right)+4\right)+8\right)\right)}{(\Gamma-1)\Gamma^4} \tag{D.10}$$

$$\langle\frac{cos(10\phi)}{1+\Gamma cos2\phi}\rangle = \frac{\left((\Gamma-2)\Gamma\left(\Gamma\left(\Gamma^2+5\frac{1}{\sqrt{1-\Gamma^2}}\Gamma+\Gamma+10\left(\frac{1}{\sqrt{1-\Gamma^2}}-1\right)\right)-8\right)+16\left(\frac{1}{\sqrt{1-\Gamma^2}}-1\right)\right)}{(\Gamma-1)\Gamma^5} \tag{D.11}$$

Bibliography

[1] V. Ahufinger and et al. Disordered ultracold atomic gases in optical lattices: A case study of Fermi-Bose mixtures. *Phys. Rev. A*, 72:063616, Dec 2005.

[2] B. L. Altshuler. *Sov. Phys. JETP*, 48:670, 1978.

[3] Y. Ando and M. Shiraishi. Spin to Charge Interconversion Phenomena in the Interface and Surface States. *Journal of the Physical Society of Japan*, 86(1):011001, 2017.

[4] A. G. Aronov and Y. B. Lyanda-Geller. Nuclear electric resonance and orientation of carrier spins by an electric field. *Soviet Journal of Experimental and Theoretical Physics Letters*, 50:431, Nov. 1989.

[5] M. N. Baibich et al. Giant Magnetoresistance of (001)Fe/(001)Cr Magnetic Superlattices. *Phys. Rev. Lett.*, 61:2472–2475, Nov 1988.

[6] G. Bastard. Wave Mechanics Applied to Semiconductor Heterostructures (Les Editions de Physique, Les Ulis). page 107, 1986.

[7] L. P. K. G. Baym. *Quantum statistical mechanics; Green's function methods in equilibrium and nonequilibrium problems.* Frontiers in physics. New York, W.A. Benjamin, 1962.

[8] L. Berger. Side-Jump Mechanism for the Hall Effect of Ferromagnets. *Phys. Rev. B*, 2:4559–4566, Dec 1970.

[9] F. S. Bergeret and I. V. Tokatly. Singlet-Triplet Conversion and the Long-Range Proximity Effect in Superconductor-Ferromagnet Structures with Generic Spin Dependent Fields. *Phys. Rev. Lett.*, 110:117003, Mar 2013.

[10] F. S. Bergeret and I. V. Tokatly. Spin-orbit coupling as a source of long-range triplet proximity effect in superconductor-ferromagnet hybrid structures. *Phys. Rev. B*, 89:134517, Apr 2014.

[11] J. Borge, C. Gorini, G. Vignale, and R. Raimondi. Spin Hall and Edelstein effects in metallic films: From two to three dimensions. *Phys. Rev. B*, 89:245443, Jun 2014.

[12] Y. A. Bychkov and E. Rashba. Properties of a 2D electron gas with lifted spectral degeneracy. *JETP Lett.*, 39(2):78, 1984.

[13] Y. A. Bychkov and E. I. Rashba. Oscillatory effects and the magnetic susceptibility of carriers in inversion layers. *J. Phys. C*, 17:6039, 1984.

[14] H. J. Chang et al. Current and Strain-Induced Spin Polarization in InGaN/GaN Superlattices. *Phys. Rev. Lett.*, 98:136403, Mar 2007.

[15] L. Chen and et al. Robust spin-orbit torque and spin-galvanic effect at the Fe/GaAs (001) interface at room temperature. *Nat. Commun.*, 7:13802, 2016.

[16] F. Cooper and et al. Nonequilibrium quantum fields in the large-N expansion. *Phys. Rev. D*, 50:2848–2869, Aug 1994.

[17] T. Darnhofer and U. Rössler. Effects of band structure and spin in quantum dots. *Phys. Rev. B*, 47:16020–16023, Jun 1993.

[18] C. Di Castro and R. Raimondi. *Statistical Condensed Matter Physics*. Cambridge University Press, 2015.

[19] G. Dresselhaus. Spin-Orbit Coupling Effects in Zinc Blende Structures. *Phys. Rev.*, 100:580–586, Oct 1955.

[20] M. Dyakonov. *Spin Physics In Semiconductors. Springer Series in Solid-State Sciences*. Springer, 2008.

[21] V. Edelstein. Solid State Commun. 73 233 Inoue JI, Bauer GEW and Molenkamp LW 2003. *Phys. Rev. B*, 67:033104, 1990.

[22] V. Edelstein. Spin polarization of conduction electrons induced by electric current in two-dimensional asymmetric electron systems. *Solid State Communications*, 73(3):233–235, 1990.

[23] H.-T. Elze and U. Heinz. Quark-Gluon transport theory. *Phys. Rep.*, 183:81–135, 1989.

[24] H.-A. Engel, B. I. Halperin, and E. I. Rashba. Theory of Spin Hall Conductivity in n-Doped GaAs. *Phys. Rev. Lett.*, 95:166605, Oct 2005.

[25] H.-A. Engel, E. I. Rashba, and B. I. Halperin. Out-of-Plane Spin Polarization from In-Plane Electric and Magnetic Fields. *Phys. Rev. Lett.*, 98(3):036602, Jan. 2007.

[26] H.-A. Engel, E. I. Rashba, and B. I. Halperin. *Theory of Spin Hall Effects in Semiconductors*. John Wiley & Sons, Ltd, 2007.

[27] J. Fabian and S. D. Sarma. Spin relaxation of conduction electrons. *Journal of Vacuum Science & Technology B: Microelectronics and Nanometer Structures Processing, Measurement, and Phenomena*, 17(4):1708–1715, 1999.

[28] L. L. Foldy and S. A. Wouthuysen. On the Dirac Theory of Spin 1/2 Particles and Its Non-Relativistic Limit. *Phys. Rev.*, 78:29–36, Apr 1950.

[29] S. Ganichev et al. Experimental separation of Rashba and Dresselhaus spin splittings in semiconductor quantum wells. *Physical Review Letters*, 92(25):256601, 2004.

[30] S. D. Ganichev and et al. Conversion of Spin into Directed Electric Current in Quantum Wells. *Physical Review Letters*, 86:4358–4361, May 2001.

[31] S. D. Ganichev et al. Spin-galvanic effect due to optical spin orientation in n-type GaAs quantum well structures. *Phys. Rev. B*, 68:081302, Aug 2003.

[32] S. D. Ganichev and et al. Electric current-induced spin orientation in quantum well structures. *Journal of Magnetism and Magnetic Materials*, 300:127–131, May 2006.

[33] S. D. Ganichev, E. L. Ivchenko, V. V. Belkov, S. A. Tarasenko, M. Sollinger, D. Weiss, W. Wegscheider, and W. Prettl. Spin-galvanic effect. *Nature*, 417:153, 2002.

[34] S. D. Ganichev, M. Trushin, and J. Schliemann. Spin polarisation by current. *arXiv:1606.02043*, June 2016.

[35] S. Giglberger et al. Rashba and Dresselhaus spin splittings in semiconductor quantum wells measured by spin photocurrents. *Phys. Rev. B*, 75(3):035327, 2007.

[36] C. Gorini, P. Schwab, R. Raimondi, and A. L. Shelankov. Non-Abelian gauge fields in the gradient expansion: Generalized Boltzmann and Eilenberger equations. *Phys. Rev. B*, 82:195316, Nov 2010.

[37] C. Gorini, A. M. Sheikhabadi, and et al. Theory of current-induced spin polarization in an electron gas. *Phys. Rev. B*, 95:205424, May 2017.

[38] E. Ivchenko, Y. B. Lyanda-Geller, and G. Pikus. Photocurrent in structures with quantum wells with an optical orientation of free carriers. *JETP Lett.*, 50:175–177, 1989.

[39] E. L. Ivchenko. *Optical spectroscopy of semiconductor nanostructures.* Alpha Science Int'l Ltd., 2005.

[40] E. L. Ivchenko and G. E. Pikus. New photogalvanic effect in gyrotropic crystals. *Soviet Journal of Experimental and Theoretical Physics Letters*, 27:604, June 1978.

[41] S. Karube, K. Kondou, and Y. Otani. Experimental observation of spin-to-charge current conversion at non-magnetic metal/Bi 2 O 3 interfaces. *Applied Physics Express*, 9(3):033001, 2016.

[42] Y. K. Kato, R. C. Myers, A. C. Gossard, and D. D. Awschalom. Current-Induced Spin Polarization in Strained Semiconductors. *Phys. Rev. Lett.*, 93:176601, Oct 2004.

[43] L. V. Keldysh et al. Diagram technique for nonequilibrium processes. *Sov. Phys. JETP*, 20(4):1018–1026, 1965.

[44] A. Khaetskii. Intrinsic spin current for an arbitrary Hamiltonian and scattering potential. *Phys. Rev. B*, 73:115323, Mar 2006.

[45] W. Knap et al. Weak antilocalization and spin precession in quantum wells. *Phys. Rev. B*, 53:3912–3924, Feb 1996.

[46] H. C. Koo and et al. Control of Spin Precession in a Spin-Injected Field Effect Transistor. *Science*, 325(5947):1515–1518, 2009.

[47] V. L. Korenev. Bulk electron spin polarization generated by the spin Hall current. *Phys. Rev. B*, 74:041308, Jul 2006.

[48] R. Kubo. The fluctuation-dissipation theorem. *Reports on Progress in Physics*, 29(1):255, 1966.

[49] D. C. Langreth. Hall Coefficient of Hubbard's Model. *Phys. Rev.*, 148:707–711, Aug 1966.

[50] A. Larkin and Y. Ovchinnikov. Nonlinear conductivity of superconductors in the mixed state. *Sov. Phys. JETP*, 41(5):960–965, 1975.

[51] E. Lesne et al. Highly efficient and tunable spin-to-charge conversion through Rashba coupling at oxide interfaces. *Nat Mater*, 15:1261, 2016.

[52] M. B. Lifshits and M. I. Dyakonov. Swapping Spin Currents: Interchanging Spin and Flow Directions. *Phys. Rev. Lett.*, 103:186601, Oct 2009.

[53] X.-J. Liu, M. F. Borunda, X. Liu, and J. Sinova. Effect of Induced Spin-Orbit Coupling for Atoms via Laser Fields. *Phys. Rev. Lett.*, 102:046402, Jan 2009.

[54] X.-J. Liu, X. Liu, L. C. Kwek, and C. H. Oh. Optically Induced Spin-Hall Effect in Atoms. *Phys. Rev. Lett.*, 98:026602, Jan 2007.

[55] M. Luengo-Kovac and et al. Current-induced spin polarization in InGaAs and GaAs epilayers with varying doping densities. *Phys. Rev. B*, 96:195206, Nov 2017.

[56] A. Maleki Sheikhabadi and R. Raimondi. Inverse Spin Galvanic Effect in the Presence of Impurity Spin-Orbit Scattering: A Diagrammatic Approach. *Condensed Matter*, 2(2):17, 2017.

[57] A. Manchon, H. C. Koo, J. Nitta, S. M. Frolov, and R. A. Duine. New perspectives for Rashba spin-orbit coupling. *Nature Materials*, 14:871–, Aug. 2015.

[58] F. MEIER and B. Z. (Eds.). *Optical Orientation*. Modern Problems in Condensed Matter Sciences 8. Elsevier Science Ltd, 0 edition, 1984.

[59] Mellnik A. R. and et al. Spin-transfer torque generated by a topological insulator.

[60] T. Miyazaki and N. Tezuka. Giant magnetic tunneling effect in Fe/Al2O3/Fe junction. *Journal of Magnetism and Magnetic Materials*, 139(3):L231–L234, 1995.

[61] V. F. Motsnyi and et al. Electrical spin injection in a ferromagnet/tunnel barrier/semiconductor heterostructure. *Applied Physics Letters*, 81(2):265–267, 2002.

[62] S. Murakami. Absence of vertex correction for the spin Hall effect in p-type semiconductors. *Phys. Rev. B*, 69:241202, Jun 2004.

[63] K. Nomura and et al. Edge-spin accumulation in semiconductor two-dimensional hole gases. *Phys. Rev. B*, 72:245330, Dec 2005.

[64] B. M. Norman and et al. Mapping spin-orbit splitting in strained (In,Ga)As epilayers. *Phys. Rev. B*, 82:081304, Aug 2010.

[65] B. M. Norman, C. J. Trowbridge, D. D. Awschalom, and V. Sih. Current-Induced Spin Polarization in Anisotropic Spin-Orbit Fields. *Phys. Rev. Lett.*, 112:056601, Feb 2014.

[66] K. Osterloh and et al. Cold Atoms in Non-Abelian Gauge Potentials: From the Hofstadter "Moth" to Lattice Gauge Theory. *Phys. Rev. Lett.*, 95:010403, Jun 2005.

[67] S. S. P. Parkin. Origin of enhanced magnetoresistance of magnetic multilayers: Spin-dependent scattering from magnetic interface states. *Phys. Rev. Lett.*, 71:1641–1644, Sep 1993.

[68] G. Pikus and A. Titkov. Spin relaxation under optical orientation in semiconductors. *Optical Orientation*, 8:73–131, 1984.

[69] R. E. Prange and L. P. Kadanoff. Transport Theory for Electron-Phonon Interactions in Metals. *Phys. Rev.*, 134:A566–A580, May 1964.

[70] R. Raimondi, C. Gorini, P. Schwab, and M. Dzierzawa. Quasiclassical approach to the spin Hall effect in the two-dimensional electron gas. *Phys. Rev. B*, 74:035340, Jul 2006.

[71] R. Raimondi, C. Gorini, and S. Tölle. Spin-charge coupling effects in a two-dimensional electron gas. *arXiv:1611.07210*, 2016.

[72] R. Raimondi and P. Schwab. Spin-Hall effect in a disordered two-dimensional electron system. *Phys. Rev. B*, 71:033311, Jan 2005.

[73] R. Raimondi and P. Schwab. Tuning the spin Hall effect in a two-dimensional electron gas. *EPL (Europhysics Letters)*, 87(3):37008, 2009.

[74] R. Raimondi and P. Schwab. Interplay of intrinsic and extrinsic mechanisms to the spin Hall effect in a two-dimensional electron gas. *Physica E*, 42(4):952–955, 2010.

[75] R. Raimondi, P. Schwab, C. Gorini, and G. Vignale. Spin-orbit interaction in a two-dimensional electron gas: a SU(2) formulation. *Ann. Phys.*, 524:153, 2012.

[76] R. Raimondi, P. Schwab, C. Gorini, and G. Vignale. Spin-orbit interaction in a two-dimensional electron gas: A SU(2) formulation. *Annalen der Physik*, 524(3-4):n/a–n/a, 2012.

[77] J. Rammer. *Quantum field theory of non-equilibrium states.* Cambridge University Press, 2007.

[78] J. Rammer and H. Smith. Quantum field-theoretical methods in transport theory of metals. *Rev. Mod. Phys.*, 58:323–359, Apr 1986.

[79] C. Reig, S. Cardoso, and S. C. Mukhopadhyay. Giant magnetoresistance (GMR) sensors. *SSMI6*, pages 157–180, 2013.

[80] U. Rössler. Nonparabolicity and warping in the conduction band of GaAs. *Solid State Communications*, 49(10):943–947, 1984.

[81] J. Ruseckas and et al. Non-Abelian Gauge Potentials for Ultracold Atoms with Degenerate Dark States. *Phys. Rev. Lett.*, 95:010404, Jun 2005.

[82] W. P. S. G. Ganichev. *Intense Terahertz Excitation of Semiconductors (Series on Semiconductor Science and Technology)*. 2006.

[83] J. C. R. Sánchez et al. Spin-to-charge conversion using Rashba coupling at the interface between non-magnetic materials. 4:2944, 2013.

[84] S. D. Sarma, J. Fabian, X. Hu, and I. Žutić. Spin electronics and spin computation. *Solid State Communications*, 119(4–5):207–215, 2001.

[85] P. Schwab and R. Raimondi. Magnetoconductance of a two-dimensional metal in the presence of spin-orbit coupling. *The European Physical Journal B - Condensed Matter and Complex Systems*, 25(4):483–495, 2002.

[86] P. Schwab and R. Raimondi. Quasiclassical theory of charge transport in disordered interacting electron systems. *Annalen der Physik*, 12(7-8):471–516, 2003.

[87] J. Schwinger. Brownian Motion of a Quantum Oscillator. *Journal of Mathematical Physics*, 2(3):407–432, 1961.

[88] A. M. Sheikhabadi, R. Raimondi, and K. Shen. The Edelstein Effect in the Presence of Impurity Spin-Orbit Scattering. *Acta Physica Polonica A*, 132(1):135–139, 2017.

[89] K. Shen, R. Raimondi, and G. Vignale. Theory of coupled spin-charge transport due to spin-orbit interaction in inhomogeneous two-dimensional electron liquids. *Phys. Rev. B*, 90(24):245302, 2014.

[90] K. Shen, R. Raimondi, and G. Vignale. Spin current swapping and Hanle spin Hall effect in a two-dimensional electron gas. *Phys. Rev. B*, 92:035301, Jul 2015.

[91] K. Shen, G. Vignale, and R. Raimondi. Microscopic theory of the inverse Edelstein effect. *Phys. Rev. Lett.*, 112(9):096601, 2014.

[92] Y. Shiomi et al. Spin-Electricity Conversion Induced by Spin Injection into Topological Insulators. *Phys. Rev. Lett.*, 113:196601, Nov 2014.

[93] V. Sih et al. Spatial imaging of the spin Hall effect and current-induced polarization in two-dimensional electron gases. *Nature Physics*, 1:31–35, Oct. 2005.

[94] J. Smit. Magnetoresistance of ferromagnetic metals and alloys at low temperatures. *Physica*, 17(6):612–627, 1951.

[95] A. Soumyanarayanan, N. Reyren, A. Fert, and C. Panagopoulos. Emergent phenomena induced by spin–orbit coupling at surfaces and interfaces. *Nature*, 539:509, 2016.

[96] T. D. Stanescu, C. Zhang, and V. Galitski. Nonequilibrium Spin Dynamics in a Trapped Fermi Gas with Effective Spin-Orbit Interactions. *Phys. Rev. Lett.*, 99:110403, Sep 2007.

[97] S. Sugahara and M. Tanaka. A spin metal-oxide-semiconductor field-effect transistor (spin MOSFET) with a ferromagnetic semiconductor for the channel. *Journal of Applied Physics*, 97(10):10D503, 2005.

[98] S. Tarasenko. Orbital mechanism of the circular photogalvanic effect in quantum wells. *JETP Lett.*, 85(3):182–186, 2007.

[99] S. Tölle, U. Eckern, and C. Gorini. Spin-charge coupled dynamics driven by a time-dependent magnetization. *Phys. Rev. B*, 95:115404, Mar 2017.

[100] M. Trushin and J. Schliemann. Anisotropic current-induced spin accumulation in the two-dimensional electron gas with spin-orbit coupling. *Physical Review B*, 75(15):155323, Apr. 2007.

[101] J. Y. Vaishnav and C. W. Clark. Observing Zitterbewegung with Ultracold Atoms. *Phys. Rev. Lett.*, 100:153002, Apr 2008.

[102] L. E. Vorob'ev and et al. Optical activity in tellurium induced by a current. *Soviet Journal of Experimental and Theoretical Physics Letters*, 29:441, Apr. 1979.

[103] I. Žutić, J. Fabian, and S. D. Sarma. Spintronics: Fundamentals and applications. *Reviews of modern physics*, 76(2):323, 2004.

[104] H. Weigert and U. Heinz. Kinetic equations for the quark-gluon plasma and their semiclassical expansion. *Z. Phys. C*, 50:195–203, 1991.

[105] R. K. Willardson and A. C. Beer. *Semiconductors and semimetals*, volume 12. Academic press, 1977.

[106] R. Winkler. *Spin-orbit Coupling Effects in Two-Dimensional Electron and Hole Systems (Springer Tracts in Modern Physics)*. Springer, 1 edition, 2003.

[107] P. Wölfle and K. Muttalib. Anomalous Hall effect in ferromagnetic disordered metals. *Annalen der Physik*, 15(7-8):508–519, 2006.

[108] Y. Yafet. g Factors and Spin-Lattice Relaxation of Conduction Electrons. volume 14 of *Solid State Physics*, pages 1–98. Academic Press, 1963.

[109] C. L. Yang et al. Spectral Dependence of Spin Photocurrent and Current-Induced Spin Polarization in an InGaAs/InAlAs Two-Dimensional Electron Gas. *Phys. Rev. Lett.*, 96:186605, May 2006.

[110] Yuasa Shinji et al. Giant room-temperature magnetoresistance in single-crystal Fe/MgO/Fe magnetic tunnel junctions. *Nat Mater*, 3(12):868–871, dec 2004. 10.1038/nmat1257.

[111] S.-L. Zhu and et al. Spin Hall Effects for Cold Atoms in a Light-Induced Gauge Potential. *Phys. Rev. Lett.*, 97:240401, Dec 2006.

Acknowledgements

Firstly, I would like to express my sincere appreciation to my advisor Prof. Roberto Raimondi for his continuous support of my Ph.D study and related research, for all his helpful comments, suggestions and enthusiastic support. His guidance helped me in all the time of research and writing of this thesis. I could not have imagined having a better advisor and mentor for my Ph.D study. I would also like to mention Dr. Cosimo Gorini, Dr. Ka Shen, Prof. Ilya V. Tokatly and Prof. Giovanni Vignale for stimulating and instructive discussions.

Last but not the least, it is my privilege to thank my wife, Mahsa. Her support, quiet patience, encouragement and unwavering love were undeniably the bedrock upon which the past eleven years of my life have been built. I owe my deepest gratitude to my family: my parents and to my brother and sisters for supporting me spiritually throughout my life in general.